2016

Behavioral Assays with Smart Worm Recognition Programs Applied to Plant-parasitic and Human-parasitic Nematodes

Zachery Njus
Iowa State University

Behavioral assays with smart worm recognition programs applied to plant-parasitic and human-parasitic nematodes

by

Zachery Njus

A dissertation submitted to the graduate faculty

in partial fulfillment of the requirements for the degree of

DOCTOR OF PHILOSOPHY

Major: Electrical Engineering

Program of Study Committee:
Santosh Pandey, Major Professor
Jaeyoun Kim
Long Que
Philip Jones
Jiming Song

Iowa State University

Ames, Iowa

2016

To my fiancée, Nikki Riha,

I could not have made it this far in my doctoral study without you.

To my family,

Thank you for your unconditional support and encouragement throughout this journey.

TABLE OF CONTENTS

LIST OF FIGURES

LIST OF TABLES

Page

ACKNOWLEDGMENTS

I would like to express my sincere gratitude to my advisor, Dr. Santosh Pandey, for his continuous guidance, motivation, and support throughout my research studies. I feel a large part of my success is due to the freedom he allowed me to pursue topics of interest and the expert advice he provided on how to proceed.

I would also like to thank my Ph.D. committee members; Dr. Jaeyoun Kim, Dr. Long Que, Dr. Philip Jones, and Dr. Jiming Song, for their guidance and support throughout the course of this research.

Collaborating with fellow graduate students Taejoon Kong, Augustine Beeman, Upender Kalwa, Jared Jensen, Riley Brien, Sreemoyee Acharya and Hiruni Harischandra, as well as undergraduate Isaac Johns, was truly an enjoyable experience. I would also like to the Dr. Archana Parashar for mentoring and training me early on in my graduate studies. Thank you all for making my time at Iowa State University a memorable experience.

Last but never the least, I would like to thank my fiancée, Nikki Riha, and my parents for their unwavering support and encouragement. Throughout this journey they have been an amazing support system and they truly deserve my thanks.

ABSTRACT

The free-living *C. elegans* roundworm has inspired an entire family of microfluidic devices to capture, culture or screen worm populations for a number of biological studies. Worm tracking programs also have been developed that can recognize body features and extract behavioral features relevant to the user. While the technological developments towards *C. elegans* research is commendable, there is far less effort in applying these technologies for parasitic nematodes. This is primarily because of the difficulty in extracting parasitic nematodes from host systems, culturing them in laboratory settings, and applying genetic techniques to a non-model organism.

The thesis starts by demonstrating our *C. elegans* microfluidic platform, specifically to test the effects of static magnetic fields on the worms (Chapter 2). It had been hypothesized that adult *C. elegans* may possess traces of magnetite within their body that helps them guide their directionality of movement. To test this hypothesis, we encapsulated single *C. elegans* in straight microchannels and exposed them to varying degrees of static magnetic fields from permanent magnets. Our experiments suggested no conclusive effects of static magnetic fields on the directionality or velocity of *C. elegans*.

Plant-parasitic nematodes are quite lethargic and sedentary compared to their *C. elegans* counterparts, and we presented microfluidic devices specifically tailored to these slow-moving nematodes (Chapter 3). The two plant-parasitic nematodes, soybean cyst nematodes and root knot nematodes, were designed to be tracked within microfluidic chips for over 18 hours with a goal to test their chemoattraction to chemical compounds and live roots. Extensive experimental runs were conducted using the microfluidic chip technology and the data was compared to runs

from the greenhouse. We showed that the microfluidic chip technology provides a reliable platform for chemotaxis studies on the two plant-parasitic nematodes and a viable alternative to greenhouse tests.

The fabrication of abovementioned microfluidic chips required considerable time commitment, and made us search for alternative chip designs that could be mass manufactured. We developed two types of devices: agarose gel membranes resting on paper and Pluronic gel membranes resting on plastic (Chapter 4). Methods of worm handling, imaging, transfer, and drug screening are shown using *C. elegans* as the subject of choice. Compared to agarose plate and microfluidic assays, the membrane devices are flexible, much more cost-effective, and easier for worm accessibility. A *C. elegans* worm tracking program is written that uses active contour model and adaptive thresholding to identify single worms from non-uniformly lit backgrounds and track their centroid as a function of time.

The human parasitic nematode, *Brugia malayi*, presents a far greater repertoire of behavioral patterns than those seen in the model nematode, *C. elegans*. Because of this reason, almost all *C. elegans* worm tracking software do not work effectively on *brugia malayi*. We built a tracking software specifically to identify movement features of *brugia malayi* while the nematode undergoes unconventional twists, coils, and occlusions. A number of parameters can be extracted from the body positions of the nematode, such as curvature, number of bends, forward/backward movement, and probing/cruising motion. We believe this tracking software can help differentiate movement patterns of untreated versus treated nematodes with minimal human intervention.

In summary, the thesis aimed to extend the technological developments in *C. elegans* microfluidics towards both plant-parasitic and human-parasitic nematodes. Through the chapters,

we discussed the challenges in studying non-model organisms especially with limited information. But because of the importance of these parasitic nematodes in agriculture and human welfare, we hope the work presented here will inspire new detection and control strategies for nematodes.

CHAPTER I

INTRODUCTION

Within the realm of bioengineering, microfluidic technology refers to the design, fabrication, and testing of microscale devices and chips for the understanding of biological processes. As is obvious, the myriad of biological processes occurring in even the simplest organism is overwhelming and mystical. The challenges in technology development for bioengineering lies in multiple domains: ability to observe the minutest processes with near real-time resolution, mastery of all known processes to adequately characterize system outputs for given inputs, and the dexterity to modify and control natural process with defined results. Some of these challenges have often resounded in the world of synthetic biology where gene sequencing, mapping, and editing are now considered very plausible goals in organismal biology. Beyond microbiology, however, these challenges are not delineated clearly and much more research efforts are needed to fully understand the working of a simple organism.

An example of a simple, multicellular organism that occurs ubiquitously in nature is the nematode or roundworm. Nematodes come in all sizes, exhibit a wide range of behavioral

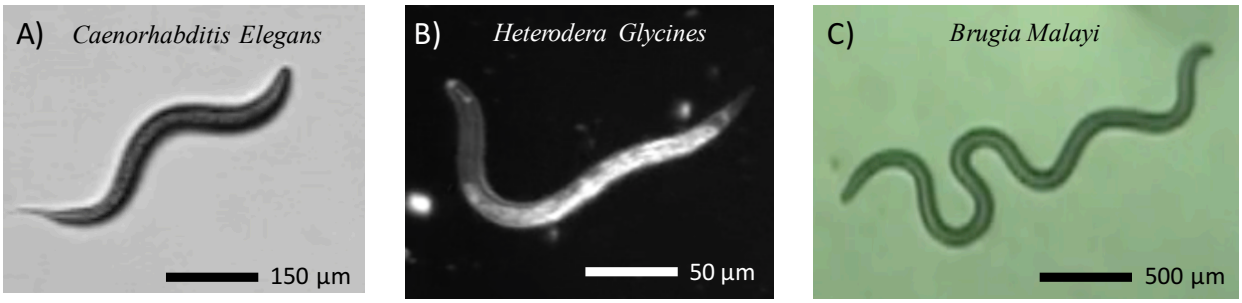

Fig. 1.1. Images of various microscopic nematode species. An image of the model organism *Caenorhabditis elegans* (A). An image of the plant-parasitic nematode *Heterodera glycines* (B). An image of the human-parasitic nematode *Brugia malayi* (C). Scale bars are indicated.

traits, and can be free living or parasitic. *Caenorhabditis elegans* is a classic example of a free living, model organism that is widely popular for its ease of culture, short lifespan, and genetic tractability. The use of *C. elegans* for clinical research was initially propelled by the fact that 40% genes of this roundworm have human homologues. Thus, as an alternative to human testing especially during preclinical studies, it would be easier to create *C. elegans* mutants with desired disease markers and use them for the screening/discovery of new drug compounds. There are a large number of nematodes that infect host plants, including soybean, corn, potatoes, rice, and wheat. Plant-parasitic nematodes are often specific to their respective host; in other words, a soybean cyst nematode usually only infects soybean crops. Strategies for the management of the plant-parasitic nematodes are often evolving as nematodes are often developing resistance to available pesticides. There are also nematodes that infect humans and animal hosts, including sheep, horses, and pigs. The level of nematode infection in an animal or human host is often assessed by the egg count of the nematode present in the faeces. *Brugia malayi* is a notoriously popular nematode that can cause filaria or elephantiasis in human populations. This nematode uses the mosquito as the intermediate host and eventually enters the human body when the mosquito bites the human subject. While the free-living *C. elegans* has been extensively studied, there is far less information available on plant- and animal-parasitic nematodes —their life cycle stages, attractive or repulsive factors, and control strategies.

Research Motivation

The work in this thesis is aimed at developing hardware and software platforms for characterizing specific behavioral traits of nematodes. There are several devices and chip-based technologies stemming from microfluidics that have been applied for nematode studies,

primarily for *C. elegans*. While the commitment and ingenuity in the published literature within the *C. elegans* microfluidic community is indeed significant, there has been far less research on technology development for plant-parasitic or human-parasitic nematodes. One of the main reasons for the dearth of literature on technology platforms for nematodes beyond *C. elegans* is the inaccessibility of these nematodes, difficulty to culture and maintain them in laboratories, and non-trivial experimental and imaging protocols while handling these nematodes. However, in our opinion, here lies the overarching motivation for my work: addressing the critical need of new technology platforms for studying the behavior of nematodes, beyond the model *C. elegans* organism.

In order to assess the need for a new technology within a certain community, it is important to understand the methodologies used in present-day nematology laboratories and come up with rational solutions for the end users. In the past years, we developed active collaborations with the laboratory of Prof. Greg Tylka in ISU Plant Pathology, the laboratory of Prof. Lyric Bartholomay in ISU Entomology and the laboratory of Prof. Michael Kimber in ISU Biomedical Sciences. These collaborations have helped us design hardware and software platforms that cater to the specific needs of their current experiments, in addition to unlimited access to their laboratories to test an existing prototype, redesign with new modifications, and retest the newer prototype.

Literature Review

There are a number of behavioral assays to study the behavior of the model organisms, *C. elegans* [1-4]. These nematodes can be cultured on multiple platforms, including agarose plates [2], well plates, and microfluidic devices [3]. For behavioral analysis of these nematodes, a

standard microscope stage is used to record the worm movement at real-time along with tracking software to identify patterns of behavior when subjected to various stimuli [4]. While the development of devices and software is more in the engineering realm, the actual data analysis linking the role of specific genes to observed behavior lies primarily within the domain of worm biologists.

A challenge in such interdisciplinary research (i.e. linking genetic makeup to behavioral traits) inherently lies in the gap between engineering and biological sciences. Generally speaking, engineers and biologists seem to perceive a problem with markedly different perspectives and present quite disparate solutions with different approaches. One way to handle these differences is through establishing and sustaining communication channels between engineers, data scientists, and biologists to identify new problems and use the worm model to speed up discoveries related to human health.

While *C. elegans* research has considerably evolved in the past decade, there is increasing interest in applying similar technologies towards the study of parasitic nematodes. For instance, laboratory platforms to study plant-parasitic nematodes are considerably outdated and there is ample scope for high-throughput benchtop assays that can quickly screen for known and unknown effectors for plant parasitism. The theme for experiments concerning plant parasitic nematodes have generally revolved around in-field test plots, greenhouse trials, agar plate and well-plate experiments [5-9]. These experiments can be considered low throughput since a field test or greenhouse experiment can last multiple weeks [7][8] or low resolution, as the worms are often scored as simply “inactive” or “active” during agar plate and well-plate experiments which is subject to experimental bias [9]. Similarly, studies on other parasitic worms have often relied on low throughput screening or imaging platforms. The measure of worm viability has often

been left to researcher expertise with similar scoring metrics [10][13] or is measured as a colorimetric signal [12-14] which cannot indicate any phenotypic changes in the worm's behavior.

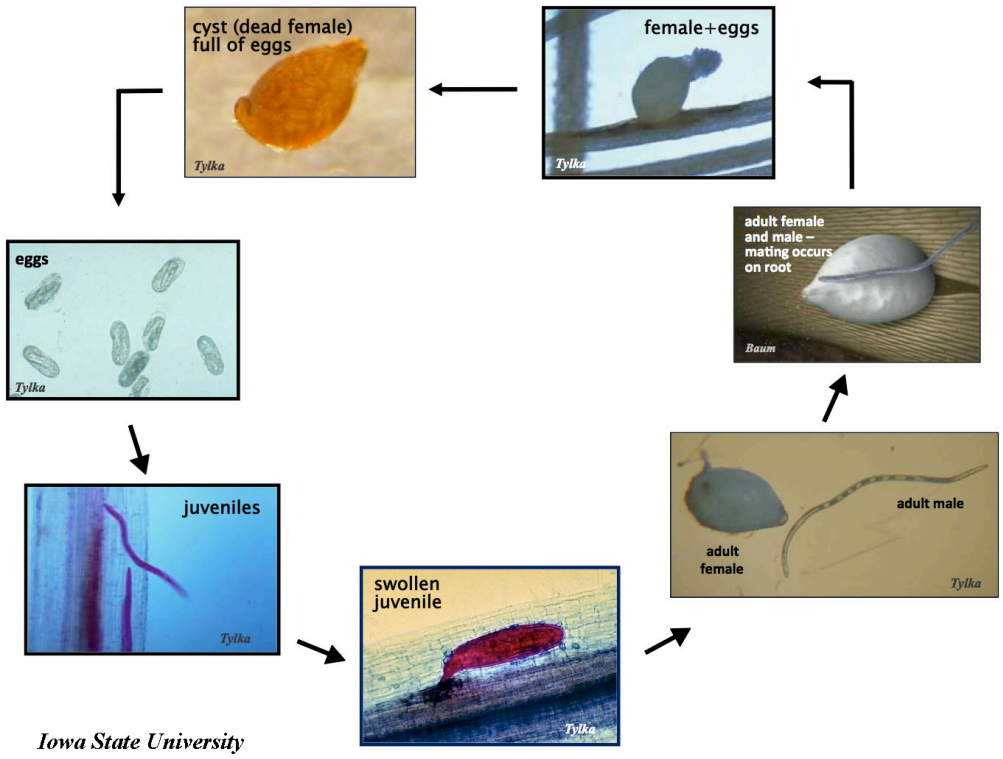

Fig 1.2. Lifecycle stages of *Heterodera glycines*.[15]

While the field of *C. elegan* research provides clues to handling many of these shortcomings, there are more challenges involved in studies of parasitic nematodes. For example, the free-living *C. elegans* are easily cultured on a bed of OP50 bacteria and maintained in a lab, whereas there is limited availability of parasitic nematodes. Parasitic nematodes are viable only within their host system, and survive for a short span outside their host. For instance, soybean cyst nematodes (SCNs) are obtained from the hatching of eggs collected from female cysts on infected roots (Fig. 1.2) [16]. Culturing the SCNs requires a greenhouse, ample space for

soybean plants, a system to separate the SCN females from the soil and a system to collect freshly hatched worms [17], which is far more complicated and difficult than the culturing procedure for *C. elegans* that simply requires agar plates and cultures of bacteria [18].

Since *Brugia malayi* is a human parasitic nematode, and is also more difficult to survive outside their intermediate host, unlike the free-living *C. elegan*. Single *brugia malayi* are obtained after excising the head of an anaesthetized mosquito, its intermediate host [19]. Culturing and handling this human parasite requires a BSL-3 facility to breed the infected mosquitoes and the food source of the mosquitos (rabbits) [20]. These nematodes usually have limited viability outside the human host and seem to succumb within a few hours outside their intermediate host [20]. The lifecycle stages of *brugia malayi* are illustrated in Figure 1.3.

Besides issues in culturing parasitic nematodes, these worms pose challenges in the design of assays to track their behavior. Specifically, the response of different nematodes vary greatly and thus the parameters being tested in the assays also differ significantly. The SCNs are much more lethargic than their *C. elegan* counterparts; thus, making it very difficult for a user to differentiate between a sedentary versus a dead worm [22]. The SCNs are also much smaller in size, ~300 μm in length, compared to *C. elegans*, ~600 μm in length [23]. Thus, any device and experiment designed for *C. elegans* cannot easily be translated to those for parasitic nematodes; we would need to modify and scale the assay to accommodate the difference in size, motility and the length of experiments (24 hours) with the SCN nematode.

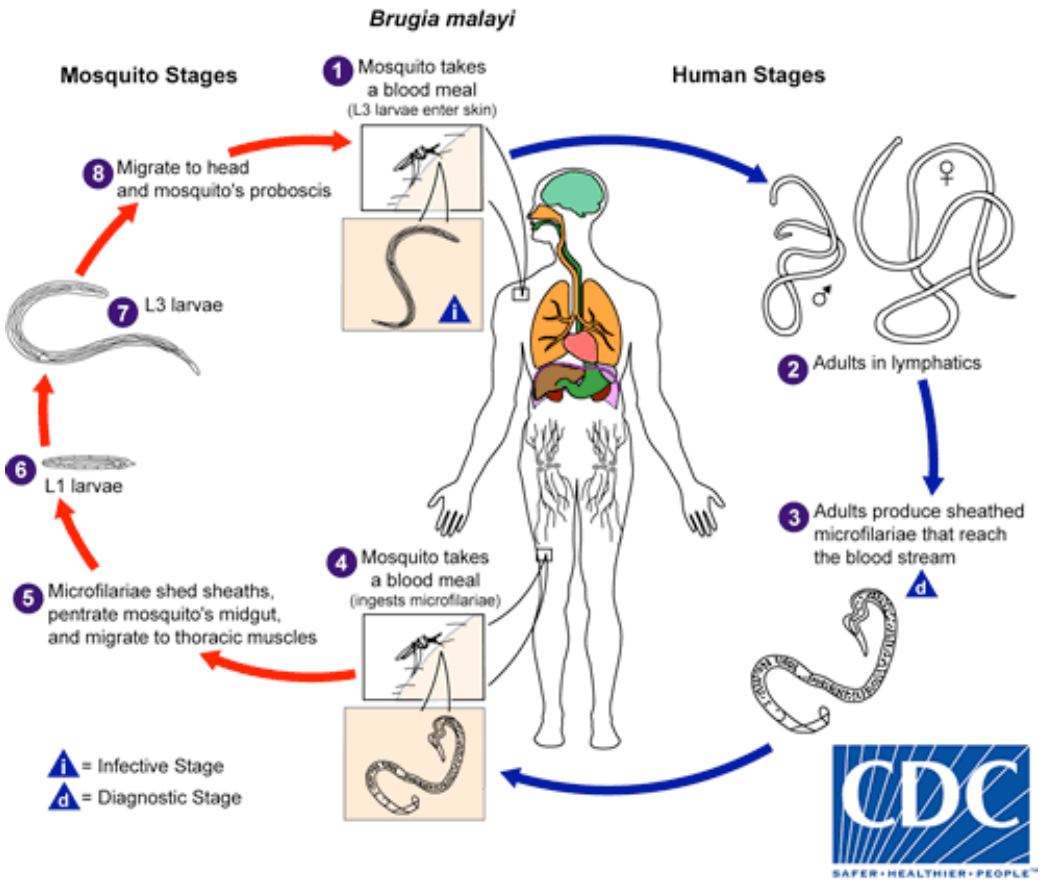

Fig. 1.3. Life cycle stages of *Brugia malayi.*[21]

Regardless of the nematode species, it is important that the measure of change in the behavior of the worm be unbiased. This leads to the need for a software-based solution to quantify the changes in the nematode's behavior which has been done for the *C. elegan* community in the form of worm-tracking programs [24-28]. The programs developed to work with *C. elegans* have been shown to be highly accurate and able to differentiate between multiple mutant species [24] as well as quantifying the effect of different chemicals on the nematodes [28]. There are a number of assumptions made in the programs with regards to the nematode of interest. Often, the visual appearance of the nematode is assumed to match specific criteria [27] or the movement characteristics of the worm are assumed to follow a derived motion model [25].

Some software tracking programs are designed to work with plant- and human-parasitic nematodes. However, these programs have not focused on high resolution data and often ignore subtle phenotypic changes while monitoring the average "motion" of multiple nematodes [29] or counting nematodes in a single location at one point in time [6]. Thus, while the background information used in the development of *C. elegan* tracking programs can be useful to a certain degree, more sophisticated programs are needed for experiments with plant- and human-parasitic nematodes that can track subtle behavioral traits not often seen in *C. elegan* videos.

The above review indicates that there has been substantial progress in *C. elegan* research in three distinguishable fronts: device development, video tracking, and phenotype-genotype relationships. However, there are significant challenges in the studies of parasitic nematodes: culturing worms outside hosts, variations in shapes and postures, and understudied biology of the animals. Every nematode species has a set of behavioral traits that can be observed within an identifiable time and space resolution. Thus, it is challenging to formulate a general device assay or a software tracking that could be applicable to studies of different parasitic nematodes. The following chapters will demonstrate how our chip designs and software modules evolved as we started working with three species of nematodes (free-living *C. elegans*, plant-parasitic SCN, and human-parasitic *Brugia malayi*), thereby providing insights to future experimental designs for parasitic nematodes.

Dissertation Organization

This thesis is divided into chapters that discuss my work on different nematode species, namely the free-living *C. elegans*, plant-parasitic soybean cyst nematode, and human-parasitic *Brugia Malayi*. For each nematode, microscale devices have been realized to handle and image nematode populations over short or long time periods using microscopy or scanner imaging approaches. An automated scheme was developed to analyze the large number of video files and extract comprehensible information from the large data set. In other words, the thesis laid emphasis on both the hardware and software aspects of technology development for nematology.

Chapter 2 explores whether magnetoreception exists in *C. elegans*. By putting worms in straight channel microfluidic device and exposing them to a permanent magnet, we attempted to characterize the effect of static magnetic fields on the movement of single worms. The average velocities and percentage of turning or curling occurrences were captured from recorded videos of the *C. elegans* exposed to magnetic field strengths of 5 – 120 milli Tesla using our custom software program. These parameters were used to determine if exposure to these magnetic fields altered the direction and velocity of *C. elegans* movement. This chapter is modified from my first-authored journal paper "Characterizing the effect of static magnetic fields on *C. elegans* using microfluidics," published in Advances in Bioscience and Biotechnology, 6, 583-591, 2015.

Chapter 3 examines the chemotactic tendencies of two plant-parasitic nematodes, *Meloidogyne incognita* and *Heterodera glycines*, using microfluidic chips. Plant-parasitic nematodes often employ a myriad of chemical and biological cues below the soil to guide them towards the plant's root system. Because it is nearly impossible to image the chemoattraction of plant-parasitic nematodes to host roots in (natural or greenhouse) soil environments, microfluidic chemotactic screening assays have been proposed here to test a range of chemicals and live roots

against nematode populations. One chip design was used to facilitate the testing of ionic solutions while the other accommodated young plant roots. The attraction and repulsion of the two nematode species to the ionic solutions and plate roots was monitored over a 24-hour period. The work was jointly performed by Augustine Beeman in the laboratory of Prof. Greg Tylka. This chapter is modified from my jointly first co-authored journal paper "Chip technologies for screening chemical and biological agents against plat-parasitic nematodes," published in Phytopathology, 106, 12, 2016.

Chapter 4 presents a non-polymeric microfluidic device for culturing and imaging the model nematode, *C. elegans*. This family of microfluidic paper-based analytical devices (μPADs) have been popular in the area of point-of-care diagnostics where tests are conducted to detect antigens, proteins or chemical byproducts of interest. However, such flexible devices have not been applied for testing whole organisms. In our case, the structure of a μPAD simply consists of a paper or plastic substrate with a suspended membrane made of agarose or Pluronic gel. We demonstrate the experimental procedures of loading, visualization and transfer of *C. elegans* to and from these membrane devices, which are more user-friendly and less complicated than in polymeric microfluidic devices. To show the ease of device operation in this open microfluidic device, levamisole drug screening of *C. elegans* is conducted and the dose response is plotted.

Chapter 5 discusses my work on the development of a fast, objective and user-friendly program to screen for potential vaccines against the filarial parasite *Brugia malayi*. The screening for effectiveness of potential vaccines is essentially done by observing the movement patterns of the nematode suspended in a liquid buffer droplet. Currently, such observations are done manually by a trained expert who is well-versed in distinguishing any defects or alterations

in movement patterns of *brugia malayi* on a glass slide. However, with such dependency on the human eye, there is scope for error and bias that can be readily eliminated by a software tracking program. In developing the program, a set of behavioral parameters is defined and calculated by tracking the worm's body posture throughout the video sequences. This process itself is challenging and no existing *C. elegans* tracking programs could effectively track the movement of these more-convoluted *brugia malayi*. The extracted behavioral parameters were analyzed and used as metrics to quantify the level of fitness or activity associated with the parasite.

References

[1] Yanik, M.F., Rohde, C.B., Pardo-Martin, C. (2011) Annual Review of Biomedical Engineering, 13, 185-217

[2] Gray, J.M., Karow, D.S., Lu, H., Chang, A.J., Chang, J.S. (2004) Oxygen sensation and social feeding mediated by a *C. elegans* guanylate cyclase homologue. Nature 430(6997) 317–322

[3] Lockery, S.R., Lawton, K.J., Doll, J.C., Faumont, S., Coulthard, S.M. (2008) Artificial dirt: microfluidic substrates for nematode neurobiology and behavior. Journal of Neurophysiology, 99(6) 3136–3143

[4] Saldanha, J.N., Parashar, A., Pandey, S., Powell-Coffman J.A. (2013) Multiparameter Behavioral Analyses Provide Insights to Mechanisms of Cyanide Resistance in *Caenorhabditis elegans*. Toxicological Sciences, 135(1), 156-168

[5] Papademetriou, M.K., Bone, L.W. (1982) Chemotaxis of Larval Soybean Cyst Nematode, *Heterodera glycines* Race 3, to Root Leachates and Ions. Journal of Chemical ecology, 9(3), 387-396

[6] Wang, C., Lower, S., Williamson, V.M. (2009) Application of Pluronic gel to the study of root-knot nematode behaviour. Nematology, 11(3), 453-464

[7] Meyer, S.L.F., Johnson, G., Dimock, M., Fahey, J.W., Huettel, R.N. (1997) Field Efficacy of Verticillium lecanii, Sex Pheromone, and Pheromone Analogs as Potential Management Agents for Soybean Cyst Nematode. Journal of Nematology, 29(3), 282–288

[8] Chang, S.J.C., Doubler, T.W., Kilo, V.Y., Abu-Thredeih, J., Prabhu, R., Freire, V., Suttner, R., Klein, J., Schmidt, M.E., Gibson, P.T., Lightfoot, D.A. (1996) Association of Loci Underlying Field Resistance to Soybean Sudden Death Syndrome (SDS) and Cyst Nematode (SCN) Race 3. Crop Science, 37(3), 965-971

[9] Wuyts, N., Swennen, R., Waele, D. (2006) Effects of plant phenylpropanoid pathway products and selected terpenoids and alkaloids on the behaviour of the plant- parasitic nematodes *Radopholus similis*, *Pratylenchus penetras*, and *Meloidogyne incognita*. Nematology, 8, 89-101

[10] Smith, H.L., Paciorkowski, N., Babu, S., Rajan, T.V. (2000) Development of a Serum-Free System for the *in Vitro* Cultivation of *Brugia malayi* Infective-Stage Larvae. Experimental Parasitology 95**,** 253–264

[11] Taylor, M.J., Cross, H.F., Mohammed, A.A., Trees, A.J. (1996) Susceptibility of *Brugia malayi* and *Onchocerca lienalis* microfilariae to nitric oxide and hydrogen peroxide in cell-free culture and from IFNγ-activated macrophages. Parasitology, 112(3), 315-322

[12] Lakshmi, V., Joseph, S.K., Srivastava, S., Verma, S.K., Sahoo, M.K., Dube, V., Mishra, S.K., Murthy, P.K. (2010) Antifilarial activity in vitro and in vivo of some flavonoids tested against *Brugia malayi.* Acta Tropica, 116(2) 127-133

[13] Rao R.U., Moussa H., Weil G., (2002) *Brugia malayi* effects of antibacterial agents on larval viability and development in vitro. Experimental Parasitology, 101, 77–81

[14] Rao R.U., Huang Y., Fischer K., Fischer P.U., Weil G., (2008) *Brugia malayi*: Effects of nitazoxanide and tizoxanide on adult worms and microfilariae of filarial nematodes. Experimental Parasitology 121 38–45

[15] Tylka, G., (2014) Lifecycle stages of SCN, Iowa State University: Plantpathology, www.plantpath.iastate.edu, 10 August 2014.

[16] Cho, H.J., Farrand, S., Noel, G. (2000) High-efficiency induction of soybean hairy roots and propagation of the soybean cyst nematode. Planta, 210(2), 195-204

[17] Faghihi, J., Ferris, J.M. (2000) An efficient new device to release eggs from *Heterodera glycines*. Journal of Nematology, 32 411-413

[18] Serafini, T., Kennedy, T.E., Gaiko, M.J., Mirzayan, C., Jessell, T.M., Tessier-Lavigne, M. (1994) The netrins define a family of axon outgrowth-promoting proteins homologous to *C. elegans* UNC-6. Cell, *78*(3), 409-424

[19] Smillie, C., Vickery, A., Kwa, B., Nayar, J., Rao, U. (1994) Evaluation of Different Medium Supplements for In vitro Cultivation of Brugia malayi Third-Stage Larvae. The Journal of Parasitology, 80(3), 380-383

[20] Ash, L., Riley, J., (1970) Development of subperiodic *Brugia malayi* in the jird *Meriones unguiculatus*. The Journal of Parasitology 56(5), 962–968

[21] Silva, A. J., Moser, M., Life cycle stages of *Brugia malayi.* (2002) Centers for Disease Control and Prevention. www.cdc.gov. 05 November 2016

[22] Faske, T.R., Starr, J.L. (2006) Sensitivity of *Meloidogyne incognita* and *Rotylenchulus reniformis* to Abamectin. Journal of Nematology, 38(2), 240–244

[23] Tylka, G. (1994, January). Soybean Cyst Nematode. Retrieved September, 2015, from http://nematode.unl.edu/scn/scnisu.htm

[24] Geng W. (2004) Automatic tracking, feature extraction and classification of *C elegans* phenotypes. IEEE Transactions on Biomedical Engineering, 51(10), 1811–1820

[25] Fontaine E., Burdick J., Barr A. (2006) Automated tracking of multiple *C. Elegans*. Conference Proceedings Engineering in Medicine and Biology Society.1:3716-9

[26] Wang S.J., Wang Z.W. (2013) Track-A-Worm, An Open-Source System for Quantitative Assessment of *C. elegans* Locomotory and Bending Behavior. PLoS ONE 8(7), e69653

[27] Nagy S, Goessling M, Amit Y, Biron D (2015) A Generative Statistical Algorithm for Automatic Detection of Complex Postures. PLoS Computational Biology 11(10), e1004517

[28] Ramot, D., Johnson, B.E., Berry, T.L. Jr, Carnell, L., Goodman, M.B. (2008) The Parallel Worm Tracker: A Platform for Measuring Average Speed and Drug-Induced Paralysis in Nematodes. PLoS ONE, 3(5), e2208

[29] Storeya B., Marcellinoc C., Millera M., Macleana M., Mostafaa E., Howella S., Sakanaric J., Wolstenholmea A., Kaplana R. (2014) Utilization of computer processed high definition video imaging for measuring motility of microscopic nematode stages on a quantitative scale: "The Worminator." International Journal for Parasitology: Drugs and Drug Resistance, 4(3), 233–243

CHAPTER 2

CHARACTERIZING THE EFFECT OF STATIC MAGNETIC FIELDS ON *C. ELEGENS* USING MICROFLUIDICS

Modified from a paper published in Advances in Bioscience and Biotechnology

Zach Njus, Douglas Feldmann, Riley Brien, Taejoon Kong, Upender Kalwa, Santosh Pandey*

Abstract

In nature, several organisms possess a magnetic compass to navigate or migrate them to desired locations. It is thought that these organisms may use biogenic magnetic matter or light-sensitive photoreceptors to sense and orient themselves in magnetic fields. To unravel the underlying principles of magnetosensitivity and magnetoreception, previous experiments have been conducted on bacteria, vertebrates, crustaceans, and insects. In this study, the model organism, *C. elegans*, is used to test their response and sensitivity to static magnetic fields in the range of 5 milli Tesla to 120 milli Tesla. Single wild-type *C. elegans* are put in microfluidic channels and exposed to permanent magnets for five cycles of thirty-second time intervals. The worm movement is recorded and analyzed with custom software to calculate the average velocity and the percentage of turning and curling. Contrary to some published studies, our results did not show a significant difference compared to control experiments. This suggests that *C. elegans* may not sense static magnetic fields in the range of field strengths that we tested.

Introduction

Over a century ago, it was first postulated that animals possess some sort of a "magnetic compass" to explain the navigation behavior of migratory birds [1-3]. Early experiments showed that the navigation of carrier pigeons (*Columbidae livia*) could be disrupted by attaching magnets to their body [4]. Experiments with magnetic coils demonstrated that European robins (*Erithacus rubecula*) orient themselves to artificially generated magnetic fields [5] [6]. The evidence in early studies indicated that some birds may possess a magnetic sense, but the underlying mechanisms behind this sense remain a fascinating and bewildering mystery of nature.

Even though very few organisms have been identified as being responsive to external magnetic fields, the phenomenon of magnetosensitivity is thought to be much more pervasive in nature. Some examples of magnetosensitivity have been observed in bacteria, vertebrates, crustaceans, insects, and a mollusk species [7]. In one study, migratory lobsters (*Panulirus argus*) were disoriented by an artificially generated magnetic field, which prompted the lobsters to migrate in the opposite direction of their intended destination [8]. In another study, the mole-rat (*Fukomys anselli*) was shown to use magnetic fields to orient their nest construction in a specific direction of a circular arena [9]. When magnetic coils were employed to alter the ambient magnetic field, the mole-rats were found to re-orient the construction of their nests in the direction of the new magnetic field.

To explain the underlying principles of magnetosensitivity, two broad mechanisms of magnetoreception have been proposed. The first proposed mechanism suggests that magnetite (Fe3O4) particles, which are naturally found in many organisms, could be integrated into the nervous system of the organism. As supporting evidence, magnetite has been found in the heads of homing pigeons, and the amount of magnetite present could theoretically enable detection of

small changes in the magnetic field strength [10]. Brain studies found that the trigeminal brainstem complex in European robins is stimulated by magnetic fields, and an increased neural activity is measured when the birds are exposed to non-uniform magnetic fields [11]. The exact site and distribution of magnetite within the bird's head are less understood, but are hypothesized to be stored in macrophages or in magnetosensitive neurons [12]. In simpler organisms, such as magnetotactic bacteria, the role of magnetite is clearer. Magnetotactic bacteria rely on magnetite-containing organelles to migrate to anaerobic environments that are more favorable for growth [13]. These bacteria interact with and move into alignment each other using magnetic forces produced by the magnetite particles.

The second proposed magnetoreception mechanism suggests that magnetic sensitivity is mediated by the photoreceptor cryptochrome. Studies have shown that the magnetic sense is light-dependent and has been investigated on monarch butterflies (*Danaus plexippus*), fruit flies (*Drosophila melanogaster*), and migrating birds [14]. As an example, it was shown that by filtering light in the ultraviolet-A/blue wavelengths, monarch butterflies did not exhibit the same directional flight compared to in white light [15]. It was hypothesized that the photoreceptor cryptochrome molecules were sensitive to these wavelengths of light, and generated magnetically sensitive radical pair products that eventually enabled magnetosensistivity in the butterflies. In another example, Drosophila mutants with cryptochrome deficiency were shown not to display the magnetosensitive response found in wild-type flies, indicating that the photoreceptor cryptochrome was required to produce the magneto-sensitive behavior in the flies [16]. A combination of both magnetite-based and photoreceptor-mediated mechanisms mediates and regulates the magnetic sensory system in migrating birds. [17].

Designing experiments to isolate the exact role of magnetic fields in the navigation or migration of organisms is challenging. This is because the response to magnetic fields is often influenced by several biological and environmental factors that work in unison to produce a behavioral trait. For instance, birds and insects can use other senses to navigate, making it difficult to isolate the response to magnetic fields. Pigeons, for example, use the position of the sun to navigate during migration periods [7]. Early magnetic experiments found that navigation of pigeons was only disrupted on overcast days when magnets were attached to the birds [4]. Birds and higher vertebrates have a large and complex nervous system that can be difficult to interrogate during experiments. As such, there is an increasing interest to study magnetoreception in model organisms, such as Drosophila and Caenorhabditis elegans, which have a simple nervous system and a well-established genetic model.

The *C. elegans* is a model nematode worm (around 1.3 mm in length at the adult stage) with a short lifespan of 21 days, tractable genome, a simple nervous system comprising 302 neurons, and the relative ease of culture on agarose plates. This worm has been a great candidate for studies on behavior, development, toxicity screening, and neuronal signaling [18]-[20]. In lines with the earlier discussion on the first mechanism of magnetoreception, traces of biogenic magnetite were found in adult *C. elegans* using a superconducting quantum interference device (SQUID) and transmission electron microscopy [21]. The thermal decay of remanence (TDR) measurements confirmed magnetite as the particle of interest near the edges of the nematode's body. Subsequently, several studies examined the (detrimental) effects of magnetic fields on nematodes. In one study, *C.elegans* were exposed to a 1.7 tesla magnetic field at 60 hertz for 84 hours to investigate biohazardous effects of magnetic fields over the lifespan of the worm. The high-power, alternating magnetic fields were shown to disrupt locomotion and reproduction in *C.*

elegans [22] [23]. Besides alternating magnetic fields, static magnetic fields also can affect the locomotion and lifespan in *C. elegans*. Hung et al. reported reduced crawling speeds when worms were exposed to static magnetic fields [24] [25]. Investigations regarding the directional ability of worms in magnetic fields have been less conclusive. Using a 3-axis coil system, Pichler studied the response of different species of worms to static magnetic fields of varying intensity and direction. No significant effect was found in turning frequency, velocity, or average direction upon exposing the worms to magnetic fields of up to 3.4 Gauss [26]. In a similar experiment using magnetic coils, Garcia et al. tested if the average direction of worm movement was affected by magnetic field strength and direction. At field strengths up to a 10 Gauss, no significant effect was found in average direction of movement [27].

In this paper, we attempt to verify whether static magnetic fields affect the crawling speed or any other movement traits in the wild-type *C. elegans*. A microfluidic chip is designed and a stage is built to apply static magnetic fields using permanent magnets. Here worms are confined to a channel to restrict their movement to two directions, in contrast to being unconstrained on an open agar plate. This eliminates interaction among multiple worms and reduces the field of view for imaging worm behavior. Measurements of worm position are recorded over time under different field strengths. Using custom software, two movement parameters, average velocity and percentage of turning and curling, are calculated. Both parameters did not show a significant change upon exposure to static magnetic fields of up to 120 milli Tesla (mT).

Materials and Methods

Fabrication of Microfluidic Chip

A microfluidic chip is designed to study the behavior of *C. elegans* upon exposure to static magnetic fields. (Figure 2.1(a)). Each microfluidic chip comprises eight straight channels (length: 1 cm, width: 250 μm, depth = 40 μm) (Figure 2.1(b)). The channel length is optimized to be within the field of view of a Leica MZ16TM transmission stereozoom microscope during the entire length of the experiment. The channel width and depth are chosen to permit unrestricted sinusoidal movement of individual worms (Figure 2.1(c)). To further avoid interaction between worms, only one worm is used in one channel. The physical layout of the microfluidic chip is drawn in AutoCAD and the mask is printed on a transparency sheet. Afterwards, SU-8 is spin-coated on a silicon wafer (diameter: 3 inches, thickness: 300 μm) and the patterns on the mask are transferred on the SU-8 polymer by exposure by ultraviolet light and subsequent developing in a SU-8 developer. A polydimethylsiloxane (PDMS) polymer is poured on the SU-8 mold and allowed to harden in a low-pressure chamber. The PDMS layer is peeled, punched with holes for inlet/outlet ports, exposed to air plasma, and irreversibly sealed onto a standard glass slide (Figure 2.1(b)).

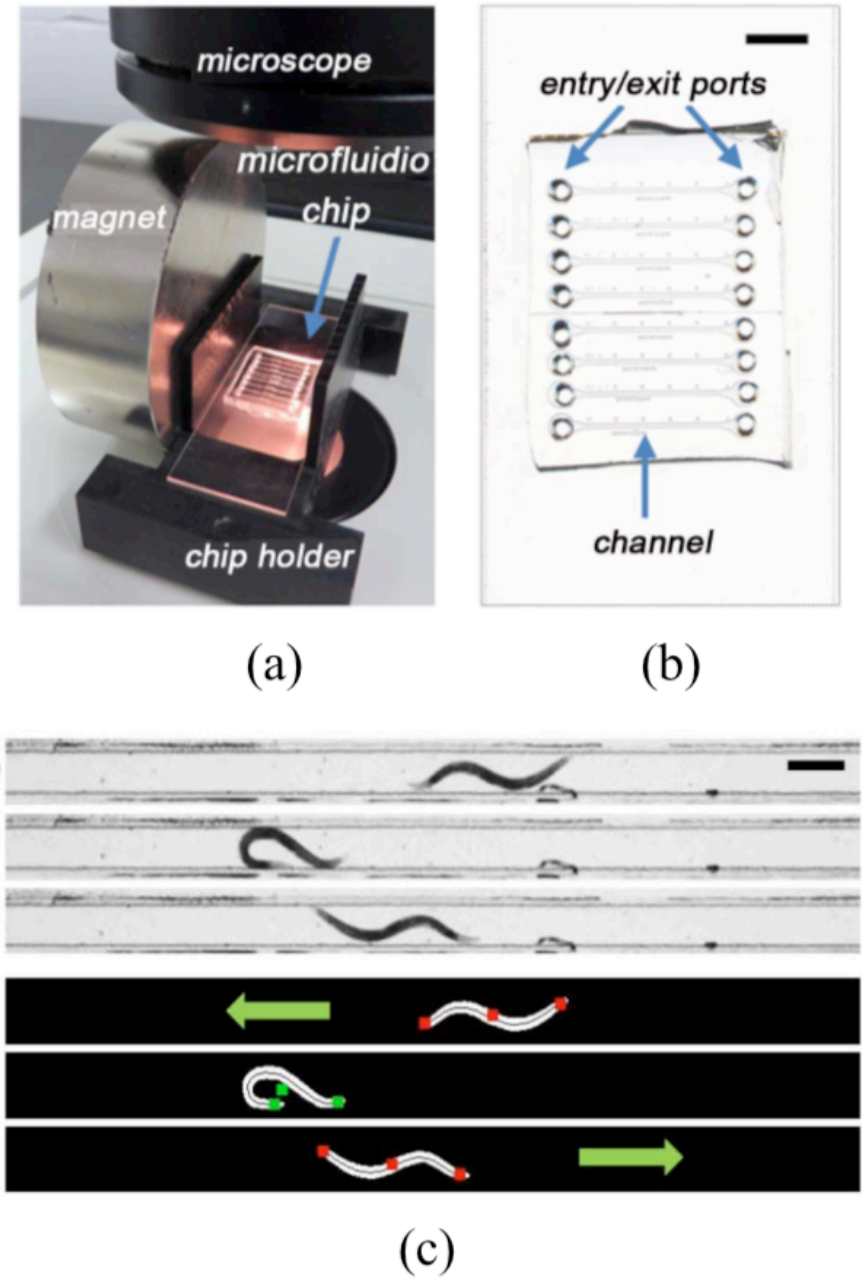

Figure 2.1. (a) Snapshot of the experimental setup showing the microfluidic chip, chip holder, and a permanent magnet; (b) Image of our fabricated microfluidic chip having eight parallel, straight channels; each with its port for worm entry and exit; (c) The top panel shows three lanes of channels as recorded by the camera. The bottom panel shows the processed images from the custom software that removes the background and identifies the centroid, head, and tail (indicated by dots). The green arrows indicate the direction of worm movement. As the worm reverses direction, the software detects that the spacing between the head and tail is decreased, and records a turning event (indicated by green dots on the worm).

Chip Filling with Agarose Gel

Agarose is a reliable medium for observing worm movement within microfluidic devices. With liquid media, there is an internal fluid pressure in the channels that can influence the worms' natural movement. The chip is filled with 0.7% agarose in M9 buffer. Previously, *C. elegans* were grown at 20˚C on standard Nutrient Growth Media (NGM) agarose plates with *Escherichia coli* OP50 food [28]. For the magnetotaxis experiments, single L4-stage and young adult worms are picked with a sterilized worm picker and dropped at the chosen entry ports of the microfluidic channels. A custom chip holder houses the microfluidic chip and holds the magnet at fixed distances from the entry ports. All experiments are performed at 22˚C. To nullify any effects of gravity, the chip holder is placed on the flat, horizontal stage of the microscope. For every experiment of a specific magnetic field, around 3 to 5 separate chips are tested with around 3 to 5 worms in every chip.

Steps for Exposure to Static Magnetic Fields

Figure 2.2 illustrates the procedure for performing the magnetotaxis experiment. After dropping in the entry port, the worms enter the channels within 5 minutes. The movement of all worms in the channels is recorded simultaneously by a QICamTM 24-bit Color digital camera interfaced with QCapture PROTM software. Once the worms appear in their respective channels, image frames are captured every one second for the pre-decided length of the experiment and stitched together to create a video file. The initial worm movement is recorded for over one minute to ensure that the worms are healthy. Unhealthy or inactive worms are ignored in the image recording step. Next, we wanted to test whether the natural worm movement is affected by the presence of static magnetic fields. To test this, the magnetic field is applied by placing the

magnet at a chosen distance from the microfluidic chip for definite time duration (i.e. 30 seconds). Conversely, the magnetic field is removed by moving the magnet at least 24 inches away from the microfluidic device for definite time duration (i.e. 30 seconds). We also tried applying and removing the magnetic field multiple times (i.e. 5 times) to test if the observed effect in worm behavior is repeatable and/or cumulative. After an experiment, the worms are visually inspected to see if they appear healthy and then the microfluidic chip is discarded.

Image Analysis to Compute Worm Movement

A custom object tracking software is developed to process the recorded videos of worm movement and to extract the x- and y-coordinates of the central skeleton of worm body (i.e. head, tail, and centroid) (Figure 2.1(c)). Briefly, the software converts the video frames into grayscale and identifies the background. The background image is calculated by averaging all the frames of the video together. The difference between the background image and a current frame gives a foreground image containing only the moving worm from that frame. Thereafter, the software performs segmentation and recognizes the boundaries of the worm body, which are used to calculate the coordinates of the central skeleton. Average velocity is estimated by computing the instantaneous velocities using the worm centroid locations in successive frames and then averaging these instantaneous velocities over the length of the video [28]. The information from the central skeleton's head and tail locations is used to identify the time instances when the body curls. Both the average velocity and curling/turning behavior are important parameters of worm movement, and the developed software alleviates the trouble of manual image analysis. Statistical analysis of the movement data is performed using GraphPad PrismTM software.

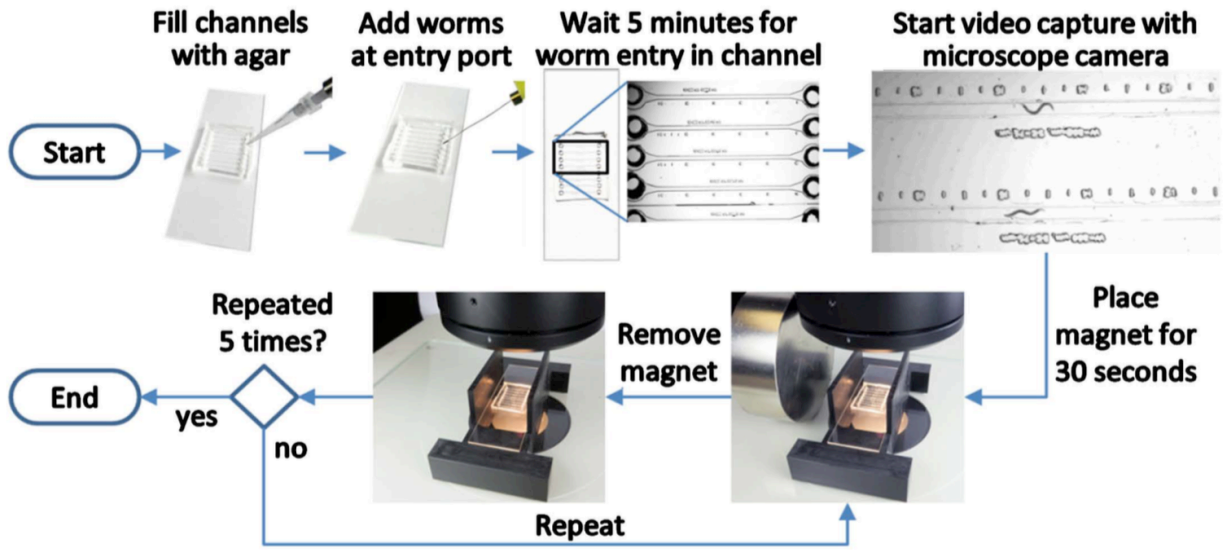

Figure 2.2. Steps involved in conducting the magnetic field experiment are depicted in the flow chart. The channels are filled with 0.7% agarose and worms are added to the entry port. After the worms enter the channels, the video recording is started. The permanent magnet is placed at a specified distance from the chip holder for 30 seconds and removed. The process is done once or repeated five times. Later the chip is discarded and the video is analyzed.

Results

Characterization of Magnetic Field Strengths

We designed a simple method to apply the static magnetic fields at fixed distances from the microfluidic chip using a permanent magnet. A plastic chip holder is built where the fabricated chip can be placed in. An adhesive tape is used to firmly hold the chip and chip holder on the microscope stage. Because the permanent magnet is heavy, extra caution is required to move the magnet and to ensure that the chip orientation is not changed during moving the magnet. Figure 2.3(a) shows the configuration of the magnet and chip holder. Using wooden blocks as spacers, the magnet is spaced between 0 and 4.5 inches from the chip holder housing the microfluidic chip. We use a cylindrical neodymium permanent magnet (diameter: 3 inches,

thickness: 1 inch). With the magnet placed at a specific distance, the field strength at the center of the chip holder is measured with a gaussmeter and a Hall probe (Model 410, Lake Shore CryotronicsTM). The measured field strengths at the six positions used in our experiments are shown in Figure 2.3(b). When the magnet is held closest to the chip holder, the field strength is around 120 milli Tesla (mT). When the magnet is 4.5 inches away from the chip holder, the field strength reduces to nearly zero.

Effect on the Average Velocity

After recording videos of each experiment, the movement of each worm is analyzed separately. The centroid coordinates and the body skeleton in each image frame (image capture speed: 1 frame per second) are extracted using our imaging software. This geometric information is used to identify changes from the worm's natural sinusoidal movement. In general, a worm may exhibit a relative increase or decrease in velocity when exposed to external stimuli. The worm body may turn away from a directional repellant or may curl up to avoid exposure to the repellant. Such curling and omega turns are often observed when worms are exposed to drug chemicals and toxins, such as potassium cyanide [28]. However, in the presence of physical stimuli without any chemicals, such as magnetic and electric fields, the behavioral response of these organisms may be subtle and difficult to quantify by direct observations. As such, we employed our imaging software to automatically extract the average velocities and the percentage of curling and turns.

The average velocity is calculated by taking the mean of all instantaneous velocities (i.e. ratio of net displacement to time interval) between successive image frames (Figure 2.4(a)). In Figure 2.4(b), we plot the average velocities from the different magnetic field experiments. We

conducted experiments on the effects of the following field strengths: 5 mT, 10 mT, 60 mT, 80 mT, 90 mT, and 130 mT. In a specific experiment, the average velocity of every worm is further averaged to obtain an overall average velocity. In the control experiment, worms are allowed to move in their respective channels in the absence of external magnetic field, and the average velocity is 97.38 ± 48.3 μm/second. For experiments with magnetic fields, worms are allowed to enter the channel and the permanent magnet is placed at a definite distance as shown by Figure 2.3. The magnet is placed for 30 seconds (i.e. field ON) and removed for 30 seconds (i.e. field OFF). The process is repeated for 5 cycles. The recorded videos are partitioned into two sections: image frames where the field is ON (blue bars, Figure 2.4(b)) and image frames where the field is OFF (red bars, Figure 2.4(b)). The average velocities of the two sections are calculated and shown in Figure 2.4(b). In all experiments with magnetic field exposure, the range of average velocities is between 84 μm/second to 128 μm/second. The average velocity at 60 mT (with field ON) is statistically significant ($p < 0.05$) compared to others in the group with magnetic field exposure. There is no significant difference amongst the other average velocities. Interestingly, in all experiments, the average velocities with field OFF (red bars, Figure 2.4(b)) are lower than the average velocities with field ON (blue bars, Figure 2.4(b)), even though the relative decrease in velocity (7 μm/second to 30 μm/second) is not significant.

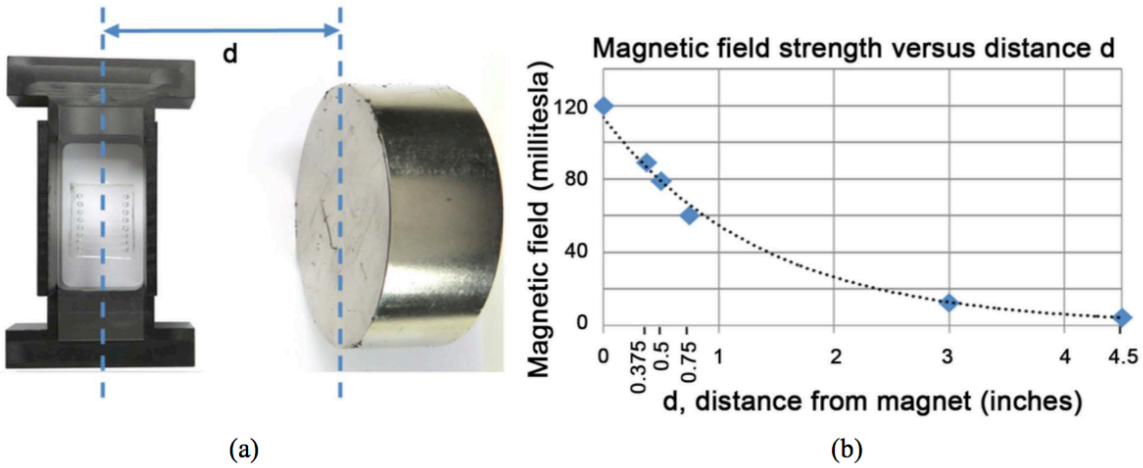

(a) (b)

Figure 2.3. (a) The permanent magnet is placed at a specific distance (labeled as "d") from the center of the chip holder; (b) The strength of the magnetic field is measured at the center of the chip holder and plotted in the graph.

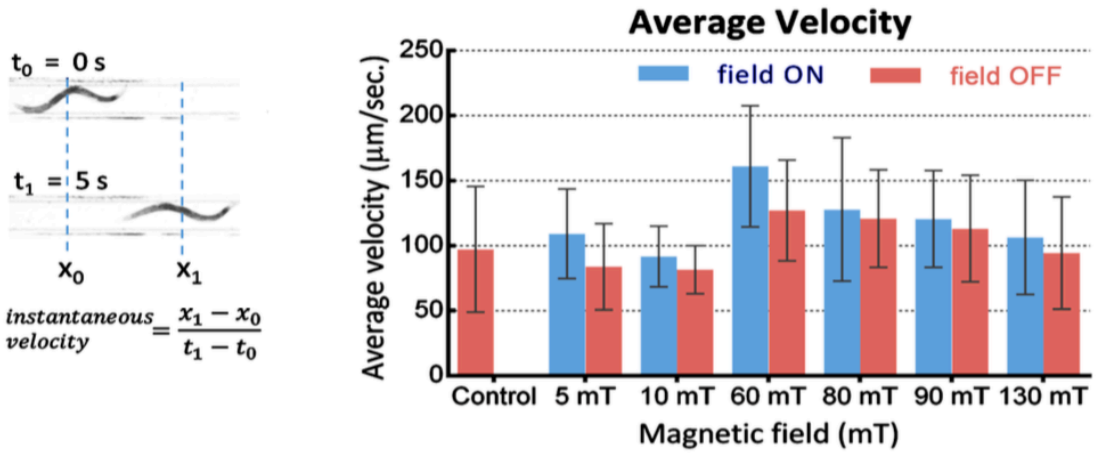

(a) (b)

Figure 2.4. (a) The instantaneous worm velocity is calculated as the ratio of net displacement to the time interval. All the instantaneous velocities are averaged to produce the average velocity of an individual worm; (b) The average velocities of all worms for the different magnetic field strengths are plotted; both during the periods of placing the magnet (i.e. field ON) and removing the magnet (i.e. field OFF).

Effects on the Turning and Curling Behavior

A worm tends to turns away from an aversive environment (e.g. drug chemicals or toxins) or can curl its body to avoid exposure to the environment [28]. However, such turning and curling actions are also a part of their repertoire of behavioral traits in the natural environment. Hence it is important to identify whether the frequency of turning and curling events are significantly different in experimental tests. Figure 2.5 shows representative images of the worm's body posture during turning and curling in different magnetic field strengths. Images are grouped in two categories: with field ON and field OFF. The time points of the images are labeled next to individual images and red arrows indicate the direction of worm movement. In all magnetic fields, the changes in body postures and the time taken to accomplish a turn appear similar with no noticeable differences. High magnetic field strengths (90 mT to 120 mT) do not appear to hinder the turning and curling of *C. elegans*.

Figure 2.6 shows the percentage of worms that turned and curled during the first 30 seconds of placing the magnet or removing it (i.e. field ON and field OFF periods, respectively). The imaging software identifies a turn or curl when the head and tail turn inwards such that the net distance between them is less than one half of the body length. The time instances when a turn or curl occurred is outputted by the software and random videos are manually verified for accuracy and consistency of this result. Typically, a worm takes around 7 to 12 seconds to complete a turn. If a worm decides to turn away from the magnet, it would possibly indicate that the worm does not prefer being in the magnetic field. In the control experiment where no magnetic field is applied throughput the video, the average percentage of turns and curls is around 71.5% ± 49%. There is no statistically significant difference between the percentage of

curls and turns in experimental and control groups. The result indicates that curling or turning is probably not a clear indication of sensitivity to magnetic fields.

In the earlier discussion, we counted the number of body turns or curls within the first 30 seconds of placing or removing the magnet, which is sufficient time for worms to complete a turn or curl. We wished to confirm whether the worm response was different if the steps of placing and removing the magnet were repeated over multiple cycles. Figure 2.7 shows the percentage of worms that turned or curled during the first 30 seconds of placing or removing the magnet through 5 consecutive cycles. Here the results from all magnetic field experiments are combined with field strengths between 5 mT to 120 mT (Figure 2.3). The plot indicates that percentage of turning or curling is consistently within a fixed range (30% to 70%) over the course of the experiment, and there is no statistically significant difference between the values.

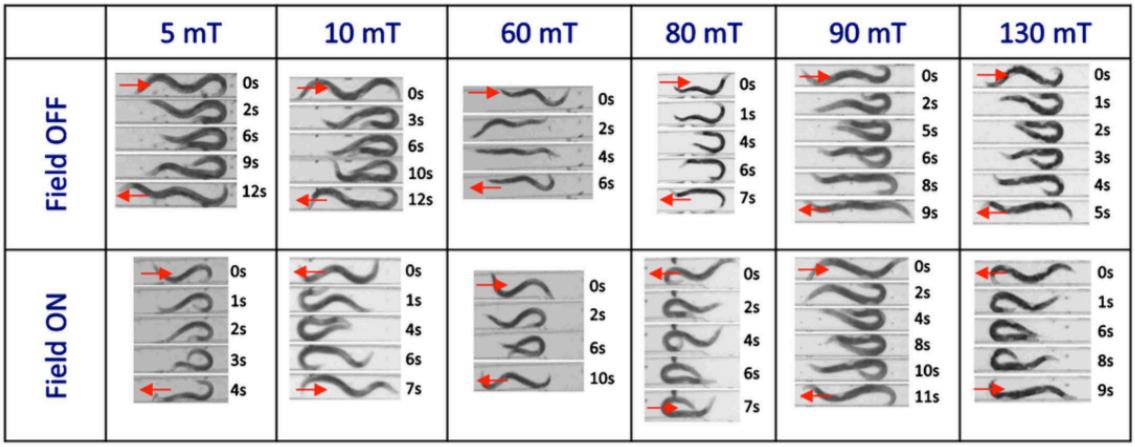

Figure 2.5. Shown are the time-lapsed images of the worm during the turning behavior and under different magnetic field. Images are grouped into time periods of placing the magnet (i.e. field ON) and removing the magnet (i.e. field OFF).

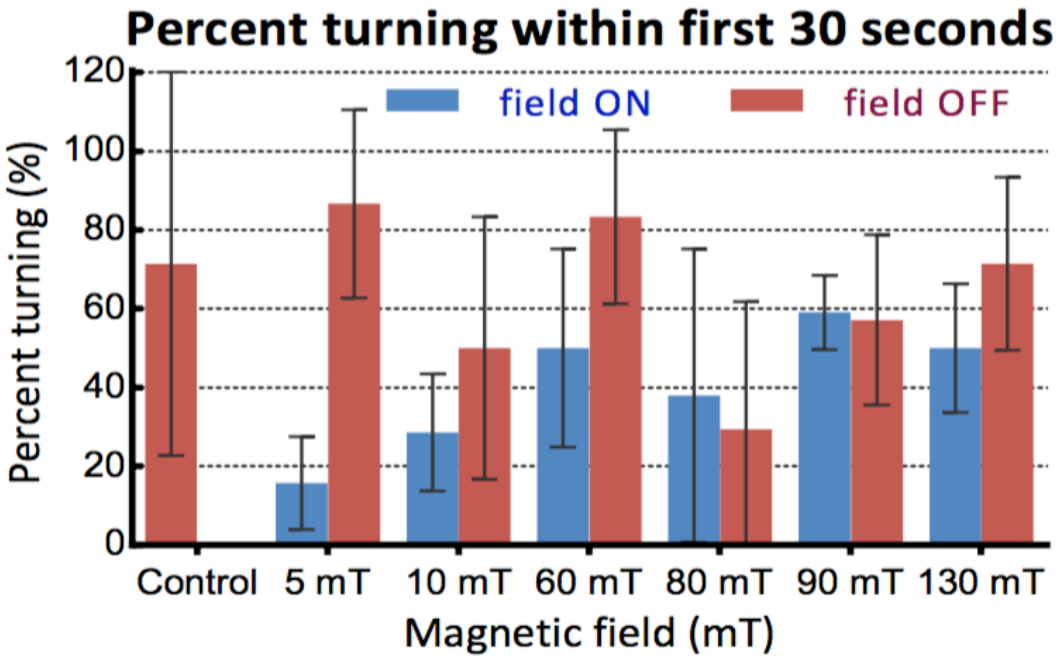

Figure 2.6. The plot shows the percentage of worms turning or curling within first 30 seconds of placing the magnet (i.e. field ON) or removing the magnet (i.e. field OFF).

Discussion

We reviewed the protocols used in our experimental procedure and tested a number of alternatives to see if the behavioral response of worms changed because of the alterations. A discussion of some alternatives to our previously discussed experimental protocols follows here.

The choice of media for filling the microfluidic channels was 0.7% agarose in M9 buffer. The standard aqueous M9 buffer solution also could be used as the migration media. But we observed significant drifts in the worm movement when an aqueous media was used. In addition, because the liquid is exposed to the outside air through the entry and exit ports, even a small change in liquid pressure is noticeable under the microscope. The liquid pressure also can alter the worm movement and influence the derived results. On the other hand, agarose gel provides a good resistance for worms to push against and attempts to mimic the natural soil environment.

The choice of the permanent magnet was selected based on the available physical sizes and strengths of the magnets. The chosen permanent magnet has a wide diameter to produce a uniform field near and around the chip holder. A gaussmeter was used to check the uniformity of the magnetic field. Magnets with smaller diameter (<2 inches) were seen to produce non-uniform magnetic fields around the chip holder. Permanent magnets with field strengths greater than 120 mT were not readily available. Alternating magnetic fields can be tested with duty cycles around 60 Hz and considerably high power than permanent magnets [22] [23].

Our tests were performed on L4-stage and young adult *C. elegans*. We chose not to use adult worms as they may have eggs within them that could influence their natural movement. Since the literature suggested that adult worms have some levels of magnetite particles within their bodies [21], we also tested adult worms in the experimental setup. However, with adult worms, we did not see any noticeable difference in behavior upon exposure to static magnetic fields. Rather, the adult worms appeared more sluggish than young adults and more hesitant to enter the channels, even in control experiments.

To test the effect of field directionality on worm behavior, we tried flipping the magnet and thereby changing the direction of the field. We saw no convincing results to indicate worms prefer the north/south pole or can sense the change in field directions. We further tested putting two magnets on either side of the chip holder and re-orienting them to different directions and distances. No noticeable change in worm movement was observed.

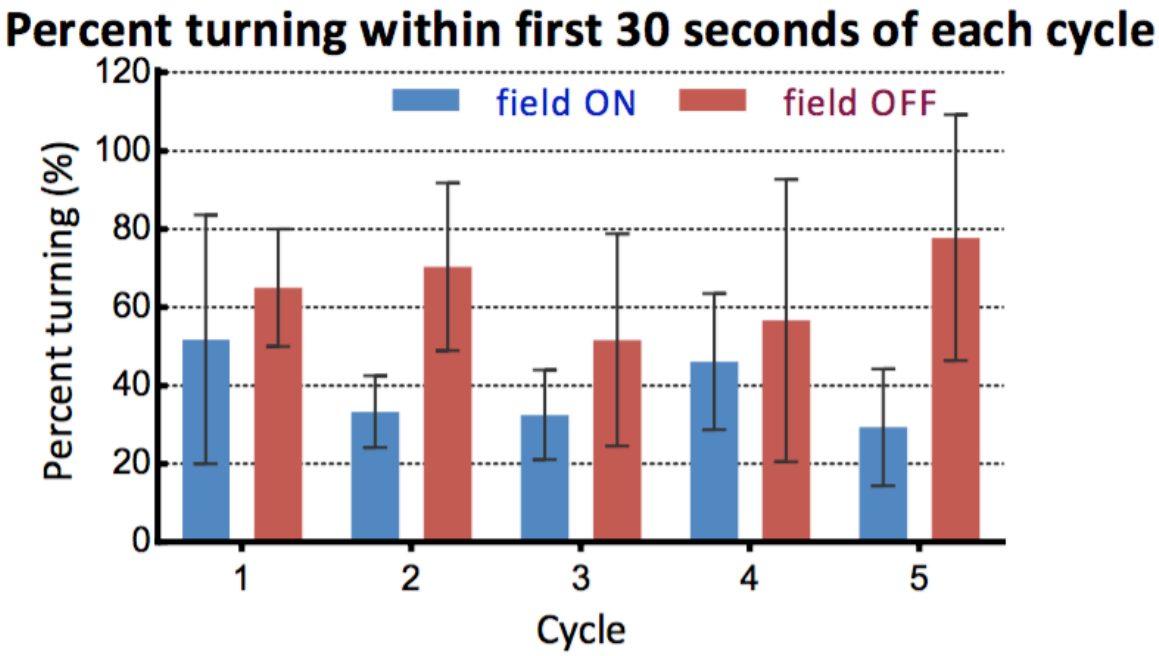

Figure 2.7. The plot shows the percentage of worms turning or curling within first 30 seconds of placing the magnet or removing the magnet, repeated over five cycles. The results are combined from all magnetic field experiments.

Conclusion

In conclusion, the results presented here indicate that effects of static magnetic fields, in the range of 5 mT to 120 mT, on the average velocity and the turning and curling behavior of wild-type *C. elegans*, are not significant. A microfluidic device setup was used to test single worms under different field strengths and an imaging software was used to automate the steps involved in computing worm movement. A number of alterations in the experimental protocol were tested, and our data suggest that static magnetic fields do not produce significant change in movement or direction of *C. elegans* nematodes.

Acknowledgements

This work was partially supported by US National Science Foundation (CBET-1150867 to S.P. and DGE1247194 to R.B). The *C. elegans* culture plates were generously provided by Dr. JoAnne Powell-Coffman and Dr. Jenifer Saldanda. We also thank Dr. Ravi Hadimani for stimulating discussions on the experiments.

References

[1] von Middendorf, A. (1855) Die Isepiptesen Russlands. Mem. Acad. Sci. St Petersbourg VI, Ser. Tome, 8, 1-143.

[2] Viguier, C. (1882) Le sens de l'orientation et ses organes chez les animaux et chez l'homme. Rev. phil. France Etranger, 14, 1-36.

[3] Wiltschko, W. and Wiltschko, R. (1996) Magnetic Orientation in Birds. Journal of Experimental Biology, 199, 29-38.

[4] Keeton, W.T. (1971) Magnets Interfere with Pigeon Homing. Proceedings of the National Academy of Sciences of the United States of America, 68, 102-106.

[5] Wiltschko, W. (1968) Über den Einfluß statischer Magnetfelder auf die Zugorientierung der Rotkehlchen (Erithacus rubecula). Zeitschrift für Tierpsychologie, 25, 537-558.

[6] Wiltschko, W. (1978) Further Analysis of the Magnetic Compass of Migratory Birds. In: Animal Migration, Naviga-tion and Homing, Springer Verlag, New York, 302-310.

[7] Wiltschko, W. and Wiltschko, R. (2005) Magnetic Orientation and Magnetoreception in Birds and Other Animals. Journal of Comparative Physiology A: Neuroethology, Sensory, Neural, and Behavioral Physiology, 191, 675-693.

[8] Boles, L.C. and Lohmann, K.J. (2003) True Navigation and Magnetic Maps in Spiny Lobsters. Nature, 421, 60-63.

[9] Marhold, S., Wiltschko, W. and Burda, H. (1997) A Magnetic Polarity Compass for Direction Finding in a Subterra-nean Mammal. Naturwissenschaften, 84, 421-423.

[10] Kirschvink, J.L. and Gould, J.L. (1981) Biogenic Magnetite as a Basis for Magnetic Field Detection in Animals. Bio-Systems, 13, 181-201.

[11] Heyers, D., Zapka, M., Hoffmeister, M., Wild, J.M. and Mouritsen, H. (2010) Magnetic Field Changes Activate the Trigeminal Brainstem Complex in a Migratory Bird. Proceedings of the National Academy of Sciences of the United States of America, 107, 9394-9399.

[12] Treiber, C., Salzer, M., Riegler, J., Edelman, N., Sugar, C., Breuss, M., et al. (2012) Clusters of Iron-Rich Cells in the Upper Beak of Pigeons Are Macrophages Not Magnetosensitive Neurons. Nature, 484, 367-370.

[13] Blakemore, R. (1975) Magnetotactic Bacteria. Science, 190, 377-379.

[14] Gegear, R.J., Foley, L.E., Casselman, A. and Reppert, S.M. (2010) Animal Cryptochromes Mediate Magnetoreception by an Unconventional Photochemical Mechanism. Nature, 463, 804-807.

[15] Guerra, P.A., Gegear, R.J. and Reppert, S.M. (2014) A Magnetic Compass Aids Monarch Butterfly Migration. Nature Communications, 5, 4164.

[16] Gegear, R.J., Casselman, A., Waddell, S. and Reppert, S.M. (2008) Cryptochrome Mediates Light-Dependent Magne-tosensitivity in Drosophila. Nature, 454, 1014-1018.

[17] Liedvogel, M. and Mouritsen, H. (2010) Cryptochromes—A Potential Magnetoreceptor: What Do We Know and What Do We Want to Know? Journal of the Royal Society Interface, 7, S147-S162.

[18] Kaletta, T. and Hengartner, M.O. (2006) Finding Function in Novel Targets: *C. elegans* as a Model Organism. Nature Reviews Drug Discovery, 5, 387-399.

[19] Li, S., Armstrong, C.M., Bertin, N., Ge, H., Milstein, S., Boxem, M., et al. (2004) A Map of the Interactome Network of the Metazoan *C. elegans*. Science, 303, 540-543.

[20] White, J.G., Southgate, E., Thomson, J.N. and Brenner, S. (1986) The Structure of the Nervous System of the Nema-tode Caenorhabditis elegans. Philosophical Transactions of the Royal Society of London B: Biological Sciences, 314,1-340.

[21] Cranfield, C.G., Dawe, A., Karloukovski, V., Dunin-Borkowski, R.E., de Pomerai, D. and Dobson, J. (2004) Biogenic Magnetite in the Nematode Caenorhabditis elegans. Proceedings of the Royal Society of London B: Biological Sciences, 271, S436-S439.

[22] Bessho, K., Yamada, S., Kunitani, T., Nakamura, T., Hashiguchi, T., Tanimoto, Y., et al. (1995) Biological Responses in Caenorhabditis elegans to High Magnetic Fields. Experientia, 51, 284-288.

[23] Miyakawa, T., Yamada, S., Harada, S., Ishimori, T., Yamamoto, H. and Hosono, R. (2001) Exposure of Caenorhabdi-tis elegans to Extremely Low Frequency High Magnetic Fields Induces Stress Responses. Bioelectromagnetics, 22, 333-339.

[24] Lee, C.-H., Chen, H.-M., Yeh, L.-K., Hong, M.-Y. and Huang, G.S. (2012) Dosage-Dependent Induction of Behavioral Decline in Caenorhabditis elegans by Long-Term Treatment of Static Magnetic Fields. Journal of Radiation Research, 53, 24-32.

[25] Hung, Y.-C., Lee, J.-H., Chen, H.-M. and Huang, G.S. (2010) Effects of Static Magnetic Fields on the Development and Aging of Caenorhabditis elegans. Journal of Experimental Biology, 213, 2079-2085.

[26] Pichler, P. (2011) A Screen for Magnetosensitive Nematodes. E-Thesis, University of Vienna, Vienna.

[27] Garcia, E., Racioppo, P., Niizawa, S., Zedwick, J., Mendoza, S. and Arisaka, K. (2014) Search for Magnetotaxis in Caenorhabdits elegans. Poster Presented at UCLA Science Poster Day, Los Angeles.

[28] Saldanha, J., Parashar, A., Pandey, S. and Powell-Coffman, J. (2013) Multiparameter Behavioral Analyses Provide In-sights to Mechanisms of Cyanide Resistance in Caenorhabditis elegans. Toxicological Sciences, 135, 156-168.

CHAPTER 3

CHIP TECHNOLOGIES FOR SCREENING CHEMICAL AND BIOLOGICAL AGENTS AGAINST PLANT-PARASITIC NEMATODES

Modified from a paper published in Phytopathology

Augustine Q. Beeman, Zach L. Njus, Santosh Pandey,* and Gregory L. Tylka

Abstract

Plant-parasitic nematodes cause substantial damage to agricultural crops worldwide. Long-term management of these pests requires novel strategies to reduce infection of host plants. Disruption of nematode chemotaxis to root systems has been proposed as a potential management approach, and novel assays are needed to test the chemotactic behavior of nematodes against a wide range of synthetic chemicals and root exudates. Two microfluidic chips were developed that measure the attraction or repulsion of nematodes to chemicals ("chemical chip") and young plant roots ("root chip"). The chip designs allowed for chemical concentration gradients to be maintained up to 24 hours, the nematodes to remain physically separate from the chemical reservoirs, and for images of nematode populations to be captured using either a microscope or a flatbed scanner. In the experiments using the chemical chips, seven ionic solutions were tested on second-stage juveniles (J2s) of *Meloidogyne incognita* and *Heterodera glycines*. Results were consistent with previous reports of repellency of M. incognita to a majority of the ionic solutions, including NH4NO3, KNO3, KCl, MgCl2, and CaCl2. *Heterodera glycines* was found to be attracted to both NH4NO3 and KNO3, which has not been reported previously. A software program was written to track the location of nematodes at regular time intervals using the root chip. In experiments with the root chip, *H. glycines* J2s were

attracted to roots of 3.day.old, susceptible (cv. Williams 82) soybean seedlings, and attraction of *H. glycines* to susceptible soybean was similar across the length of the root. Attraction to resistant (cv. Jack) soybean seedlings relative to the water only control was inconsistent across runs, and *H. glycines* J2s were not attracted to the roots of resistant or susceptible cultivars when both were placed on opposite sides of the same root chip. The chips developed allow for direct tests of plant-parasitic nematode chemotaxis to chemicals and roots with minimal human intervention.

Introduction

The soybean cyst nematode, *Heterodera glycines*, and the root-knot nematode, *Meloidogyne incognita*, are economically important plant-parasitic nematodes, each causing billions of dollars in crop loss annually (Sasser and Freckman, 1987). Plant-parasitic nematodes locate their hosts using a range of chemical cues exuded from host roots (Perry, 1996). The selective movement of nematodes towards known and unknown chemical cues is referred to as chemotaxis. In the soil, chemotaxis is a complex phenomenon where an interplay among multiple attractants and repellents produce long-range and short-range spatiotemporal signals for the nematode (Reynolds et al., 2011). With limited energy reserves, nematodes need to decipher competing chemical cues and infect their host within a restricted time. Understanding the factors involved with plant-parasitic nematode chemotaxis is a scientifically intriguing topic that could lead to advances in managing these pests.

A number of assays have been developed and used to study the chemotaxis of nematodes. Many of these laboratory assays use agar as the migration matrix and use a number of different physical configurations (Castro et al., 1989; Devine and Jones, 2003; Papademetriou and Bone,

1983; Riddle and Bird, 1985; Shinya et al., 2015). The configuration and dimensions of the area used to conduct these assays depends on the scientific hypotheses being tested. For example, a Y-shaped olfactometer was created in a Pluronic gel matrix to study whether *Meloidogyne incognita* and *M. graminicola* used the shortest path to navigate a maze and reach host roots (Reynolds et al., 2011). Besides the choice of the physical device, different ways to quantify the chemotactic behavior on plate assays have been reported. For instance, relative values can be assigned to nematodes depending on their proximity to a source compound (Wuyts et al., 2006), the number of nematodes can be counted that are in contact with a live root (Wang et al., 2009b), or the tracks created by nematodes on agar surfaces can be visualized as they move towards a filter paper disk soaked with a test compound (Huettel and Jaffe, 1987; Papademetriou and Bone, 1983). Although agar-based plate assays are widely adopted for their inherent simplicity, there are some compromises associated with their use. Agar plate assays require carefully drying the agar (Wuyts et al., 2006), followed by adding a treatment compound in a well cut into the agar or saturated filter paper disk (Hu et al., 2013, Papademetriou and Bone, 1983) potentially introducing a source of variability between experiments. On plates with agar, some of the nematodes may not be visible throughout the length of the experiment as some nematodes can move beneath the agar surface, migrate to the edges of the plate, or become obscured as they reach the source of the chemical gradient (i.e. agar plug, filter paper disk, etc.). Recording tracks made by nematodes to a test compound can also be challenging if there are many nematodes on a given plate.

As an alternative to agar-based plate assays, microfluidic technology offers the advantage of diffusing compounds within custom-designed chip geometries to suit a desired chemotaxis experiment. Microfluidics can be defined as “the handling and analyzing of fluids in structures of

micrometer scale" (Beebe et al., 2002). In the past two decades, there have been exciting applications of microfluidics in biology, such as in electrophysiology, pharmaceutical drug screening, cell sorting and analysis, biomolecule separation and screening, point-of-care diagnostics, and tissue engineering (Beebe et al., 2002). Microfluidic systems may also be paired with technology to allow the user to automatically load samples, perfuse chemicals, monitor real-time activity, record and analyze data and conduct multiple tests in parallel. In nematology, the development of microfluidic assays have been primarily focused on the behavioral modeling of *Caenorhabditis elegans* (Saldanha et al., 2013) and some parasites of veterinary importance (Chen et al., 2011). These studies have also used image analysis combined with microfluidics to aid in data acquisition (Njus et al., 2016; Saldanha et al., 2013).

While the goals of automation, real-time imaging and high-throughput screening are necessary in certain studies (e.g. those involving pharmacology, toxicity, olfactory functions, and ion-channel kinetics of whole nematodes) that run over ten or twenty minutes (Carr et al., 2011; Lockery et al., 2012; Peytavi et al., 2005), experiments to investigate the chemotaxis of plant-parasitic nematodes require longer time periods. Plant-parasitic nematodes exhibit a far more sedentary lifestyle than *C. elegans*, so microfluidic devices must be designed with these behavioral attributes in mind.

The objectives of our study were to 1) design, optimize and fabricate two microfluidic chips, a "chemical chip" and "root chip" 2) determine the effect of multiple ionic solutions on movement of second-stage juveniles (J2s) of *H. glycines* and *M. incognita* using the chemical chip and 3) study the movement of *H. glycines* J2s in response to young soybean roots growing on the root chip. The combination of microfluidic chips and imaging tools can potentially lead to faster screening of novel chemical compounds that disrupt nematode migration to roots,

characterizing nematode-resistant traits of host plants, and answering fundamental questions in root-nematode interactions.

Materials and Methods

Microfluidic Chips

The overall design of the chemical microfluidic chip is shown in Figure 3.1. Each lane on the chip consisted of a central port (i.e. the nematode entry port) where nematodes were inserted for chemotaxis experiments (Figure 3.1A). Two resting chambers on either side of the nematode entry port allowed for unrestricted movement of the nematodes from the central port. Two resting chambers at opposite ends of the lane provided access to reservoirs that contained treatment solutions. The treatment reservoir housed the test compound of interest while the control reservoir housed the experimental control. The resting chambers were connected to the treatment and control reservoirs by microscale filters (Figure 3.1B). The filters allowed slow diffusion of chemicals from the treatment and control reservoirs into the resting chambers and also prevented nematodes from moving into the treatment and control reservoirs. The chemical microfluidic chip contains four parallel lanes for separate, simultaneous tests (Figure 3.1C). The dimensions of all components of the chip are shown in Figure 3.2.

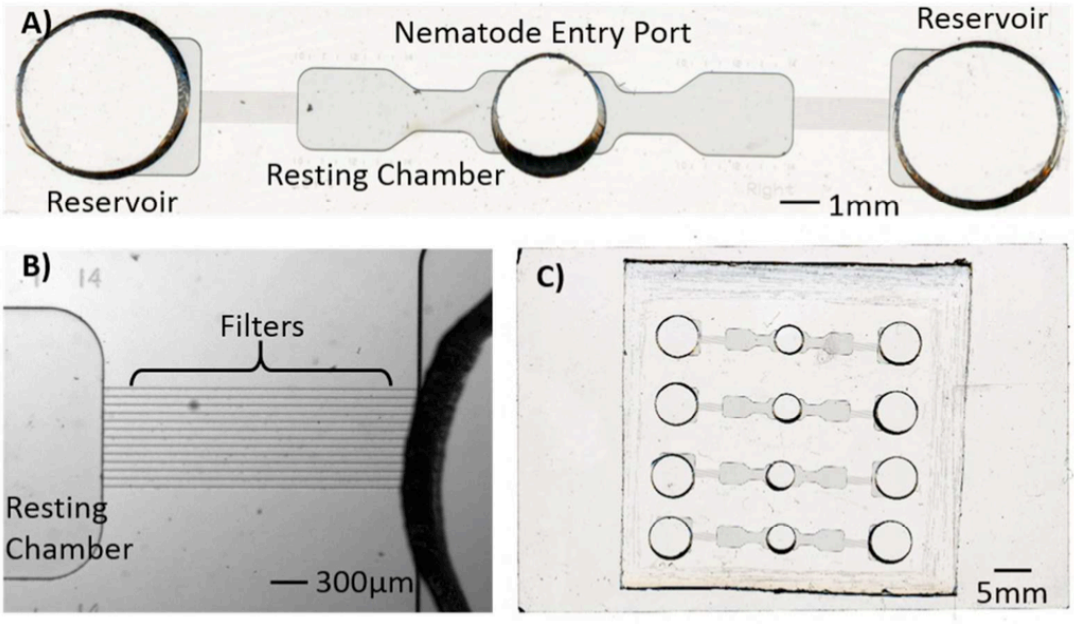

Figure 3.1. Images of the chemical chip used for chemotaxis experiments. **(A)**, Each lane comprised a nematode entry port, left and right resting chambers, left and right reservoirs and microscale filters connecting the reservoirs to the resting chambers. **(B)**, Magnified image of the filters that permitted chemical diffusion but restricted the nematodes to the resting chambers. **(C)**, Image of a whole chip comprising four parallel lanes and bonded to a glass slide. Scale bars in the images depict the relative sizes of the microfluidic chip.

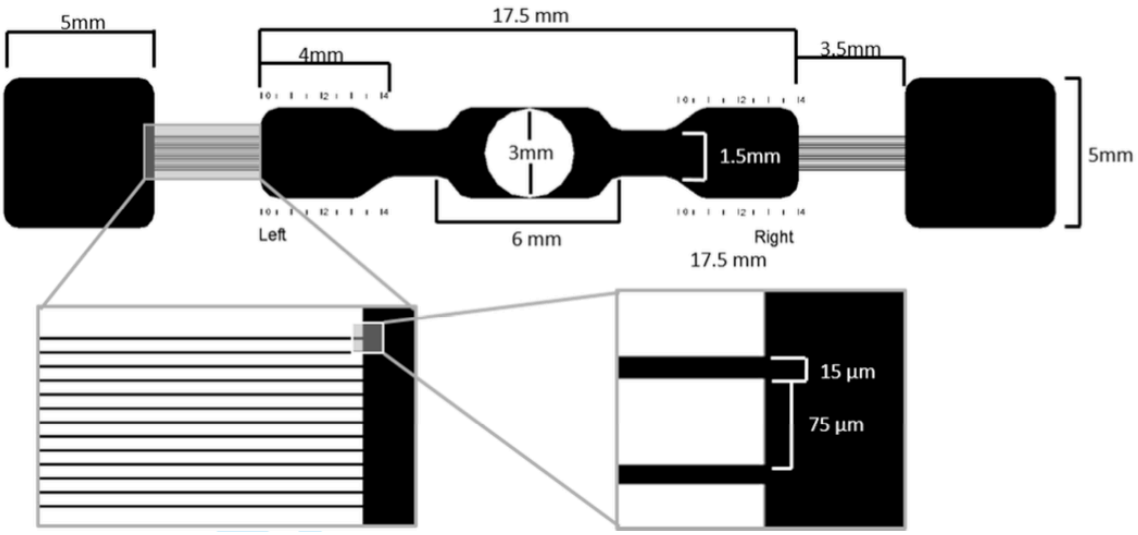

Figure 3.2. Schematic of microfluidic chip with dimensions of all major components.

The chip design was drawn in AutoCAD™ and sent to an outside vendor (FineLine Imaging™) to print the mask template. Standard soft lithography was used to fabricate the microfluidic chip. Briefly, an ultraviolet-sensitive polymer, SU-8, was spin coated on a 7.62 cm silicon wafer to a height of around 80 µm. The SU-8 layer was selectively exposed to ultraviolet light (350 nm) using the mask template. A SU-8 developer was used to remove the unexposed photoresist leaving a negative mold of the final chip. Thereafter, polydimethylsiloxane (PDMS) was poured on the SU-8 mold and baked on a hotplate for 3 hours at 100˚C. The solidified PDMS structure was peeled off and holes were punched to create the treatment and control reservoirs and nematode entry port. Finally, the PDMS chip was bonded to a glass slide using a plasma cleaner. Preliminary experiments were conducted with *H. glycines* J2s to determine the optimal device layout and dimensions, particularly the size of the filters and the relative volumes of resting chambers and reservoirs for use with plant-parasitic nematodes.

Figure 3.3A shows diffusion tests with colored dyes taken at different time points to confirm the slow diffusion of chemicals into the resting chambers over the length of proposed experiment. A microfluidic lane in the chip was pre-filled with water, and red and blue dyes were added to the treatment and control ports. As shown in the figure, the two dyes are localized in their respective resting chambers, and there is virtually no mixing of the dyes in the central nematode entry port. This visual observation suggests that the microfluidic chip can be used to perform chemotaxis experiments for up to 24 hours. Figure 3.3B demonstrates how nematodes move through the chemical chip over the length of an experiment with KNO 3. The *H. glycines* J2s in this run were attracted to KNO 3 as early as 4 hours, and a majority of the nematodes in the chip were in the resting chamber nearest to the filters connected to the KNO 3 reservoir by 24 hours. The chemical chip was modified into a root chip by converting the four separate treatment

and control reservoirs in the four lanes of the chip into two elongated root channels. This was done by carefully cutting a PDMS layer with a clean razor blade and bonding two rectangular pieces of PDMS over the top of the root channels. This design provided coverage of the root and slowed the evaporation of fluids from the root channel. The root chip comprised four lanes that are exposed to different sections of the growing root, from nearest the seed to nearest the root tip.

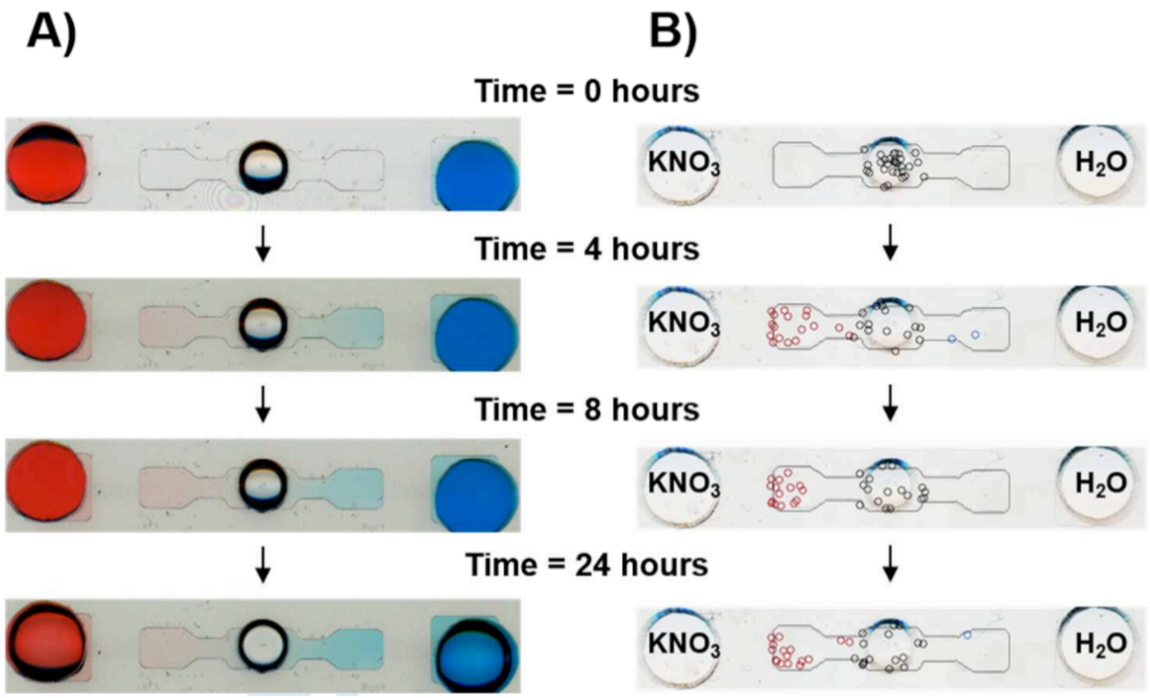

Figure 3.3. Diffusion of red and blue dye **(A)** and movement of *H. glycines* second-stage juveniles in response to KNO 3 versus water **(B)** in chemical chips at four time points after incubation at 25 °C. The diffusion of the dyes into the resting chambers of the lane over time is apparent in the images on the left. The colored circles represent *H. glycines* second-stage juveniles that moved toward (red) or away (blue) from the KNO 3 or stayed in or near the entry ports (black) of the lane in the microfluidic chip in the images on the right.

Nematode Collection for Experiments

Populations of *H. glycines* and *M. incognita* were maintained in the greenhouse on soybean, *Glycine* max (cv. Williams 82) and tomato, *Lycopersicon esculentum* (cv. Rutgers), respectively. Females and cysts (dead females filled with eggs) of *H. glycines* were collected from four- to eight-week-old plants by rinsing roots with water to remove soil and then spraying the roots with a stream of water on an 850-µm-pore sieve nested above a 250-µm-pore sieve. The debris was collected on the 250-µm-pore sieve, and the females and cysts were separated from the debris by sucrose centrifugation (Jenkins, 1964) using 1,362 g/L of sucrose. The females and cysts were crushed with a motorized rubber stopper, and eggs were collected on 25-µm-pore sieve nested under a 75-µm-pore sieve (Faghihi and Ferris, 8 2000). Eggs of *M. incognita* were collected by washing soil from the roots of six- to eight-week-old *M. incognita*-infected tomato plants, cutting the roots into 2-cm-long pieces, and incubating the root pieces with agitation in 0.5% sodium hypochlorite (bleach) for two minutes (Hussey and Barker, 1973). The suspension was poured over a nested pair of 75-µm-pore and 25-µm-pore sieves to recover the nematode eggs on the bottom 25-µm-pore sieve. The eggs were rinsed with water several times to remove all residues of the bleach.

Extracted eggs of both nematode species were further separated from debris with sucrose centrifugation in 454 g/L sucrose (Jenkins, 1964). The eggs were washed with sterile, distilled water and incubated in the dark at 25°C for 48 hours on 30-µm-pore mesh (Elko Filtering, Miami, FL) to hatch J2s (Wong et al., 1993). The hatched J2s (2 to 3 days old) moved downward through the 30-µm-pore mesh and were collected by centrifuging the incubation suspension at 2,000 g for approximately 4 minutes. The concentrated J2 suspension was diluted with sterile, distilled water to achieve the appropriate nematode population density for use in the experiments.

Chemical Chip Experimental Setup

Each lane of the microfluidic chip was filled with approximately 100 µL of sterile, distilled water added through the worm entry port using a 100-mL syringe connected to rubber tubing (inner diameter: 1 mm). A custom-made PDMS connector was put over the nematode entry port to apply sufficient fluid pressure to completely fill the chip. The connector was a cylindrical piece of PDMS (outside diameter: 5 mm, height 3 mm) with a 0.8-mm-diameter hole punch in the center, which allowed the tubing to be attached the connector. The chips were visually inspected after filling to ensure that each entire lane was completely filled with water. If air bubbles were trapped in any section of the lane, more water was added until the bubbles had exited the lane through openings of the treatment reservoirs. Chips that had large bubbles in the resting chambers or in the filters that could not be removed were discarded. Next, 30 to 70 *H. glycines* or *M. incognita* J2s were suspended in 10 to 15 µL of water and added to the central nematode entry port, then 50 µL of test chemical was added to the treatment reservoir and 50 µL of water was added to the control reservoir. The compounds used in the experiments were ionic solutions that had been reported to be attractants or repellants for *H. glycines* (Papademetriou and Bone, 1983) or *M. incognita* (Castro et al., 1998; Le Saux and Queneherve, 2002; Prot, 1979; Riddle and Bird, 1985). These included sulfates (Na 2SO 4, ZnSO 4), nitrates (NH 4NO 3, KNO 3), and chlorides (MgCl 2, CaCl 2, KCl). All ionic solutions were prepared at a concentration of 500 mM. To check for any bias of nematode movement from other factors (such as chip dimensions, fluid flow, or filling process), some lanes were filled with water in both the treatment and control reservoirs. The chips were incubated in darkness at 25°C. For each ionic

solution, between 482 to 712 *H. glycines* J2s were tested over a total of 9 to 10 replications and 441 to 666 J2s *of M. incognita* were tested over a total of 9 to 12 replications (Table 3.1).

Table 3.1. Effect of different ionic solutions (500 mM) on chemotaxis of two plant-parasitic nematodes. Results of chemotaxis experiments at 24 hours. A total of 9 to 12 replications were done for each ionic solution tested. For each species of nematode, the response was rated as either A = attracted, N = neutral response, R = repelled at the $P = 0.05$ level using a Student's paired t-test.

Meloidogyne incognita

Ionic solution	Replicates	Total nematodes	Outcome	*P* value	Standard Error
$CaCl_2$	12	626	R	0.0007	7.79
$MgCl_2$	10	496	R	0.0004	9.05
KCl	11	441	R	<0.0001	6.08
NH_4NO_3	12	768	R	<0.0001	6.63
KNO_3	11	666	R	0.0002	7.36
$ZnSO_4$	10	515	N	0.1798	6.28
Na_2SO_4	9	555	N	0.2435	4.46
water	23	1363	N	0.9185	5.26

Heterodera glycines

Ionic solution	Replicates	Total nematodes	Outcome	*P* value	Standard Error
$CaCl_2$	10	690	R	0.0332	7.42
$MgCl_2$	10	483	A	0.0195	7.79
KCl	10	627	N	0.6436	9.52
NH_4NO_3	9	473	A	0.0058	5.83
KNO_3	10	712	A	<0.0001	6.20
$ZnSO_4$	9	561	N	0.5131	0.05
Na_2SO_4	9	546	N	0.2157	0.04
water	23	1458	N	0.1634	0.06

Software Program

To eliminate the need for manual microscopic observation for data collection throughout the length of the experiment, a custom software program was written to control a high-resolution (2400 dpi) flatbed scanner (EPSON Perfection V750-M Pro Scanner) onto which the microfluidic chips were placed. The program also controlled the time interval for scanning the chips. A temperature-controlled chamber (25 °C) housed the scanner system, and multiple chips (up to four) were placed on the scanner bed to be monitored simultaneously during an experiment. When the experimental run was completed, the program organized and formatted the scanned images to allow a user to identify the locations of all of the nematodes in a lane at each time point. Thereafter, the program calculated x- and y-coordinates of each identified nematode and scored individuals as either being attracted, repelled or having no preference to the treatment based on their location in the resting chambers or nematode entry port. The movement of J2s to a resting chamber adjacent to a reservoir holding a test compound was considered an attraction behavior, and movement of J2s to a resting chamber in the opposite direction was considered a repulsion behavior. We used the scanner setup to demonstrate the slow diffusion of chemicals through the filters from the treatment ports (Figure 3.3).

Root Chip Experimental Setup

Experiments were conducted with *H. glycines* and soybean seedlings in root chips. Soybean seeds of *H. glycines*-susceptible (cv. Williams 82) and *H. glycines*-resistant (cv. Jack) cultivars were plated on 1.5% agar and germinated in darkness at 25˚C for three days. Roots of these seedlings were inserted arbitrarily in a channel on either side of the root chip, and J2s of *H. glycines* were added to the central port of the chip as described previously. The movement of *H.*

glycines J2s toward or away from the root of each cultivar was tested. In a separate experiment, roots of the two soybean cultivars were placed on opposite sides of a chip and movement of *H. glycines* J2s towards one or the other cultivar was assessed. Similar to the chemical chip setup, water only controls were used to check for any directional bias in the chips in which the root channels were filled with water on both sides. Root chips were placed flat on a scanner that was enclosed in the temperature-controlled (25˚C) chamber described previously and scanned every hour for 18 hours. A total of 4 chips were used for each treatment, with the number of *H. glycines* J2s tested for each treatment ranging from 502 to 574.

Data Collection

For the chemical chip experiments, all data was collected using a dissecting microscope at 60X magnification. The locations of the nematodes in the chemical chips were initially recorded at 1, 6, 24 and 48 hours after the start of the experiment. It was then determined that the maximum response occurred at 24 hours, and data collection for some chemical chip experiments was done only at 24 hours. For root chip experiments, nematode location was scored every hour using a flatbed scanner and analyzed using the custom software program described above.

Statistical Analysis

For each nematode species in the chemical chip experiments, there were between 9 to 12 runs for each ionic solution tested and 23 runs for the water only control treatment. The percentages of J2s in the two resting chambers and nematode entry port at 24 hours were calculated. For the chemical chip experiments, the percentage of nematodes in a resting chamber

adjacent to the treatment reservoir was compared with the percentage of nematodes in the resting chamber adjacent to the control reservoir using a paired Student's t-test in SAS using PROC TTEST (Devine and Jones, 2003; Hu et al., 2013).

Root chips were used to assess the following set of treatments: *H. glycines*-susceptible soybean (cv. Williams 82) versus water, *H. glycines*-resistant soybean (cv. Jack) versus water, *H. glycines*-susceptible soybean versus *H. glycines*-resistant soybean and water versus water. For the root chip experiments, the percentage of nematodes in the each of the resting chambers were analyzed similarly to the chemical chip experiments. First, an ANOVA was conducted in PROC GLM of SAS to test the effect of lane at each hour time point. If the effect of lane was found not to be significant, the data from all lanes were subsequently combined for analysis and the effect of each treatment in the root chips at 18 hours was tested using a paired t-test in PROC TTEST. A chemotaxis index (chemoindex) modeled after Le Saux and Quénéhervé, (2002) was calculated to determine overall movement of the nematode population inside each lane of the chip. The equation for the chemoindex was defined as: (pT-pC), where pT is the percentage of nematodes in the chip residing in the resting chamber adjacent to the treatment reservoir and pC is the percentage of the nematodes in the resting chamber adjacent to the control reservoir. Therefore, a positive value (i.e. greater than zero) denoted that the nematodes were attracted to the treatment, while a negative value (i.e. less than zero) indicated that they were repelled from the treatment. The chemoindex value was calculated for each lane of a chip at every time point in the experiment. Standard errors of the mean (SEM) of the chemoindex values for each lane were calculated and plotted for every hour of the experiment.

Results

Chemical Chip Experiments

Maximum movement of both plant-parasitic nematode species occurred by 24 hours of incubation (data from other time points are not shown). No directional bias towards the right or left side of the chip was observed (Figure 3.4). *Heterodera glycines* and *M. incognita* exhibited differential chemotactic responses to the ionic solutions. In general, 32 to 52.3 percent of the *H. glycines* J2s added to the chemical chips moved towards or away from test compounds, while 37.6 to 76.6 percent remained in the nematode entry point after 24 hours. In contrast, only 14.1 to 51 percent of the *M. incognita* J2s moved towards or away from compounds used in the experiments.

A compound was determined to be an attractant or repellent if a significantly higher proportion of nematodes moved toward the nematode resting chamber adjacent to treatment reservoir or away from a compound being tested (i.e. toward the resting chamber adjacent to the control reservoir). Compounds that elicited no significant movement towards or away from the source were considered neutral. Among the compounds to which *H. glycines* was exposed, three were attractants, one was a repellant, and three had no significant effect. Specifically, there was significant movement of *H. glycines* J2s towards MgCl 2, KNO 3, and NH 4NO 3. *Heterodera glycines* J2s were most strongly attracted to KNO 3, where an average of 51% of the J2s in the chip moved towards the compound and only 10.1% away. Conversely, *H. glycines* was repelled by CaCl 2, with an average of 13.2% moving toward the compound and 32% moving away. There was no significant movement detected towards or away from KCl, ZnSO 4, Na 2SO 4, and the water only control. In contrast to the results obtained with *H. glycines*, *M. incognita* J2s were repelled by KNO 3, NH4NO 3, KCl, MgCl 2, and CaCl 2. For example, while an average of 51%

of the *M. incognita* J2s move away by KCl, only 1.3% moved toward the compound. Like *H. glycines*, *M. incognita* J2s were not attracted or repelled by ZnSO 4 and Na 2SO 4.

Root Chip Experiment

These experiments were limited to 18 hours, largely because water uptake from roots resulted in empty root channels after this time. The *H. glycines* J2s were successfully tracked moving in the chip during the course of the experiment using a temperature-controlled flatbed scanner (Figure 3.5). For the treatments with roots, the lane positions had negligible effect on the nematode migration patterns and data were subsequently combined and analyzed (Table 3.2). Williams 82, an *H. glycines*-susceptible cultivar, attracted *H. glycines* J2s regardless of which lane the nematodes were placed in, with positive chemotaxis index values ranging by lane from 12.1 to 16.8 after 18 hours (Figure 3.6A). When lanes were combined for analysis Williams 82 this attraction was found to be significant (P = 0.001). *H. glycines* J2s were attracted to *H. glycines*-resistant soybean in some runs, but the attractive response was not consistently seen across all replications, with chemotaxis index values ranging by lane from -9.2 to 3.5 after 18 hours (Figure 3.6C). However, there was no strong preference to either root when roots from both *H. glycines*-resistant and *H. glycines*-susceptible cultivars were placed on opposite sides (Figure 3.6C), and there was no directional bias in the water control chips (Figure 3.6D).

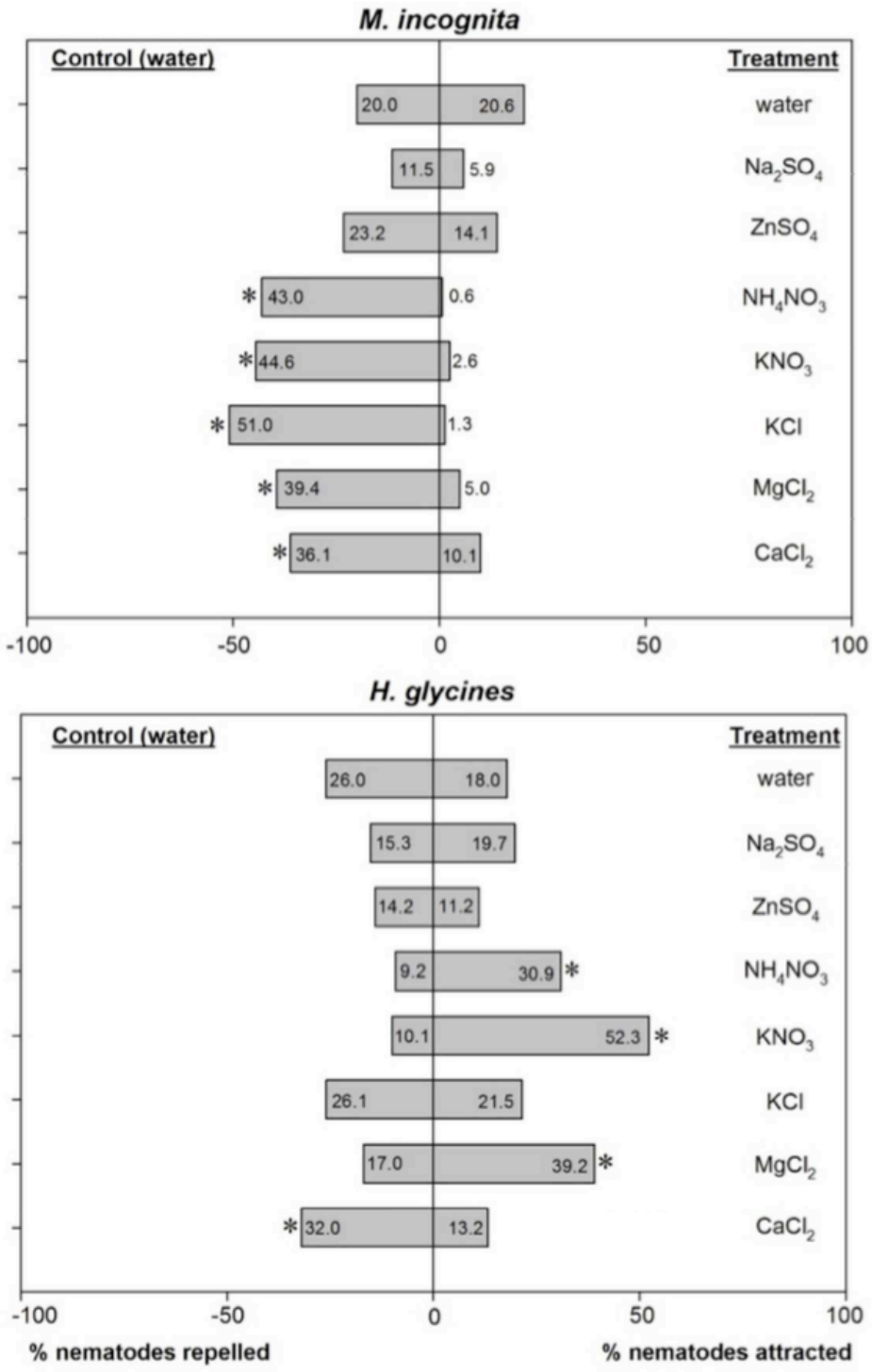

Figure 3.4. Results after 24 hours from the chemical chip chemotaxis experiments using different ionic solutions (500 mM) on juveniles of *M. incognita* and *H. glycines*. Bars represent the percentage of total nematodes in each lane moving either towards or away from ionic

solutions. Asterisks indicate a significant difference between the percentage of attracted and repelled juveniles at $P = 0.05$, using a Student's paired t-test.

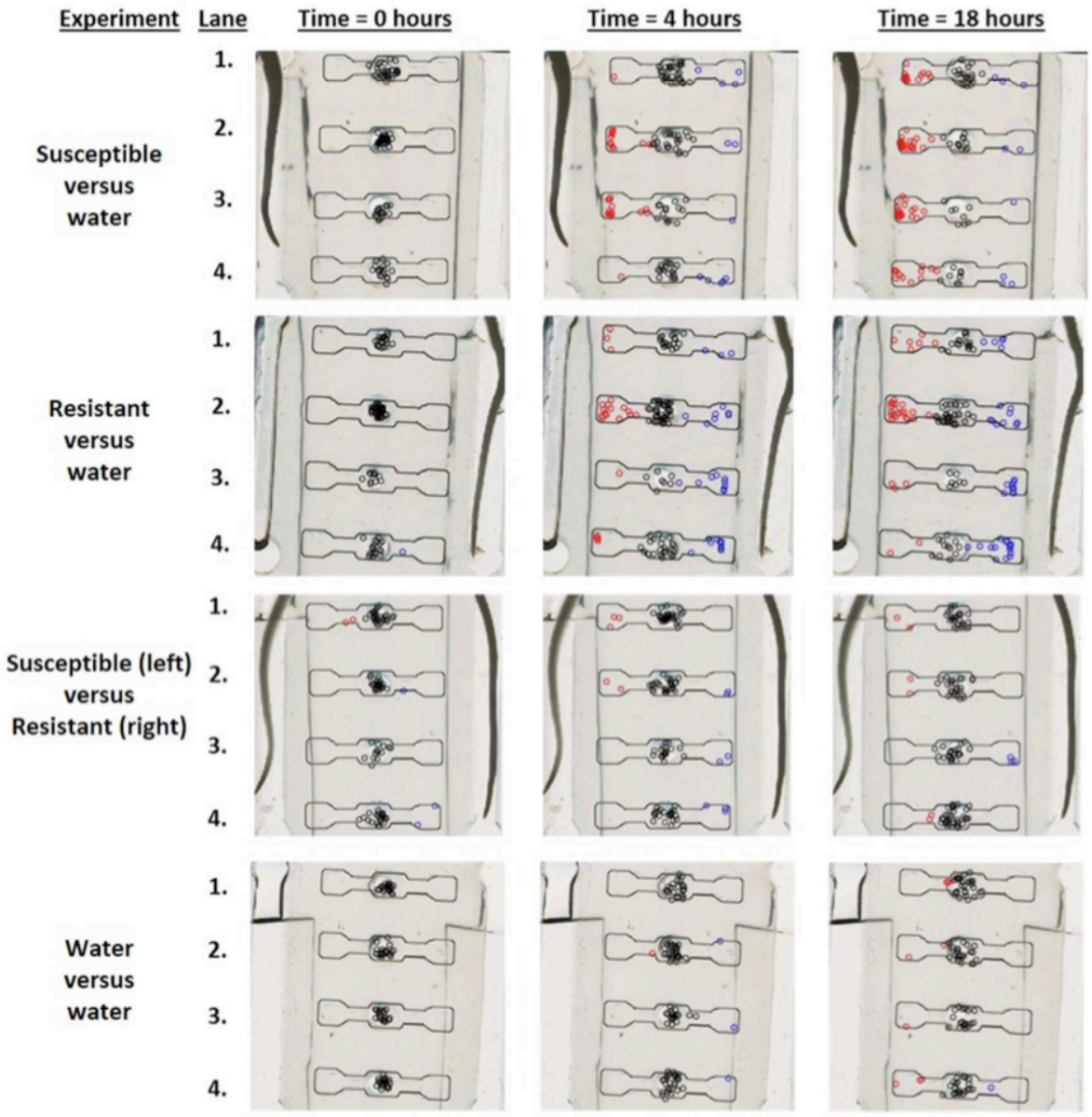

Figure 3.5. Results from root chip experiments conducted on flatbed scanner measuring the effect of the presence of roots of 3-day-old soybean seedlings on *H. glycines* chemotaxis. Each circle represents a single juvenile. Black dots represent juveniles in the center of the chip, while red and blue circles represent juveniles that have migrated to the left and right portions of the chip, respectively.

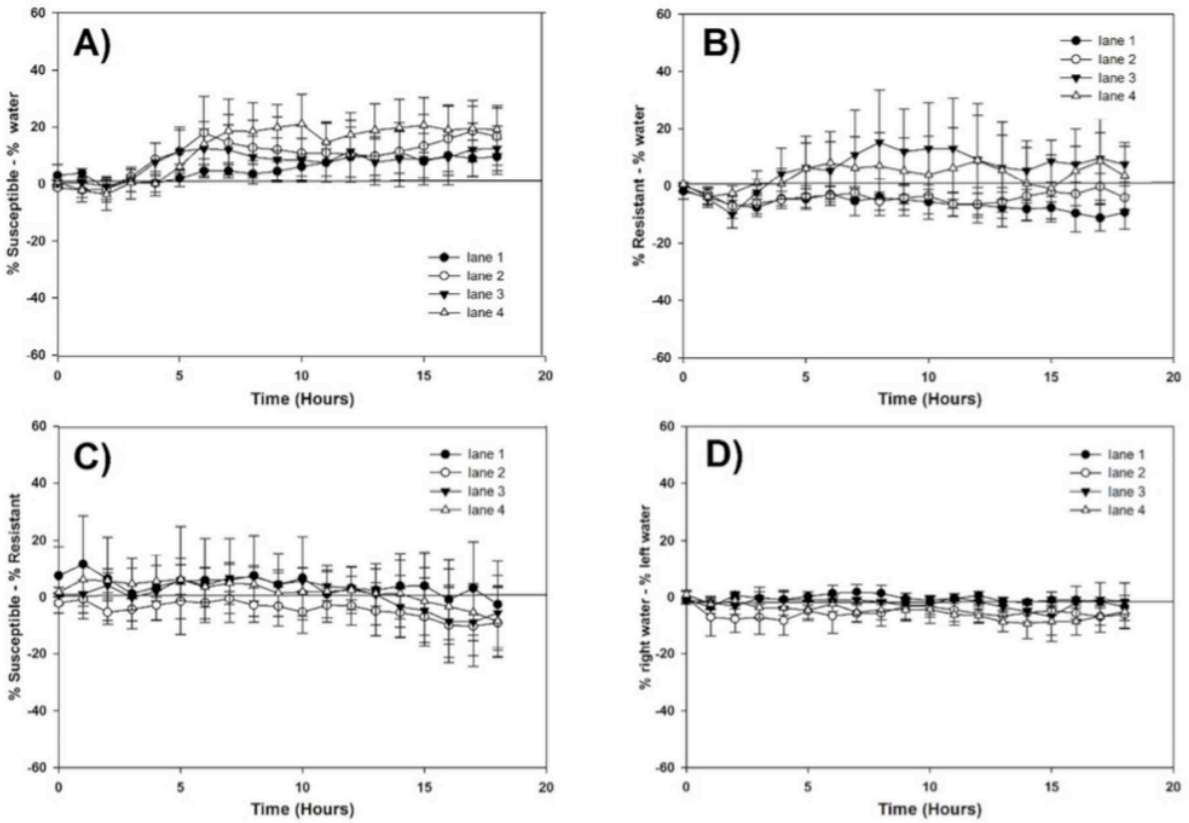

Figure 3.6. Chemotaxis of *H. glycines* J2s in root chips with Williams 82 (*H. glycines*-susceptible soybean) **(A)**, Jack (*H. glycines*-resistant soybean) **(B)**, Williams 82 versus Jack **(C)**, and water only controls **(D)**. Positive values indicate attraction and negative values indicate repulsion towards hypothesized attractant for **A-C**, while **(D)** shows limited directional bias in the absence of roots. Error bars represent the standard error of the mean (SEM) for each lane-hour combination.

Discussion

Plant-parasitic nematodes use chemical signals in the soil to guide them to host roots. This provides scientists with an opportunity to search for chemical compounds and biological agents that disrupt nematodes from traveling to host roots. Known chemical signals to which nematodes respond to include plant hormones, CO 2, ionic gradients, pH gradients, and secondary metabolites (Curtis, 2008; Dusenbery, 1983; Kerry, 2000; Riddle and Bird, 1985; Wang and Williamson, 2009a; Wuyts et al., 2006). Root exudates likely contain components that

both attract and repel nematodes (Devine and Jones, 2003; Tefft and Bone, 1985). Some scientists have tried to characterize the effects of root exudates on nematodes (Devine and Jones, 2003), but more studies are needed to understand the role of various factors in nematode chemotaxis. A better understanding of nematode chemotaxis can lead to identifying compounds that could serve as crop protection chemicals (Le Saux and Quénéhervé, 2002) or biological antagonists (Sikora 19 et al., 1992; Hu et al., 2013). Host plant resistance has been reported based partially on reduced nematode attraction to roots (Linsell et al., 2014), and exudates from root-cap cells have been reported to induce quiescence in certain plant-parasitic nematodes (Hiltpold et al., 2014). Furthermore, production of peptides *in planta* that disrupt chemotaxis of cyst nematodes has been reported (Lui et al., 2005). The microfluidics chips described in this paper can aid in conducting research to answer these basic and applied questions and develop novel management strategies.

In this paper, we describe two microfluidic chips to study the chemotaxis of plant-parasitic nematodes to both chemical compounds and live roots from intact soybean seedlings. The designs incorporate microscale filters that physically separate the nematodes from the source while permitting the establishment of chemical gradients over a period of 18 to 24 hours. The chips enable increased standardization in chemotaxis experiments because the mask template is reusable, allowing us to fabricate new batches of microfluidic chips with consistent repeatability in chip dimensions. Additionally, we developed a software program that helps to analyze a large set of saved images - identifying moving nematodes and tracking their locations as a function of time. Seven ionic solutions were tested on chemotaxis of *M. incognita* and *H. glycines* J2s using visual observation of large numbers of nematodes (>5,000 of each species) with the chemical chip. And we measured the effect of soybean roots on chemotaxis of *H. glycines* with the root

chip using a flatbed scanner paired with software to identify the position of each nematode in a device at 1 hour time points over the course of an 18 hour experiment.

The results of the experiments with the chemical chip revealed an interesting differential chemotactic response of *M. incognita* and *H. glycines* J2s to various ionic solutions. *Meloidogyne incognita* J2s were significantly repelled by all but two ionic solutions tested, which was consistent with results from previous studies reporting strong repellency of *M. incognita* to various ionic solutions (Prot, 1980; Castro et al., 1990; Le Saux and Quénéhervé, 2002; Riddle and Bird, 1985). The mechanism behind this repellent behavior of *M. incognita* J2s to ionic solutions has not been explained. Chemotaxis of *H. glycines* J2s has been less studied, but Papademetriou and Bone (1983) found that ZnSO 4 and MgCl 2 attracted *H. glycines* J2s. In our experiments MgCl 2 attracted *H. glycines* J2s, but ZnSO4 did not elicit an attractive or repellent response. Differences between our results and those reported by the literature can possibly be attributed to the differences in rate in different incubation media (water, agar, Pluronic gel, etc.) or the layout of the assay. For example, the assay of Papademetriou and Bone (1983) only measured attractive behavior indirectly based on agar tracks as an indication to whether the nematodes moved towards filter paper saturated with a test compound over a 24 hour period and found ZnSO 4 to be an attractant. Our chip allows for direct observation of nematode movement towards or away from a test compound. The fundamental differences in the two assay setups (measuring tracks versus direct nematode observation) may explain the differences in observed results. Our results found *H. glycines* J2s to be strongly attracted to both KNO 3 and NH 4NO 3, and repelled by CaCl 2, which has not been reported previously. As shown in Figure 3.3B, the attraction of *H. glycines* to KNO 3 occurred within a few hours, with a large number of J2s being attracted to the chemical as early as 4 hours after the start of the

experiment. A KNO 3 solution can serve as a good positive control for future *H. glycines* chemotaxis studies.

The root chip system provides an alternative to experiments that test nematode behavior (e.g. hatching, chemotaxis) in response to collected root exudates. Previous work has relied on collecting root exudates from growing plants and applied them to nematodes in separate steps (Levene et al., 1998; Tefft and Bone, 1985; Zhao et al., 2000). Our root chip allows for undisturbed growth of the soybean seedlings in the presence of the nematode. Therefore, the nematode can react to exudates as they are directly being emitted from the roots. A single chip has four separate lanes that allow spatial effects of roots of plant-parasitic nematode chemotaxis to be discerned. Spatial preference has been noted for species such as *M. incognita*, which migrates to root tips of host plants for penetration (Wyss et al., 1992). The results of our experiments with three-day-old soybean seedlings suggest there is no spatial preference on chemotaxis of *H. glycines* (Table 3.2).

Table 3.2. Effect of 3-day-old *H. glycines*-susceptible (cv. Williams 82) and *H. glycines*-resistant (cv. Jack) soybean roots on chemotaxis on *H. glycines* juveniles. Results of root chip experiments at 18 hours. Effect of lane was determined by ANOVA at 18 hours for each of the treatments. Data from the percentage of juveniles migrating to each side of the chip was then analyzed, and the response was rated as either A = attracted, N = neutral response, R = repelled at the $P = 0.05$ level using a Student's paired t-test.

Treatment	Control	Replicates (all lanes)	Total nematodes	*P* value for effect of lane	Outcome (combined lanes)	*P* value for paired t-test	Standard Error
Susceptible	water	16	502	0.8499	A	0.001	3.70
Resistant	water	16	573	0.4183	N	0.90	3.79
Susceptible	Resistant	16	576	0.9845	N	0.21	5.81
Water	water	16	524	0.9253	N	0.11	2.33

Experiments with the root chip were conducted by taking high resolution scans of the chips under controlled conditions over a period of 18 hours. The *H. glycines* J2s tested with the root chip were successfully monitored and analyzed with custom software program for automatic image capture as well as to streamline image processing and analysis. Results from the root chip found *H. glycines* J2s to be attracted to roots of susceptible (cv. Williams 82) soybean across multiple runs. The *H. glycines* J2s were attracted to resistant (cv. Jack) soybean in some runs (Figure 3.5), but this effect was not consistent across runs (Figure 3.6). There was no attraction of *H. glycines* J2 toward susceptible or resistant roots when both were placed on opposite sides of the chip (Figure 3.6). This result is consistent with the findings of Colgrove and Niblack (2005) who reported no differences in *H. glycines* J2 penetration into roots with or without resistance. However, others have reported host and cultivar effects on chemotaxis of plant-parasitic nematodes (Zhao et al., 2000), indicating that this assay might be useful for further host and cultivar preference studies. Additionally, this assay may be useful for testing the effect of seed treatments, particularly systemic compounds, on chemotaxis of different nematode species. Recently, Hida et al. (2015) described a microfluidic chip that measured chemotaxis of *M. incognita* J2s to KNO 3. There are similarities and differences between both their approaches and ours. Both chips were constructed from PDMS using soft lithography, incorporate microscale filters to form concentration gradients of a chemical, and require the J2s to migrate to a final resting chamber. The chip described by Hida et al. (2015) is a two-dimensional design that requires the nematodes to migrate through a channel before making a choice towards or away from a test chemical. Our chips require the J2s to make an immediate choice to the right or left. Additionally, Hida et al. (2015) used agarose gel as the migration medium, and our chips

were filled with sterile distilled water. The chips described in Hida et al. (2015) as well as in this paper can aid in understanding plant-parasitic nematode chemotaxis.

There are some limitations of the microfluidic chips presented in this paper. As with other *in vitro* assays, it is difficult to ascertain if the results obtained from laboratory assays can be reliably reproduced in the field setting. For instance, the chemotactic gradients established in our assays may be different from those in natural soil environment, since these gradients may be altered by abiotic or biotic factors in the soil. In this context, Spence et al. (2008) cautioned that while laboratory assays can be useful in studying plant-parasitic and entomopathogenic nematodes, the effects observed in an *in vitro* assay can only provide predictions of field-relevant interactions and that extrapolations of laboratory results are often unjustified. Advances in replicating the soil environment within chemotactic assays may aid in providing better predictions of field-relevant interactions (Lockery et al., 2008). Additionally, microfluidic chips constructed from PDMS are unable to test the chemotaxic effects of hydrophobic compounds without additional fabrication steps (Mukhopadhyay, 2007; Toepke and Beebe, 2006). Our chips rely on diffusion of compounds in water, and hydrophobic compounds would be immiscible and tend to get adsorbed along the PDMS sidewalls. In order to use PDMS microfluidic chips with hydrophobic compounds, the chips must be coated with a suitable hydrophobic coating (e.g. Teflon, paralyne) to prevent the hydrophobic compound from being adsorbed to the PDMS material.

Microfluidic technology offers an attractive alternative to agar-based plate assays for studying chemotaxis of plant-parasitic nematodes. Our results demonstrate the direct benefits of microfluidic chips for testing a large number of nematodes, creating a controlled chemical gradient for long time periods, running concurrent, parallel experiments on the same chip,

monitoring root-nematode interactions, and using automated imaging and tracking tools during the experiments. The use of microfluidic chips paired with image capture tools can provide a wealth of information about nematode behavior. Increased adoption, improvements, and modifications of microfluidic chips to answer specific research questions may result in greater data granularity and faster screening of the chemotactic effects of chemicals and root exudates on plant-parasitic nematodes.

Acknowledgements

This work was partially supported by funding from the National Science Foundation CBET-1150867 to S.P. This material is based upon work supported by the National Science Foundation I/UCRC, the Center for Arthropod Management Technologies under Grant No. IIP-1338775 and by industry partners. We are grateful for the support and advice provided by Dr. Bryony Bonning (Iowa State University) and the Center's advisory board members, and Jared Jensen for assistance in research and manuscript preparation.

References

[1] Beebe, D.J., Mensing, G.A., and Walker, G.M. 2002. Physics and applications of microfluidics in biology. Annu. Rev. Biomed. Eng. 4:261-286

[2] Carr, J.A., Parashar, A., Gibson, R., Robertson, A.P., Martin, R.J., and Pandey, S. 2011. A microfluidic platform for high-sensitivity, real-time drug screening on *C. elegans* and parasitic nematodes. Lab Chip. 11:2385-2396.

[3] Castro, C. E., Belser, N. O., McKinney, H. E., and Thomason, I. J. 1990. Strong repellency of the root knot nematode, *Meloidogyne incognita* by specific inorganic ions. J. Chem. Ecol. 16:1199-1205.

[4] Chen, B., Deutmeyer, A., Carr, J., Roberts, A. P., Martin, R. J., and Pandey, S. 2011. Microfluidic bioassay to characterize parasitic nematode phenotype and antihelminthic resistance. Parasitology 138:80-88.

[5] Colgrove, A.L., and Niblack, T.L. 2005. The effect of resistant soybean on male and female development and adult sex ratios of *Heterodera glycines*. J. Nematol. 37:161-167.

[6] Curtis, R. H. C. 2008. Plant-nematode interactions: Environmental signals detected by the nematode's chemosensory organs control changes in the surface cuticle and behaviour. Parasite 15:310-316.

[7] Devine, K.J., and Jones, P.W. 2003. Investigations into the chemoattraction of the potato cyst nematodes *Globodera rostochiensis* and *G. pallida* towards fractionated potato leachate. Nematology 5:65-75.

[8] Dusenbery, D. B. 1983. Chemotactic behavior of nematodes. J. Nematol. 15:168-173.

[9] Faghihi J., and Ferris J. M. 2000. An efficient new device to release eggs from *Heterodera glycines*. J. Nematol. 32:411-413.

[10] Hida, H., Nishiyama, H., Sawa, S., Higashiyama, T., and Arata, H. 2015. Chemotaxis assay of plant-parasitic nematodes on a gel-filled microchannel device. Sensors Actuat. B 221:1483-1491.

[11] Hiltpold, I., Jaffuel, G., and Turlings, T.C.J. 2014. The dual effects of root-cap exudates on nematodes: from quiescence in plant-parasitic nematodes to frenzy in entomopathogenic nematodes. J. Exp. Bot. 66:421-424.

[12] Hu, Y., Zhang, W., Zhang, P., Ruan, W., and Zhu, X. 2013. Nematicidal activity of chaetoglobosin A produced by *Chaetomium globosom* NK102 against *Meloidogyne incognita*. J. Agric. Food Chem. 61:41-46.

[13] Huettel, R.N., and Jaffe, H. 1987. Attraction and behavior of Heterodera glycines, the soybean cyst nematode, to some biological and inorganic compounds. Proc. Helminthol. Soc. Wash. 54:122-125.

[14] Hussey R. S., and Barker K. R. 1973. A comparison of methods of collecting inocula of *Meloidogyne spp.*, including a new technique. Plant Dis. Rep. 57:1025–1028.

[15] Jenkins, W. R. 1964. A rapid centrifugal-flotation technique for separating nematodes from soil. Plant Dis. Rep. 48:692.

[16] Kerry, B. R. 2000. Rhizosphere interactions and the exploitation of microbial agents for the biological control of plant-parasitic nematodes. Annu. Rev. Phytopathol. 38:423-441.

[17] Le Saux, R., and Quénéhervé, P. 2002. Differential chemotactic responses of two plant-parasitic nematodes, *Meloidogyne incognita* and *Rotylenchulus reniformis*, to some inorganic ions. Nematology 4:99-105.

[18] Levene, B.C., Owen, M.D., and Tylka, G.L. 1998. Influence of herbicide application to soybeans on soybean cyst nematode egg hatching. J. Nematol. 30:347-352.

[19] Linsell, K.J., Riley, I.T., Davies, K.A., and Oldach, K.H. 2014. Characterization of resistance to *Pratylenchus thornei* (nematoda) in wheat (*Triticum aestivum*): Attraction, penetration, motility, and reproduction. Phytopathology 104:174-187.

[20] Liu, B., Hibbard, J.K., Urwin, P.E., and Atkinson, H.W. 2005. The production of synthetic chemodisruptive peptides *in planta* disrupts the establishment of cyst nematodes. Plant Biotech. J. 3:487-496.

[21] Lockery, S.R., Lawton, K.J., Doll, J.C., Faumont, S., Coulthard, S.M., Thiele, T.R., Chronis, N., McCormick, K.E., Goodman, M.B., and Pruitt, B.L. 2008. Artificial dirt: microfluidic substrate for nematode neurobiology and behavior. J. Neurophysiol. 99:3136-3143.

[22] Lockery, S.R., Hulme, S.E., Roberts, W.M., Robinson, K.J., Laromaine, A., Lindsay, T.H., Whitesides, G.M., and Weeks, J.C. 2012. A microfluidic device for whole-animal drug screening using electrophysiological measures in the nematode *C. elegans*. Lab Chip 12:2211-2220.

[23] Mukhopadhyay, R. 2007. When PDMS isn't the best. What are its weaknesses, and which other polymers can researchers add to their toolboxes? Anal. Chem. 79:3249-3253.

[24] Njus, Z., Feldmann, D., Brien, R., Kong, T., Kalwa, U., and Pandey, S. 2015. Characterizing the effect of static magnetic fields on *C. elegans* using microfluidics. Adv. Biosci. Biotechnol. 6:583-591.

[25] Papademetriou, M. K., and Bone, L. W. 1983. Chemotaxis of larval soybean cyst nematode, Heterodera glycines race 3, to root leachates and ions. J. Chem. Ecol. 9:387-396.

[26] Parashar, A., and Pandey, S. 2011. Plant-in-chip: Microfluidic system for studying root growth and pathogenic interactions in *Arabidopsis*. Appl. Phys. Lett. 98:263703.

[27] Perry, R. N. 1996. Chemoreception in plant-parasitic nematodes. Annu. Rev. Phytopathol. 34:181-199.

[28] Peytavi, R., Raymond, F.R., Gagné, D., Picard, F.J., Jia, G., Zoval, J., Madou, M., Boissinot, K., Boissinot, M., Bissonnette, L., Ouellette, M., and Bergeron, M.G. 2005. Microfluidic device for rapid (< 15 min) automated microarray hybridization. Clin. Chem. 51:1836-1844.

[29] Prot, J. C. 1979. Influence of concentration gradients of salts on the behaviour of four plant parasitic nematodes. Revue de Nématologie 2:11-16.

[30] Reynolds, A. M., Dutta, T. K., Curtis, R. H. C., Powers, S. J., Gaur, H. G., and Kerry, B. R. 2010. Chemotaxis can take plant-parasitic nematodes to the source of a chemo-attractant via the shortest possible routes. J. R. Soc. Interface 8:568-577.

[31] Riddle, D. L., and Bird, A. F. 1985. Responses of the plant parasitic nematodes *Rotylenchulus reniformis*, *Anguina agrostis* and *Meloidogyne javanica* to chemical attractants. Parasitology 91:185-195.

[32] Saldanha, J.N., Parashar, A., Pandey, S., and Powell-Coffmann, J.A. 2013. Multiparameter behavioral analyses provide insights into mechanisms of cyanide resistance in *Caenorhabditis elegans*. Toxicol. Sci. 135:156-168.

[33] Sasser, J.N., and Freckman, D.W. 1987. A world perspective on nematology: The role of the society. In: Vistas on Nematology. Edited by Veeck J.A. and Dickson D.W. Hyattsville MD: Society of Nematologists:7-14.

[34] Shinya, R., Chen, A., and Sternberg, P.W. 2015. Attraction and mating in *Bursaphelenchus okinawaensis* and *B. xylophilus*. 2015. J. Nematol. 47:176-183.

[35] Sikora, R.A. 1992. Management of the antagonistic potential in agricultural ecosystems for the biological control of plant parasitic nematode. Annu. Rev. Phytopathol. 30:245-270.

[36] Spence, K.O., Lewis, E.E., and Perry, R.N. 2008. Host-finding and invasion by entomopathogenic and plant-parasitic nematodes: evaluating the ability of laboratory bioassays to predict field results. J. Nematol. 40:93-98.

[37] Tefft, P.M., and Bone, L.W. 1985. Plant-induced hatching of eggs of the soybean cyst nematode *Heterodera glycines*. J. Nematol. 17:275-279.

[38] Toepke, M.W., and Beebe, D.J. 2006. PDMS absorption of small molecules and consequences in microfluidic application. Lab Chip 6: 1484-1486.

[39] Wang, C., Bruening, G., and Williamson, V. M. 2009. Determination of preferred pH for root-knot aggregation using pluronic F-127 gel. J. Chem. Ecol. 35:1242-1251.

[40] Wang, C., Lower, S., and Williamson, V.M. 2009. Application of Pluronic gel to the study of root-knot nematode behavior. Nematology 11:453-464.

[41] Wong, A. T., Tylka, G. L., and Hartzler, R. G. 1993. Effects of eight herbicides on in vitro hatching of *Heterodera glycines*. J. Nematology 25:578-584.

[42] Wuyts, N., Swennen, R., and de Waele, D. 2006. Effects of plant phenylpropanoid pathway products and selected terpenoids and alkaloids on the behaviour of the plant-parasitic nematodes *Radopholus similis*, *Pratylenchus penetras*, and *Meloidogyne incognita*. Nematology 8:89-101.

[43] Wyss, U., Grundler, F.M.W., and Munch, A. 1992. The parasitic behaviour of second-staged juveniles of *Meloidogyne incognita* in roots of Arabadopsis thaliana. Nematologica 38:98-111.

[44] Zhao, X., Schmitt, M., and Hawes, M.C. 2000. Species-dependent effect of border cell and root tip exudates on nematode behavior. Phytopathology 90:1239-1245.

[45] Zuckerman, B.M., and Jansson, H. 1984. Nematode chemotaxis and possible mechanisms of host/prey recognition. Ann. Rev. Phytopathol. 22:95-113.

CHAPTER 4

MICROFLUIDIC PAPER-BASED ANALYTIC DEVICES AS BEHAVIORAL TESTBEDS FOR *CAENORHABDITIS ELEGANS*

Abstract

Today, the area of point-of-care diagnostics is synonymous with paper microfluidics where cheap, disposable, and on-the-spot detection toolkits are being developed for a variety of chemical tests. In this work, we demonstrate novel microfluidic paper-based analytical devices (μPADs) with suspended membranes to study the behavior of a small model animal, *Caenorhabditis elegans.* The μPADs presented here are made in paper or plastic substrate, and have certain advantages compared to standard agarose plates or polymeric microfluidic devices for *C. elegans* studies. We discuss different schemes of μPAD fabrication and testing using agarose and Pluronic gel, as well as methods of loading, visualizing, and transferring worms to suspended gel membranes. As a sample run with levamisole, we show that drug testing on these μPADs is less complicated and more user-friendly than those in polymeric microfluidic devices.

Introduction

In recent years, microfluidic devices fabricated on low-cost, disposable substrates such as paper, plastic, and textiles have gained considerable interest with applications in resource- and power-limited settings. The acronym μPADs (i.e. microfluidic paper-based analytical devices) represents devices where microfluidic networks are realized in paper substrates by patterning hydrophobic and hydrophilic regions within them. The hydrophobic barriers restrict the fluid flow within pre-specified areas of the cellulose paper while the fluid spreads in the hydrophilic

regions by capillary action. Today, this simple concept of designing fluid handling using hydrophobic/hydrophilic patterns has evolved into a promising μPAD technology that could revolutionize the fields of quantitative screening and disease diagnostics.

It was realized early on that the major drivers of μPAD technology are the material/processing cost per device and the capability of mass manufacturing. As such, a variety of low-cost, printing techniques were explored on paper substrates that require minimalistic handling steps. Wax printing is probably the most direct ways of fabricating μPAD structures [1-5]; however other μPADs fabrication methods have been demonstrated that require additional chemical processing or machining steps (e.g. inkjet printing, wet etching, laser treatment, screen printing, and flexography) [6-12]. Compared to other methods, wax printing of μPADs is also appealing because it involves simple fabrication steps (i.e. printing using a commercial wax printer and baking on a hot plate), uses inexpensive and chemically-inert materials (i.e. paper and wax), and is environmentally friendly (i.e. no use of organic solvents). There is no need for clean room facilities and devices can be performed on-site by personnel with minimal training. The next directions of research in μPAD fabrication technologies will explore topics such as using new bioactive substrates with embedded and functionalized nanoparticles, printing biomolecules directly on testing zones, integrating multiple substrate layers into functional 3D structures, and incorporating control components to guide and regulate fluid flow in both lateral and longitudinal directions [13-17].

A number of μPAD applications have been reported in areas of medical diagnostics, environmental monitoring, and food safety. Here an unknown sample reaches the detection zone containing known reagents that triggers a certain biochemical reaction. This, in turn, generates an output signal that is detected by optical, fluorescent, chemiluminescent or electrochemical

techniques. Optical or colorimetric detection method remains the popular choice where low-cost, portable, hand-held detectors can record visual changes in the biochemical reaction. Various clinically-relevant analytes (e.g. glucose, protein, and alanine aminotransferase) have been analyzed from biological fluids (e.g. blood, serum or urine) using enzymatic, color-based detection with the possibility of imaging and transmitting the results by telemetry (using smartphones, cameras or scanners) [18-20]. Colorimetric detection of protein and DNA-based biomarkers have been demonstrated where antibodies immobilized on chemically-modified μPADs captured the targeted antigens, producing a distinct color change in the colorimetric reagent. Various attempts have been made to improve the sensitivity and lower the limit of colorimetric detection, such as using chemically-modified paper to reduce surface fouling [21], incorporating functionalized nanoparticles with high molar absorptivity to select biomarkers [22], and modifying the smartphone's camera system [23] to permit testing even under ambient lighting conditions.

As new and elegant applications of μPADs emerge, it is intriguing to consider the possibility of using paper-based devices for small animal studies, particularly those involving nematodes or worms. *Caenorhabditis elegans* is an important, small animal model organism in neuroscience and developmental biology for a variety of experiments (e.g. on gene regulation, metabolism, ageing, cell signaling, chemical screening, and drug discovery). Compared to mammalian counterparts, *C. elegans* are well-suited for high-throughput, large scale biological experiments because of the ease to culture on a diet of *Escherichia coli*, ability to grow from an egg to an adult within three days, and capacity to produce over 300 progeny. Polymer-based microfluidics has emerged as an enabling technology for *C. elegans* research where on-chip automation has streamlined the steps of worm immobilization, transport, screening, sorting,

and/or tracking. For instance, in the field of pharmacology and drug discovery, it is possible to capture individual worms within single liquid droplets in a microfluidic chip and simultaneously screen them for a range of drug concoctions [24][25]. In the field of neurobiology, individual worms can be rapidly immobilized in microfluidic chambers where laser nanosurgery can be performed on their axons [26]. These and many more examples show how microfluidics can be leveraged to create and manipulate worms and their microenvironments, with the ability of large-scale genetic and behavioral screening. Most of these worm chips necessitate the use of multi-layer device fabrication, sophisticated pumps and valve operations, and advanced programming skills to control and synchronize system operations.

However, technological advancements in polymeric microfluidics have yet to reach a significant number of *C. elegans* laboratories. One of main hurdles in the wide-scale adoption of polymeric microfluidics by biologists is the need for skilled engineers to design, fabricate, and test the microfluidic devices. The specific needs of a biological problem may demand tailored engineering solutions. But it may be challenging to foster sustained collaborations between microfluidic engineers and worm biologists due to inherent gaps (e.g. in knowledge, expectations, deliverables) between the two disciplines. The cost of chemicals and consumables in microfluidics can become expensive when a regular inventory of devices is needed to test the biological hypotheses. Because of the above reasons, routine *C. elegans* experiments are still performed on Petri dish and well-plates that offer design simplicity, experimental flexibility, standardized manufacturing, easily accessibility, and disposability.

Here we attempt to gauge whether paper-based microfluidic technology can be applied for worm biology, and if so, for what specific applications. The following reasons justify the need of paper-based microfluidics for worm biology. Firstly, paper is a ubiquitous, easily-available, and

disposable substrate that is far cheaper than standard polymers used in conventional microfluidics. Secondly, the fabrication procedure of paper-based devices is straightforward and a variety of cost-effective printing methods can be easily adopted in biological laboratories. Thirdly, there is no requirement of external instrumentation as paper-based devices are designed to work passively. However, with paper-based devices, it is not possible to achieve the resolution of device dimensions or the fluid transport capabilities seen in polymeric microfluidic devices. Thus it is certainly possible to utilize the benefits of paper-based devices for certain applications in worm biology where low cost and easy accessibility are of critical importance.

In this work, we present a family of paper- and plastic-based microfluidic devices for *C. elegans* experiments. The paper and plastic substrates are machine cut and agar membranes are suspended on the excised regions of the substrates. The suspended agar membranes serve as simple, semi-transparent platforms for observing and imaging worm behavior over extended times; both at single and population levels. We show schemes of subjecting the worms to a drug chemical and characterizing the dose response using a custom object tracking program. We also illustrate ways of transferring worms from one membrane to a Petri dish or another membrane without the need for picking individual worms. Lastly, we show a method of z-stacking where two worm populations, each on a separate membrane, is imaged simultaneously by altering the focus of the microscope lens. In short, we have shown that agar membranes suspended in paper and plastic substrates are a simple and feasible platform for worm culture, handling, screening, and imaging.

Materials and Methods

Device Fabrication

Two substrates are used for fabricating the open microfluidic devices: *paper* and *plastic*. The fabrication steps are illustrated in Figure 4.1. In general, both paper and plastic substrates are made hydrophobic by the use of wax barrier or tape. Circular areas are excised in the substrates that eventually support a thin membrane of agarose or Pluronic gel. The membrane forms the open microfluidic device on which *C. elegans* behavioral dynamics will be observed.

The paper-based microfluidic device is fabricated using Whatman™ chromatography paper (Sigma Aldrich). Initially, the device design is drawn in Adobe Illustrator™ and printed on the chromatography paper using a wax printer (Xerox Colorcube™). The paper is placed on a hot plate at 130°C with the wax pattern facing upwards. After 15 seconds, the paper is removed from the hot plate and allowed to cool at 23°C. A biopsy punch (Miltex) is used to excise a circular area within the wax pattern, which is then lowered horizontally onto a 100 mL droplet of 2% liquid agar (maintained at 80°C). When the interior of the wax pattern has come in contact with the liquid agar, the paper is lifted horizontally. This creates a suspended membrane of liquid agar in the circular excised area. This agar membrane is hydrated with 15 μL of M9 buffer and placed in a sealed, humidified petri dish.

The plastic-based device is fabricated using 8.5″ × 11″ transparency sheets (Staples) and packaging tape (Scotch™). Initially, the device design is drawn in Silhouette Cameo Studio™. Tape is applied to both sides of the transparency sheet and multiple circular patterns are excised using a Silhouette Cameo™ electronic cutter. The transparency sheet is vertically dipped into a liquid solution of 11.5% Pluronic gel and then lifted upwards out of the solution. This creates

Pluronic gel membranes in the excised areas of the transparency sheet. The gel membranes are hydrated with 15 µL of M9 buffer and placed in a sealed, humidified petri dish.

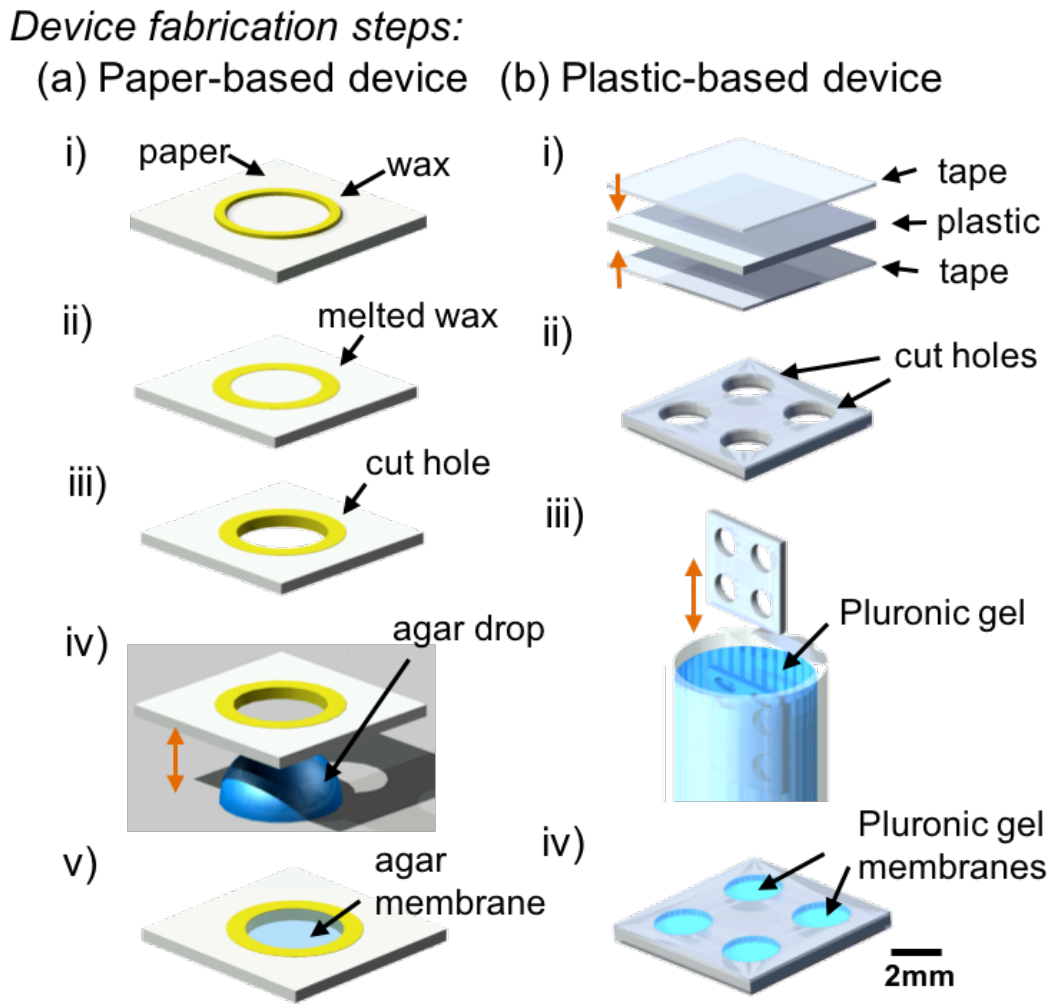

Figure 4.1. Fabrication of suspended gel membranes on paper and plastic substrates. (a) Paper-based device: A wax pattern is printed on chromatography paper and melted on a hot plate to create a hydrophobic barrier (i-ii). A circular pattern is excised using a biopsy punch to create a cut hole (iii). The paper is lowered onto a 100 mL droplet of 2% liquid agar and gently lifted, resulting in an agar membrane in the cut hole (iv-v). (b) Plastic-based device: A plastic sheet is taped on both sides and multiple circular patterns are excised using an automated design cutter to create cut holes (i-ii). The excised plastic sheet is vertically immersed into a 11.5% solution of Pluronic gel and removed, resulting in suspended membranes of Pluronic gel within the cut holes (iii-iv).

Experimental Setup

Previously wild-type *C. elegans* are grown on standard Nutrient Growth Media (NGM) agar plates with *Escherichia coli* OP50 at 20°C. The petri dish housing the open microfluidic devices (paper-based or plastic-based) is placed on the stage of a Leica MZ16 stereozoom microscope at an ambient temperature of 22°C. Two methods were attempted to put worms on the membrane devices: pipetting worm droplets and picking/insertion of worms. In the pipetting approach, individual worms are collected in a droplet of M9 buffer, and pipetted onto the agar membrane (Figure 4.2a). The worms appear to swim in the liquid droplet but, as the excess buffer is absorbed by the agar, the worms start to crawl on the agar surface. In the picking/insertion approach, individual worms are picked by a platinum picker. The picker is plunged through the Pluronic gel and extracted out, leaving behind the worms within the gel (Figure 4.2b). Based on our trials, the pipetting approach is recommended for paper-based devices consisting of agar membranes, whereas the picking/insertion approach is well-suited for plastic-based devices consisting of Pluronic gel membranes. This is because any physical contact from the sterilized wire may produce undesired irregularities on the agar membrane surface, while the Pluronic gel membrane is insensitive to any physical contact or penetration by the picker.

After the placement of the *C. elegans* on the gel membranes, the worms are observed under the microscope to ensure that they appear healthy and mobile. After a wait time of around 3 minutes, worm movement is recorded for the next 3 minutes at 10 frames per second using a QImaging 12 bit color camera. In the case of drug testing, 5 μL of levamisole solution (in M9 buffer) is added on top of the membrane and the worm response is recorded.

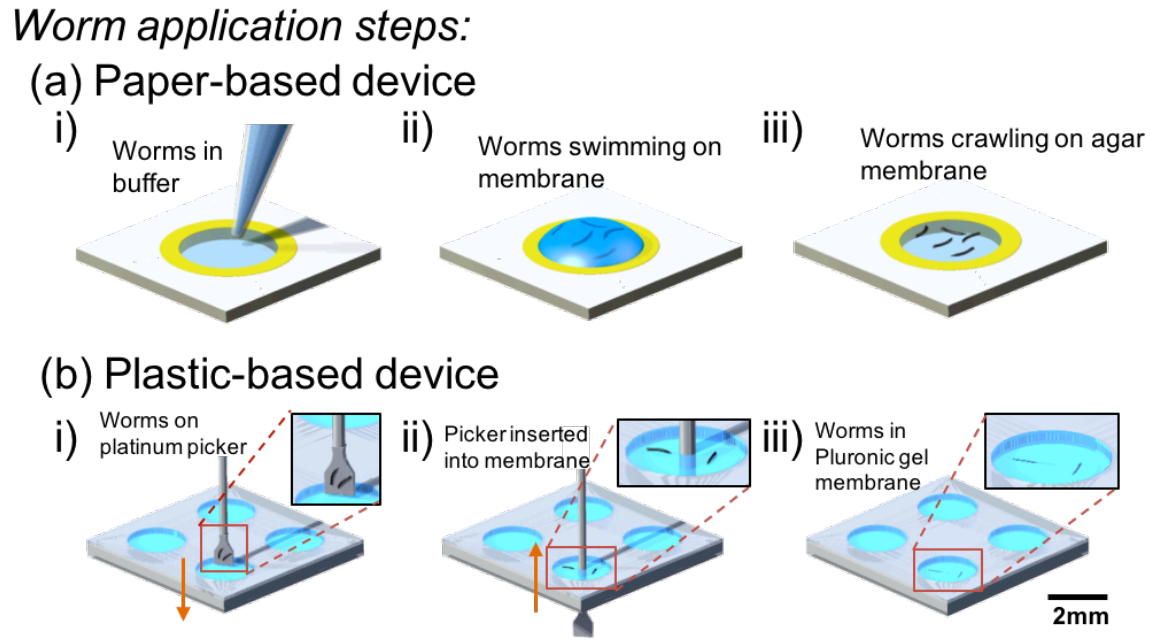

Figure 4.2. Two methods of putting *C. elegans* on suspended gel membranes. (a) Pipetting worm droplets on agar membranes: A liquid droplet containing worms is pipetted onto the agar membrane and the worms swim in the droplet (i-ii). The excess liquid is allowed to be absorbed into the agar and the worms appear crawling on the agar surface (iii). (b) Picking and inserting single worms in Pluronic gel: A platinum picker is used to pick single worms, which is then plunged through the Pluronic gel membrane (i-ii). Upon extracting back the picker, the worms remain within the Pluronic gel (iii).

Data Collection and Analysis

The videos were run through a custom worm tracking program that identifies individual worms and tracks their positional coordinates through a series of image processing steps. Initially, the worm tracking program starts by identifying circular membranes present in the fabricated devices. This step helps to limit the observed area, thereby minimizing the false identification of worm-shaped objects as well as speeding up the processing time. In order to identify the circular membranes, we used the Circular Hough Transform (CHT). The CHT is a popular algorithm for finding circular shapes in images due to its ability to handle occlusions

(overlapping or connected areas) and non-uniform illumination. We screen and qualify pixels with high gradients as candidate pixels. These candidate pixels are then used to vote in a circular pattern of a user specified radius range forming an accumulator array. Clusters that arise in the accumulator array correspond to centers of circles present in the image. Since the circles identified from the CHT algorithm are not perfect circles, the edges of the found circles need to be refined. To refine the edges, the found circles are scaled to the original size of the image and used as an initial mask input to an Active Contour Algorithm (ACA). The ACA calculates gradient field lines, which point towards edges in the image. The edge pixels of the circles are then directed into these edges, thereby refining the edges of the found circle.

Once the circular membranes are identified, the worms need to be identified and segmented from the video frames. For this, the averaging method is often used where the background image is generated by averaging a number of video frames together. Any moving objects automatically average out. The background image is subsequently subtracted from the video frames to identify the moving object. However, this averaging method is not capable to of detecting sedentary worms within a video as they become part of the background. In order to identify and segment both mobile and sedentary worms from the background, a local thresholding technique is used. A window size of 100 × 100 pixels is scanned over the frame image and any pixels that are less than 90% of the average brightness of the window are set to white. This local thresholding approach is able to detect all worms (both moving and immobile) even against a non-uniform lighting background. Later, a morphological classifier is used to remove any segmented sections are not shaped as worms. We defined sections as worm-shaped if the ratio of the perimeter length to the area of the section is in the range 0.5 - 0.6 $pixel^{-1}$ and if

the area of the section was 200 - 300 pixels. These values can be altered depending on the size and shape of a different nematode.

After the worms are segmented from the video, a minimal area-bounding box is fitted around each worm. The center point of the bounding box is considered the centroid location of the worm, which is tracked throughout the video and combined into a complete path. If multiple worms occlude with each other, the area of bounding box becomes greater than 300 pixels, and the paths are terminated until the worms resume their separate tracks. The track data is reported in the form of a Microsoft Excel workbook for individual worms. Each workbook consisted of the centroid location of the worm and instantaneous velocity at each time point. The velocity is calculated by measuring the distance moved by the worm's centroid between successive time points and dividing by the video frame rate.

Results

By the two methods described in Figure 4.2, worms are put on paper- or plastic based devices. Figure 4.4a(i) illustrates the motion of a single *C. elegans* on the agar membrane of a paper-based device. Under a light microscope, the appearance of agar membrane is clear and the paper substrate is dark in color. The worm on the agar membrane is also easily identifiable by the worm tracking program that eventually produces the centroid locations of the animal over the 3-minute length of the video (colored in red). Figure 4.4(ii) shows the velocity of the centroid location for a representative worm that is crawling on an agar membrane with M9 buffer. Similarly, worms can be put on and tracked on plastic-based devices. Figure 4.4b(i) shows four Pluronic gel membranes; each housing a single *C. elegans* in M9 buffer. The appearance of worms swimming in the Pluronic gel membranes is not visually as clear as those crawling on

agar membranes (shown in Figure 4.4a(i)). However, the worm tracking program is accurately able to identify the worms from the background and track the centroid locations of the four worms (colored in red, yellow, light blue, deep blue). Figure 4.4b(ii) shows the centroid velocities of the four representative worms that were recorded swimming in the Pluronic gel membranes over a 3-minute time period.

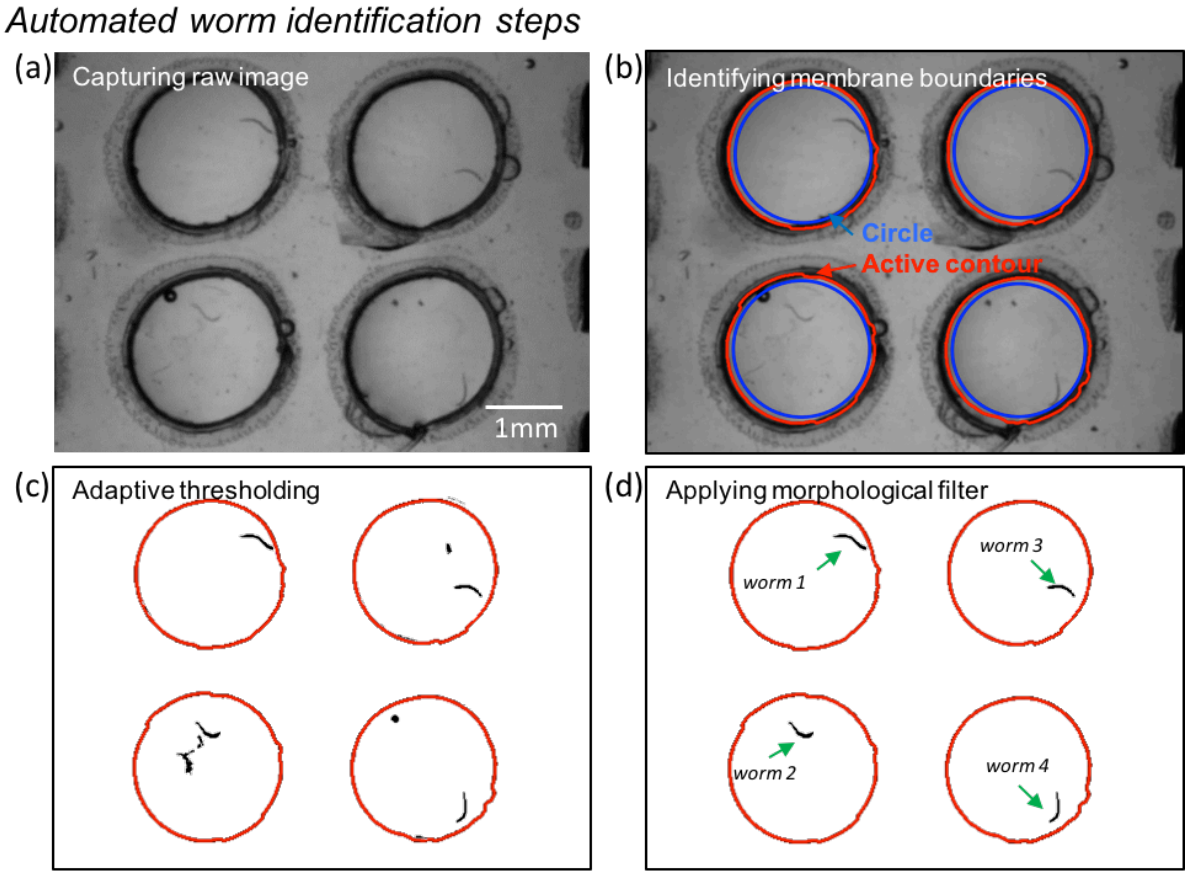

Figure 4.3. Worm tracking program. a) Original image of the plastic-based device with four suspended membranes, each housing a single worm. b) Circular membranes found by the Circular Hough Transform are illustrated in blue. Edges of the identified circles refined using the Active Contour Algorithm are shown in red. c) Sections are segmented out using an adaptive threshold with a window size of 100 x 100 pixels and a percentage of 90%. d) Using a morphological filter, specific sections are removed that do not fit within a certain threshold (area of 200 – 300 pixels; perimeter to area ratio of 0.5 – 0.6 pixels^{-1}). Arrows point to the four worms identified after the final step.

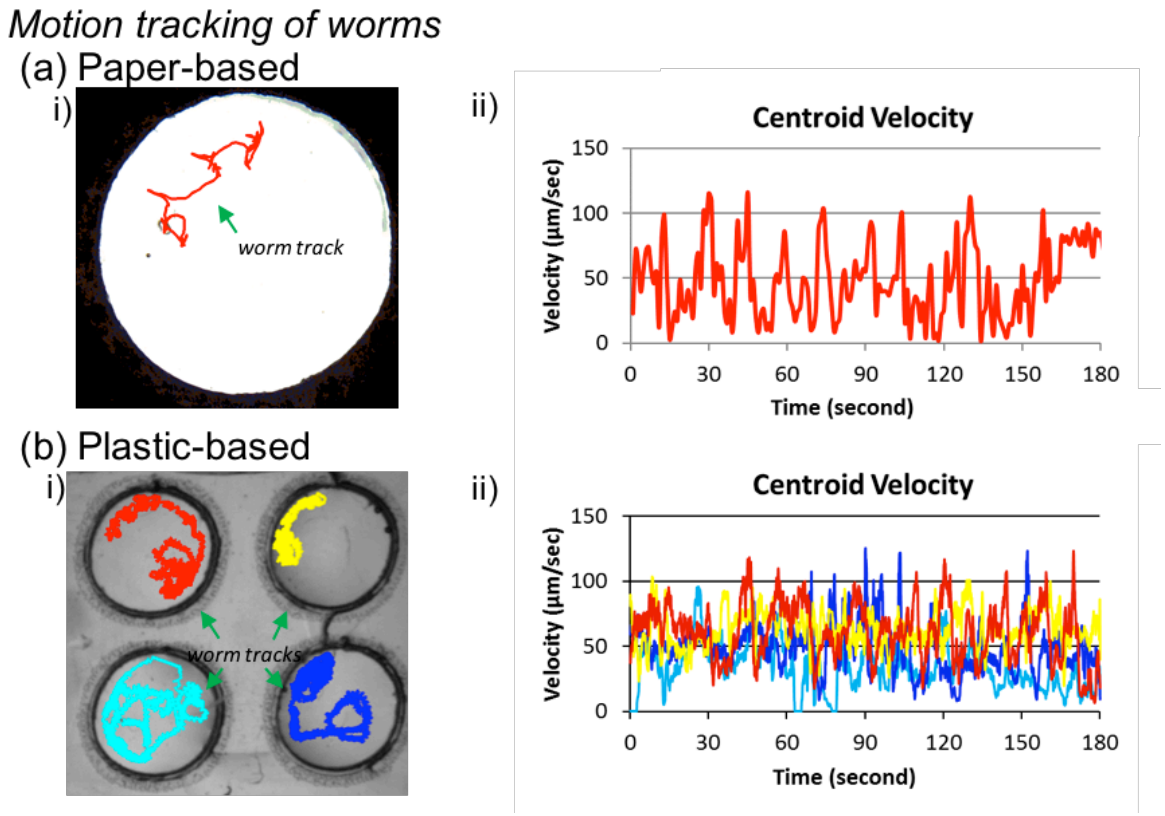

Figure 4.4. Real-time worm tracking on paper and plastic-based devices. (a) The track of a *C. elegan* crawling on an actual paper-based device is illustrated in red. (b) Velocity plot of a representative worm's centroid location is shown over the span of the 3 minutes in M9 buffer. (c) The tracks of four *C. elegans* swimming in individual plastic-based devices are illustrated. (d) Velocity plots of the four representative worms' centroid locations are shown over the course of the 3 minute in M9 buffer.

While the worms are visually observable on agar membranes or within Pluronic gel membranes, the worm tracking program clearly helps to track the physical location of the worm as a function of time. The location tracking data can then be used to calculate parameters related to behavioral traits such as attraction, aversion, toxicity, and social effects. Furthermore, it is also possible to extend the location tracking of a single worm to multiple worms on the same membrane and track individual worms simultaneously (data not shown). This, however, works

best for less than four worms per membrane device because more worms on a limited surface area lead to more collisions and shorter tracks.

One of the most important applications of microfluidic devices in the *C. elegans* community is the screening of different chemicals and drugs for their relative toxicity. Here we demonstrate the use of the proposed devices to test the *C. elegans* response to an anthelmintic drug, levamisole. A certain concentration of levamisole is prepared beforehand in M9 buffer and dropped on the suspended agar or Pluronic gel membranes. Individual worms are put on the membranes, allowed to acclimatize for 3 minutes, and then recorded for another 3 minutes. For every levamisole concentration, the worm tracking program produces the instantaneous centroid velocities of each worm which are then averaged to give an average centroid velocity (n = 5 – 10 for each concentration tested and control runs). A percent response parameter is calculated by normalizing the average centroid velocity at every levamisole concentration to the control runs. This percent response curves are plotted for paper- and plastic-based devices in Figure 4.5a and Figure 4.5b, respectively. The EC_{50} values (concentration that provokes a response half way between the maximum and minimum response) is 38.46 µM for paper-based devices and is 42.56 µM for plastic-based devices. We believe that the obtained EC_{50} values are quite close to each other, especially considering the fact that the substrate composition is different in the two membrane devices.

We show that the proposed devices with suspended membranes offer an advantage in the relative ease of worm transfer to agar plates or between devices. It is worth mentioning that the process of handling *C. elegans* (i.e. picking, transferring, discarding single or multiple worms) is requires considerable hand-eye coordination and dexterity. When working with worms on agar plates, the animals are observed under a benchtop microscope and a sterilized wire or worm

picker is used to select and pick the worms of interest. In PDMS microfluidic chips, worms are usually accessed in a similar manner through the large ports or reservoirs by pipetting or using a worm picker under a microscope. With the paper- and plastic-based devices, it is possible to transfer worms without the use of worm pickers or microscope.

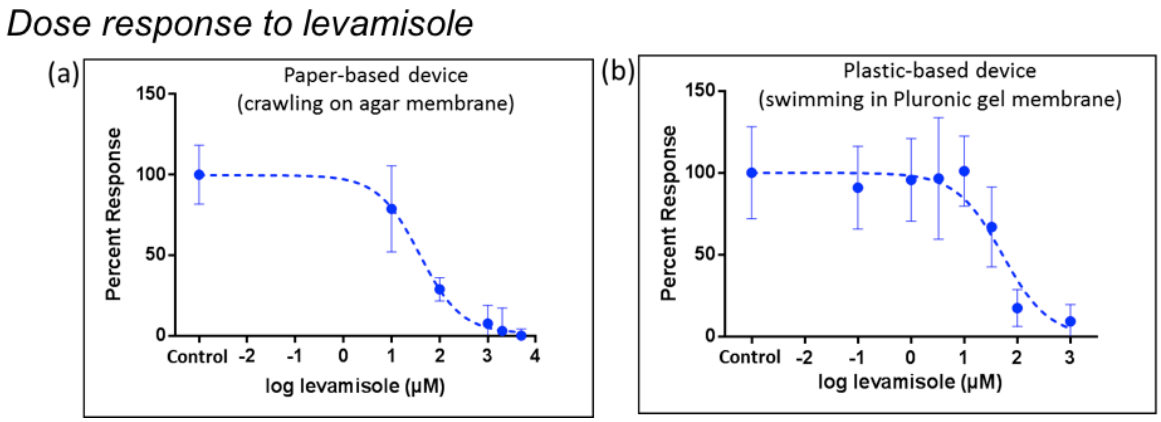

Figure 4.5. Levamisole drug testing of *C. elegans* on suspended gel membranes. Here a desired concentration of levamisole is prepared in M9 buffer and allowed to permeate into the gel membrane. The centroid velocity of individual worms is tracked at real-time and averaged over the entire recording period. The percentage response is calculated by normalizing the averaged centroid velocities from the experimental tests to those from the control tests. (a) Dose response of *C. elegans* crawling on agar membranes in a paper-based device. (b) Dose response of *C. elegans* swimming in Pluronic gel membranes in a plastic-based device.

In Figure 4.6a(i), a paper-based device contains a worm population on an agar membrane. To transfer the worms on an agar plate, the paper-based device is gently lowered on the agar plate as shown in Figure 4.6a(ii). Upon lifting the paper substrate, the membrane remains on the agar plate and the worms are able to crawl away freely (Figure 4.6a(iii)). Using a similar approach, worms in the suspended Pluronic gel can be transferred to an agar plate. Here the four plastic-based devices having worms (Figure 4.6b(i)) are lowered on the agar plate. The Pluronic gel membrane stays on the agar plate while the plastic substrate is discarded (Figure 4.6b(ii)). Thereafter worms are free to crawl on the agar plate (Figure 4.6b(iii)). In both cases, we were

able to transfer all the worms from the membrane devices to the agar plates in 5-6 independent trials for each device.

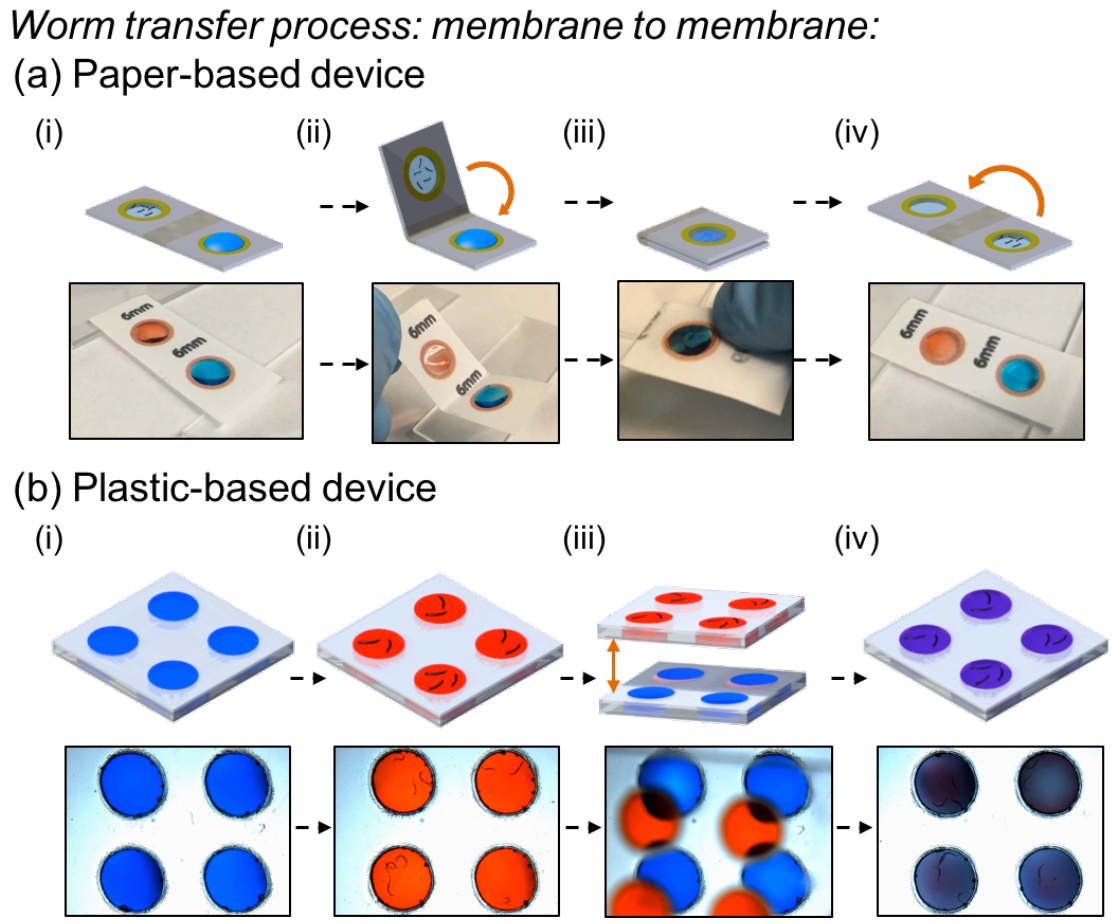

Figure 4.6. Method to transfer *C. elegans* from paper or plastic-based devices to an agar plate. The membranes are colored with a red food dye for visual ease. (a) The paper-based device having a worm population (i) is gently lowered onto the surface of agar plate (ii). When the paper substrate is lifted upwards, its suspended agar membrane detaches and is left on the agar plate (iii). The worms are now free migrate on the agar plate. (b) The Pluronic gel membranes containing worms (i) are lowered onto the agar plate. Once contact is made, the suspended membranes rupture and the worms are transferred to the agar plate (ii). The plastic substrate is removed and the worms are allowed to crawl over the agar plate (iii).

Besides transferring worms to agar plates, it is also possible to transfer worms from one device to another without the use of worm pickers or microscope. In Figure 4.7a(i), two separate paper-based devices are shown; blue membrane represents the fresh device and the red membrane

contains a worm population. As shown in Figure 4.7a(ii-iii), the paper is simply folded in to bring the red membrane in physical contact with the blue membrane. At this instance, the worms are sandwiched in between the two membranes. The paper is then folded out, which causes the worms to remain on the bottom blue membrane (Figure 4.7a(iv)).

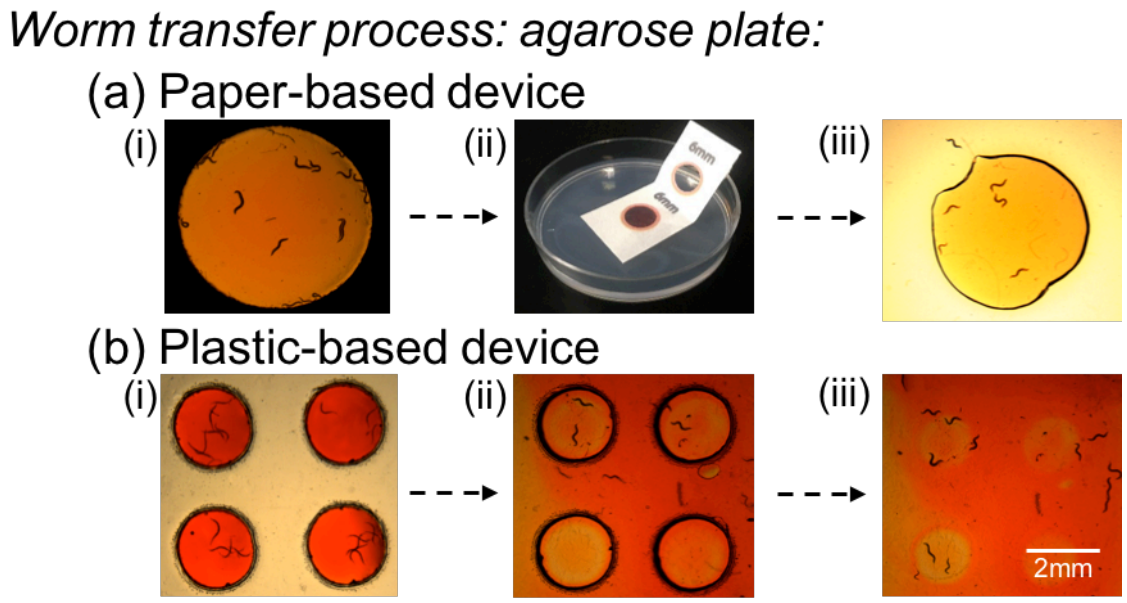

Figure 4.7. Method to transfer *C. elegans* between two paper or plastic-based devices. The worm population is to be transferred from the red-colored membranes to the 'target' blue-colored membranes. (a) To transfer worms between two agar membrane devices, a drop of buffer is added to the target membrane (i). The paper substrate is folded such that red membrane containing the worms is brought in contact with the target membrane (ii-iii). After separating the two membranes the worms will have transferred to the target membrane (iv). (b) To transfer worms between two plastic-based devices with Pluronic gel membranes, the top plastic-based device with red membranes (containing the worms) is aligned and lowered onto the bottom plastic-based device with blue membranes (i-iii) until physical contact is made. The top plastic device is then removed and the worms along with some of the gel have transferred to the bottom plastic device having the blue membrane (iv).

Following a similar approach, worms are transferred from four plastic-based Pluronic gel membranes (colored with red food dye) to four fresh Pluronic gel membranes (colored with blue food dye). In this case, the two plastic substrates are held such that the red and blue membranes

are vertically aligned. Then the plastic substrates are brought in physical contact such that the red and blue membranes mix. The top plastic substrate is now discarded while the worms stay in the membranes of the bottom plastic substrate.

It is also possible to image worms on multiple membranes that are vertically stacked and aligned together. In Figure 4.8a, we stack two Pluronic gel membranes, one on top of the other (spacing = 2 cm). By manually adjusting the focus of the microscope, we are able to change the focal plane and observe the worm population on the desired plane. Three sample planes are illustrated: yellow, red, blue planes. In Figure 4.8b, two representative worms are shown. When the focus is on the top yellow plane, worm 2 (on the upper device) is clearly visible while worm 1 (on the bottom device) appears blurred. As the focus is changed to the bottom blue plane, worm 1 is clearly visible while worm 2 appears blurred. The ability to vertically stack multiple planar devices without increasing the spatial footage and image the worm behavior on each

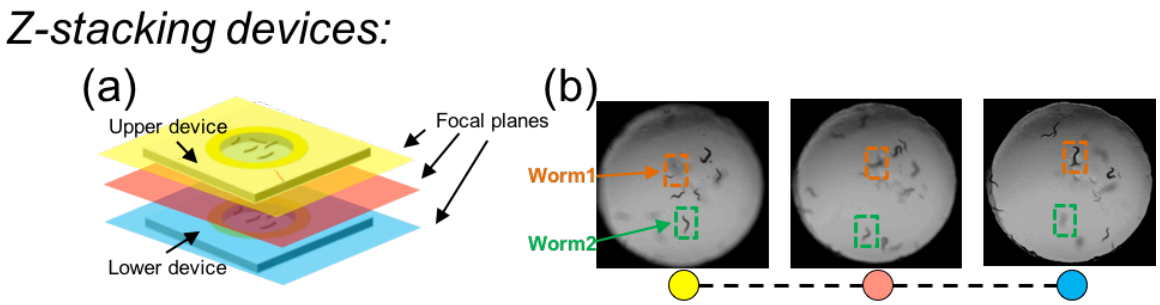

Figure 4.8. Simultaneous imaging of worms on different focal planes by z-stacking separate membranes. (a) The membrane devices are vertically stacked (spacing = 2 cm) and aligned to ensure visibility of all membranes. Then by manually adjusting the focus of the microscope, different focal planes can be independently imaged. (b) Images extracted from a video sequence taken as the focal plane of the microscope is changed from the upper membrane (yellow) through the middle plane (red) to the lower membrane (blue). Two representative worms are highlighted. Initially, as we focus on the upper device, 'worm 2' (on the upper device) is clearly visible while 'worm 1' appears blurred. When we focus to the middle of the two devices, both worms appear blurred. As the focus is now changed to the lower device, 'worm 1' (on the lower device) is clearly visible while 'worm 2' appears blurred.

membrane independently is not possible on agar plate assays. Such vertical stacking of PDMS microfluidic devices would necessitate complicated membrane fabrication and bonding techniques, and may not be practical beyond two/three layers.

Conclusion

In conclusion, paper-based and plastic-based μPADs were developed to facilitate studies on *C. elegans* model organisms. The fabrication methods demonstrated here do not require any photolithography steps, and can thus be easily adopted by non-microfluidic laboratories. There are several other advantages of the μPADs compared to agarose plate or polymeric microfluidic assays, including much lower costs per device, one-step transfer of worm populations from membranes, ability to image multiple membranes simultaneously, and easy chemical accessibility due to its open device structure. A custom software program was created to track the location of the *C. elegans* in recorded videos and extract the movement parameters of the *C. elegans* on the agar and Pluronic gel substrates. The software program incorporates active contour algorithms to successfully identify suspended membranes from background images, and uses adaptive thresholding algorithms to track the movement of worm populations over a time period. We believe the presented paper- and plastic-based devices, along with the worm tracking software program, will be appealing for *C. elegans* biologists who are accustomed to plate assays but are also seeking smarter, cheaper alternative screening assays.

Acknowledgements

The *C. elegan* culture plates were generously donated by Dr. JoAnne Powell-Coffman and Dr. Jenifer Saldanda.

References

[1] Consden, R.; Gordon, A. H.; Martin, A. J. P. (1944) Qualitative analysis of proteins: a partition chromatographic method using paper. Biochemical Journal, 38, 224−232.

[2] Carrilho, E.; Martinez, A. W.; Whitesides, G. M. (2009) Understanding Wax Printing: A Simple Micropatterning Process for Paper-Based Microfluidics Analytical Chemistry 81, 7091−7095.

[3] Zhang, Y.; Zhou, C.; Nie, J.; Le, S.; Qin, Q.; Liu, F.; Li, Y.; Li, J. (2014) Naked-Eye Quantitative Aptamer-Based Assay on Paper Device. Analytical Chemistry, 86, 2005−2012.

[4] Lu, Y.; Shi, W.; Jiang, L.; Qin, J.; Lin, B. (2009) Rapid prototyping of paper-based microfluidics with wax for low-cost, portable bioassay. Electrophoresis, 30, 1497−1500.

[5] Martinez, A. W.; Phillips, S. T.; Butte, M. J.; Whitesides, G. M. (2007) Patterned paper as a platform for inexpensive, low-volume, portable bioassays. Angewandte Chemie International Edition, 46, 1318−1320.

[6] Abe, K.; Suzuki, K.; Citterio, D. (2008) Inkjet-Printed Microfluidic Multianalyte Chemical Sensing Paper. Analytical Chemistry, 80, 6928− 6934.

[7] Yamada, K.; Takaki, S.; Komuro, N.; Suzuki, K.; Citterio, D. (2014) An antibody-free microfluidic paper-based analytical device for the determination of tear fluid lactoferrin by fluorescence sensitization of Tb^{3+}. Analyst, 139, 1637−1643.

[8] Dungchai, W.; Chailapakul, O.; Henry, C. S. (2011) A low-cost, simple, and rapid fabrication method for paper-based microfluidics using wax screen-printing. Analyst, 136, 77−82.

[9] Fenton, E. M.; Mascarenas, M. R.; Lopez, G. P.; Sibbett, S. S. (2009) Multiplex Lateral-Flow Test Strips Fabricated by Two-Dimensional Shaping. Applied Materials and Interfaces, 1, 124−129.

[10] Nie, J.; Liang, Y.; Zhang, Y.; Le, S.; Li, D.; Zhang, S. (2013) One-step patterning of hollow microstructures in paper by laser cutting to create microfluidic analytical devices. Analyst, 138, 671–676.

[11] Olkkonen, J.; Lehtinen, K.; Erho, T. (2010) Flexographically printed fluidic structures in paper. Analytical Chemistry, 82, 10246–10250.

[12] Määttänen, A.; Fors, D.; Wang, S.; Valtakari, D.; Ihalainen, P.; Peltonen, (2011) Paper-based planar reaction arrays for printed diagnostics. Sensors and Actuators B: Chemical, 160, 1404–1412.

[13] Liana, D. D.; Raguse, B.; Wieczorek, L.; Baxter, G. R.; Chuah, K.; Gooding, J. J.; Chow, E. (2013) Sintered gold nanoparticles as an electrode material for paper-based electrochemical sensors. RSC Advances, 3, 8683–8691.

[14] Martinez, A. W.; Phillips, S. T.; Whitesides, G. M. (2008) Three-dimensional microfluidic devices fabricated in layered paper and tape. Proceedings of the National Academy of Sciences of the United States of America, 105, 19606–19611.

[15] Liu, H.; Crooks, R. M. J. (2011) Three-dimensional paper microfluidic devices assembled using the principles of origami. American Chemical Society, 133, 17564–17566.

[16] Martinez, A. W.; Phillips, S. T.; Nie, Z.; Cheng, C.-M.; Carrilho, E.; Wiley, B. J.; Whitesides, G. M. (2010) Programmable diagnostic devices made from paper and tape. Lab on a Chip, 10, 2499–2504.

[17] Fu, E.; Lutz, B.; Kauffman, P.; Yager, P. (2010) Controlled reagent transport in disposable 2D paper networks. Lab Chip, 10, 918–920.

[18] Martinez, A. W.; Phillips, S. T.; Carrilho, E.; Thomas, S. W., III; Sindi, H.; Whitesides, G. M. (2008) Simple telemedicine for developing regions: camera phones and paper-based microfluidic devices for real-time, off-site diagnosis. Analytical Chemistry, 80, 3699–3707.

[19] Yetisen, A. K.; Martinez-Hurtado, J. L.; Garcia-Melendrez, A.; da Cruz Vasconcellos, F.; Lowe, C. R. (2014) A smartphone algorithm with inter-phone repeatability for the analysis of colorimetric tests. Sensors and Actuators, B: Chemical, 196, 156–160.

[20] Oncescu, V.; O'Dell, D.; Erickson, D. (2013) Smartphone based health accessory for colorimetric detection of biomarkers in sweat and saliva. Lab on a Chip, 13, 3232–3238.

[21] Guan, L.; Cao, R.; Tian, J.; McLiesh, H.; Garnier, G.; Shen, W. (2013) A preliminary study on the stabilization of blood typing antibodies sorbed into paper. Cellulose, 21, 717–727.

[22] Shen, L.; Hagen, J. A.; Papautsky, I. (2012) Point-of-care colorimetric detection with a smartphone. Lab on a Chip, 12, 4240– 4243.

[23] Thom, N. K.; Lewis, G. G.; Yeung, K.; Phillips, S. T., (2014) Quantitative Fluorescence Assays Using a Self-Powered Paper-Based Microfluidic Device and a Camera-Equipped Cellular Phone. RSC Advances, 4, 1334–1340.

[24] Shi, W.; Wen, H.; Lu, Y.; Shi, Y.; Lin, B.; Qin, J., (2010) Droplet microfluidics for characterizing the neurotoxin-induced responses in individual Caenorhabditis elegans. Lab on a Chip, 10, 2855-2863

[25] Aubry, G.; Zhan, M.; Lu, H., (2015) Hydrogel-droplet microfluidic platform for high-resolution imaging and sorting of early larval Caenorhabditis elegans. Lab on a Chip, 15(6), 1424-1431.

[26] Fang-Yen, C.; Gabel, C. V.; Samuel, A. D. T.; Bargmann, C. I.; Avery, L., (2012) Laser Microsurgery in Caenorhabditis elegans. Methods in Cell Biology, 107, 177–206.

CHAPTER 5

TRACKING THE COMPLEX BODY POSTURES OF THE FILARIAL PARASITE *BRUGIA MALAYI*

Abstract

Filarial parasites infect millions of people worldwide, and is thus important to develop objective and user-friendly platforms to rapidly screen for potential vaccines. We have designed a cross-platform open source nematode tracking program capable of tracking the complex postures exhibited by the filarial parasite, *Brugia Malayi*. The program requires minimal intervention from the user, and employs a limited number of built-in assumptions to track a wide range of nematode movement patterns. The raw movement data is further analyzed to identify quantifiable changes in posture and behavior of the parasite.

Introduction

It is estimated that around 150 million people are infected and over 1 billion people are at-risk of infection from filarial parasitic nematodes [1-7]. Diseases caused by filarial nematodes include, but are not limited to, onchocerciasis (river blindness), loiasis (African eye worm), and lymphatic filariasis (elephantitis) [3][4]. People affected by these diseases often live in developing countries where medical treatment options are relatively expensive or difficult to obtain.

Brugia malayi is a filarial parasite that is endemic in Indonesia and Southeast Asia causing the disease elephantitis [3][6-8]. Elephantitis is the second leading cause of permanent, long-term disability in the world [3]. Infection occurs when an infected mosquito

feeds on a human host, causing the nematode to exit the mosquito and enter into the human through the feeding site [6]. Once inside the human body, the filarial parasite matures after migrating to the lymphatic vessels and then proceeds to mate. A fertilized female can release hundreds or thousands of microfilariae (mf) daily, which will then be transferred to the mosquito host via a feeding event [3]. Symptoms of elephantitis include an altered immune system and enlarged body parts, leading to pain and physical disability [3][8]. Commonly available treatment options include chemotherapy and single-dose combination of ivermection or diethylcabamazine paired with albendazole; however, there is no cure for elephantitis [9]. More research opportunities need to be created in this area of medicine to identify safe, practical and viable treatments that can cure the filarial infection.

To rapidly screen the effects of potential drugs on *brugia malayi*, the movement of the parasite is visually assessed. Recent studies that have quantified the nematodes' movement have used a visual scoring system that rates the activity level of the nematodes, [10] or a video is recorded and the mean motility unit percentage is calculated [11]. These systems can be subject to observer bias and may not provide the high-resolution information about the movement of the nematodes. In recent years, advanced software-based solutions for whole-body nematode tracking have been developed [12][13]; however, these tracking programs have primarily been developed for *C. elegans*, which are the most widely used nematode model organism. Many different systems have been developed to track *C. elegans* at single worm or population level in different types of assays and quantify their behavioral parameters with a relatively high degree of resolution [14-20].

As the present-day worm tracking systems are built around *C. elegans*, there are often assumptions to be made regarding the visual appearance, speed, size, and movement parameters

of the worms. The use of these assumptions make it difficult to tailor the tracking program for other nematode species or other experimental scenarios. Furthermore, there are vast differences in size and shape of *brugia malayi* to those of *C. elegans*, thus rendering it nearly impossible for a *C. elegans* tracking method to work for our case. *Brugia malayi* have a much longer body compared to *C. elegans*, which can exhibit one or more occlusions along the length of the body. As such, we have designed a nematode tracking program that incorporates minimal assumptions regarding locomatory kinematics and visual appearance of the worm and has the ability to track the body through self-occlusions. Thereafter, our program computes key behavioral parameters to quantify the movement of the nematode. We have successfully tested our program to detect and quantify speed, curvature, number of bends, direction of motion and frequency of head oscillations of *brugia malayi* worms crawling on agar throughout multiple video sequences.

Methods

Image Processing

Before a midline spline can be produced, the recorded images are processed through several steps. First the images, if color, are converted to grayscale with brightness values ranging from 255 (white) to 0 (black). The mean pixel intensity for that image is estimated. This pixel intensity is then multiplied by a user defined percentage, resulting in a threshold value to be used to create a binary image. The user defined percentage is particularly relevant for image sequences gathered under conditions that would cause the entirety of the image to become brighter or darker (Fig. 5.1) i.e. an auto exposure setting on the camera or a user adjusting the brightness of the light. The threshold value is used to create a binary image where all pixels above the threshold are set to white and all pixels below the threshold are set to black. There is

an optional parameter to fill in holes that may appear in the center of the worm where the brightness values fall outside of the threshold; however, this parameter should only be used in situations where the worm does not self-occlude. After a binary image has been created, the image will be saved to a directory to be read by the tracking section of the program. This process is illustrated in Fig. 5.2.

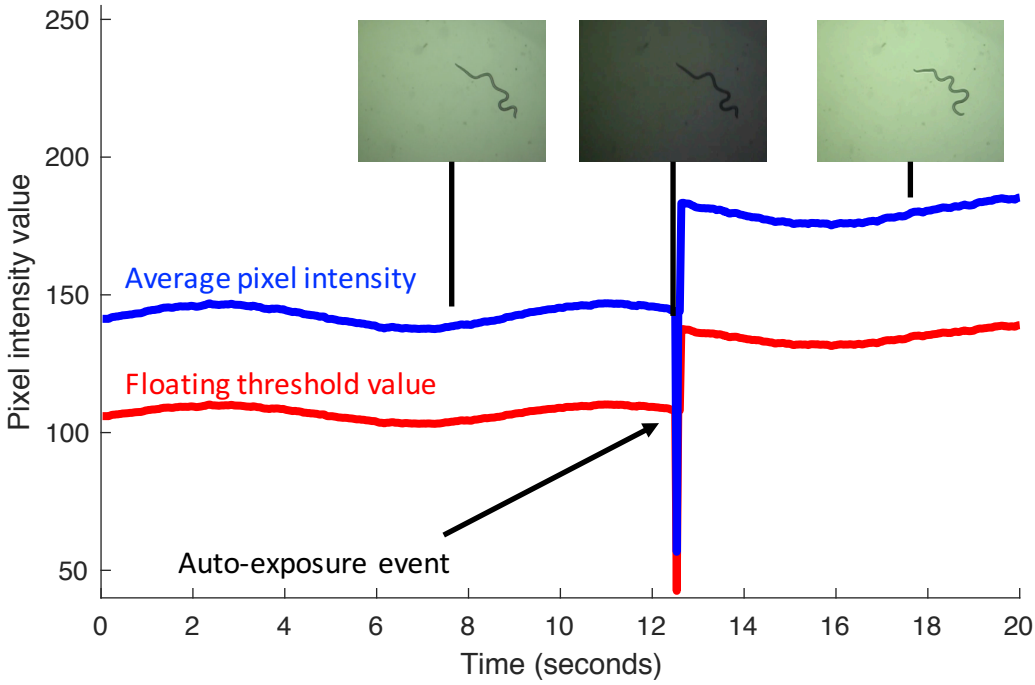

Fig. 5.1. Average pixel intensity values for a 20 second video (blue) and the associated threshold values (red). Often lighting conditions in a video can change due to interactions from the user or other software. For this video, the pixel intensity values are oscillating over time, which can cause a static threshold value to only be applicable to a subset of frames in the video. Another cause of pixel intensity changes can be an auto-exposure event happening with the camera software. This event causes a sudden drop and rise in the pixel intensity values for which a static threshold will fail to compensate, thus leading to improper segmentation. Our method of segmentation takes these issues into account and can accurately perform the segmentation.

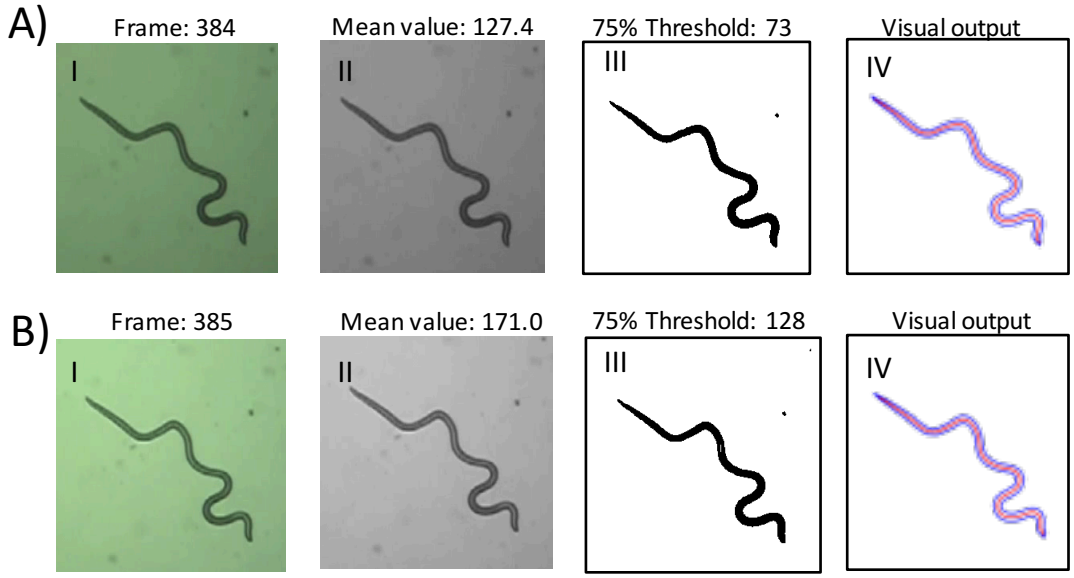

Fig. 5.2. Process of segmenting the nematode from the background and displaying the result to the user. First the original image is converted to a gray-scale image and the mean pixel intensity is calculated. The threshold is then set to 75% of the mean pixel intensity and the image is converted to a binary. This adaptive threshold allows for changes in lighting conditions throughout the experiment. (A-B) The binary image is then processed through the tracking program.

Head and Tail Identification

Identifications of the head and tail are performed automatically by finding an appropriate starting image, smoothing the boundaries found, and then highlighting statistically significant values. The program begins by searching through the binary images created in the "Image processing" step to find an image that has a single body of appropriate size, does not have any holes, and is not touching an edge of the image. The raw border pixel locations will then be smoothed and recorded as x-y pairs. The signed curvature equation is used to determine the curvature values along each border point. By only highlighting points that are 2 standard deviations lower than the average curvature value along the entire boundary, we segment out the points belonging to the head and tail. Using a k-means clustering algorithm, the segmented boundary points are clustered into two spatially separate groups and only the point with the

lowest curvature value in each group is retained. It is assumed that the tail will always form a sharper bend than the head so the border point with the lowest curvature value is assigned to the tail and the other to the head. This step produces a graphic for the user to easily verify the correctness of the assignment.

Midline Generation (No Occlusion)

If no occlusion is present in the image, then the midline of the worm is determined by splitting the boundary into two sections using the head and tail identification process previously described. For each point in the shorter of the two sections, the closest point in the longer section is found. Taking the average of these two points produces a point along the midline of the body. A cubic spline is then used to join all the points together and a user defined number of points are equally spaced throughout the spline; thereby producing the midline of the worm. From each midline point, the closest border pixel is then found and the distance between the two points reveals the width of the worm at that midline point.

Midline Evolution (Occlusion)

Monitoring the shape of a nematode's body through occlusions remains an active area of research today. When an occlusion occurs, the standard process used to generate a midline would fail due to the loss of border information through the occluded area. We perform a number of steps that will ensure the midline trends towards the centerline of the worm. To achieve this, first we calculate vectors normal to the boundary points and facing towards the body (Fig. 5.3). For every midline point, the closest border point is found and if the distance between the points is less than the width associated with that midline point, then the midline point is moved in the

direction of the border point's normal vector. This allows points that are not presently on the body to be migrated back onto the body as well as naturally tending towards the centerline of the body. Our program attempts to prevent midline points from overlapping with one another when an occlusion happens parallel to the midline. To do this, the normal vectors at each midline point are calculated and then the vector from a single midline point to all other midline points are found. If the difference in direction of the vectors is below a user specified threshold and the distance between the points is less than the width associated with that midline point, the midline point is then moved in the opposite direction of the normal vector. After the points have been moved due to the border points and fellow midline points for one iteration, they will be redistributed to ensure that the distance between points is kept equal. This is done by creating a cubic spline between them and then evenly distributing the user defined number of points.

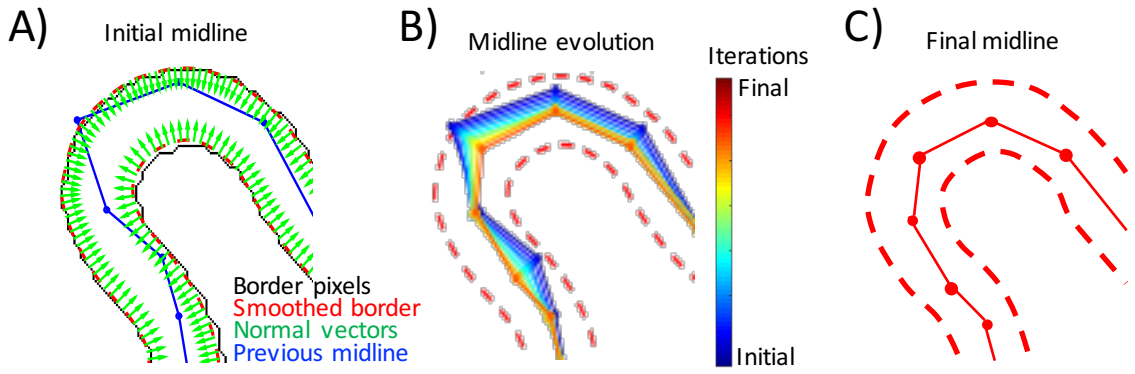

Fig. 5.3. Process of updating midline points from frame to frame. The x,y locations of the binary border pixels are recorded. A smoothed border is then calculated applying a moving point filter over the border locations. Next the normal vectors pointing into the body at every point on the smoothed border are calculated (A). At each iteration a body point is adjusted by locating a suitable border point (within 150% the width of the body at that point). The body point is then moved in the direction of the normal line to that point (B). This process continues until the combined movement of all points falls below a user specified threshold (C).

Directed Motion

To describe the direction of worm motion, we have devised a method of distinguishing between forward and backward motion in the head and tail portions of the worm. This is accomplished by monitoring the distance from the 3rd point to the head or tail in the current frame (Fig. 5.4) and the distance from the 3rd point in the previous frame and the current head or tail location. If the distance from the head to the current 3rd point is smaller than the distance from the head to the previous 3rd point, then the worm is said to be moving forward (Fig. 5.4B). Vice versa, if the distance from the head to the current 3rd point is larger than the distance from the head to the previous 3rd point, then the worm is said to be moving in the reverse direction (Fig. 5.4C). For the tail section of the worms, these distance criteria are simply reversed (data not shown).

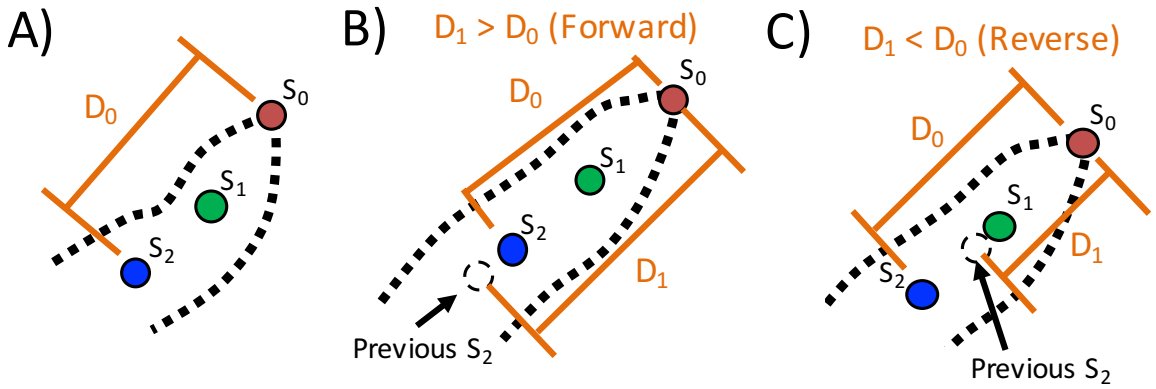

Fig. 5.4. Determination of forward or backward movement. The distance (D_0) between the head (S_0) and 3rd point (S_2) is determined for the previous frame (A). Then the distance between the head and the 3rd point of the previous frame is measured. If the distance between the head and the 3rd point (D_0) for the current frame is smaller than the distance between the head and the previous 3rd point (D_1) then the worm is said to be moving forward (B). If the worm is moving in the reverse direction D_0 would be less than D_1 (C).

Quantifying Number of Bends

One parameter that stands out among longer nematodes, as opposed to shorter nematodes, is the number of shapes and bends the nematode can perform. To classify the number of bends, we used the signed curvature equation to monitor curvature values along the midline. A bend is then classified as a change in the sign of curvature for 3 consecutive points. Consecutive points are used as a hysteresis window for when the worm is not bent a lot, and the curvature values can fluctuate between positive and negative around 0 leading to a false number of bends recorded (Fig. 5.5). A subset of shapes that the nematode can make are shown in Fig. 5.6 with arrows indicating bend locations and the total curvature (sum of all curvature values along midline).

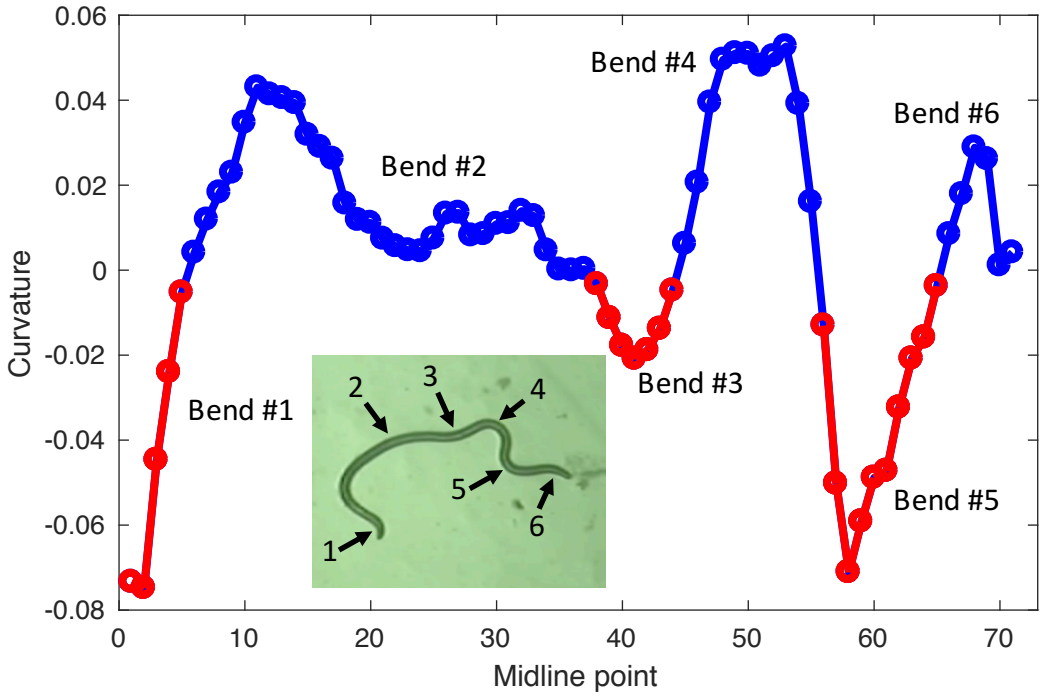

Fig. 5.5. Sample curvature values from one instance of time used to calculate the number of bends in the midline. When the sign of the curvature value changes for more than 3 consecutive points a bend is recorded. In this instance there is a total of 6 registered bends in the worms' midline. Bends are indicated on the worm body with black arrows.

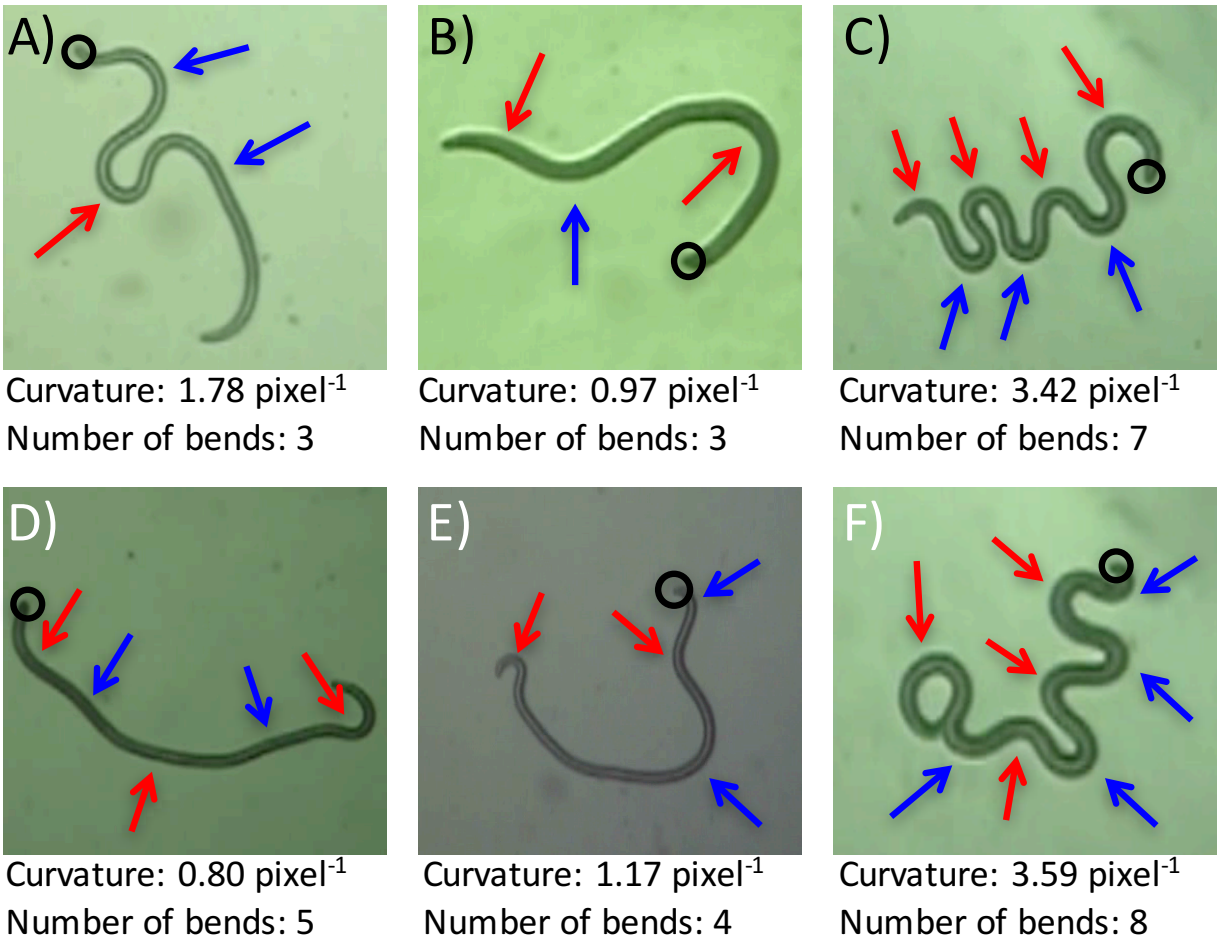

Fig. 5.6. Variety of simple and complex body postures that can be formed. The head (black circle) and bends in the worm's body (colored arrows) are highlighted; red arrows indicate negative curvature values along the midline and blue arrows indicate positive curvature values. A bend is classified as a change from positive to negative curvature or vice versa along the midline. Indicated below each image is the total absolute value of the curvature of the worm, i.e. how bent the midline of the worm is, along with the number of bends present in the body.

Results

Our program monitors several different parameters that were previously discussed and provides raw data output as well as visual representation of the output for user insight and verification.

Movement Trends

One parameter that can be used to distinguish between different worms is the tendency for directed movement. In Fig. 5.7, we show a colored visual representation of the position of the worm throughout a 20 second video. The tendency for the worm to move in the forward and backward direction is also shown as a percentage of the total length of the video. It is easy to see in video numbers 2, 6, 7, 8 and 9 that the worm crawls in a directed, forward motion for a large portion of the video. In contrast, video numbers 1, 3, 4, 5, and 10 show the worm moving in the backward direction almost as much as in the forward direction. In these videos, the worms appear to elongate and then contract repeatedly while not displacing their entire body significantly. From this data, it is possible to measure how much of the total movement of the worm is concentrated in a particular direction as opposed to random perturbations.

Head Velocity

Monitoring the movement of the head of the worm can be very useful. The velocity of the head of the worm is shown in Fig 5.8 with the positive values indicating a forward direction and the negative values indicating a backwards direction. The signed value of the head velocity allows for motion patterns such as entirely forward, entirely backward and probing (mixture of forward and backward) to be classified. In Fig. 5.8J the velocity of the worm's head is alternating between positive (forward) and negative (backward) values indicating that the worm was behaving in a probing pattern, while Fig. 5.8B show the worm's head velocity is almost entirely positive (forward) meaning the worm was crawling in a very forward directed manner.

Curvature Analysis

Often the curvature along the worm's midline can be used to distinguish movement patterns and general body shape. Plots of several worm's curvature values throughout a 20 second video are shown in Fig. 5.9. When monitoring the curvature of a nematode, it is common to view undulatory motion represented as bands moving diagonally across the plot such as in Fig. 5.9B, H and I which correspond quite well to forward directed motion from Fig. 5.7 and Fig. 5.8. Another movement pattern that can be seen is a probing motion (alternating between forward and backward). This probing action is shown as jagged horizontal bands across the plot such as Fig. 5.9J. We can also see that these worms do not always propagate a wave/ bend through their entire body and can even generate new waves at any point in the body which can be seen in Fig. 5.9C at the 5 second mark. The divergence of the red band near the center of the body into two separate bands is the creation of 1 bend into 3 different bends. From the magnitude and total intensity of the curvature plots, we can also gather how curled up the worm is. Fig. 5.9C is much more curled up than Fig. 5.9A and this can also be verified from Fig. 5.7A and C.

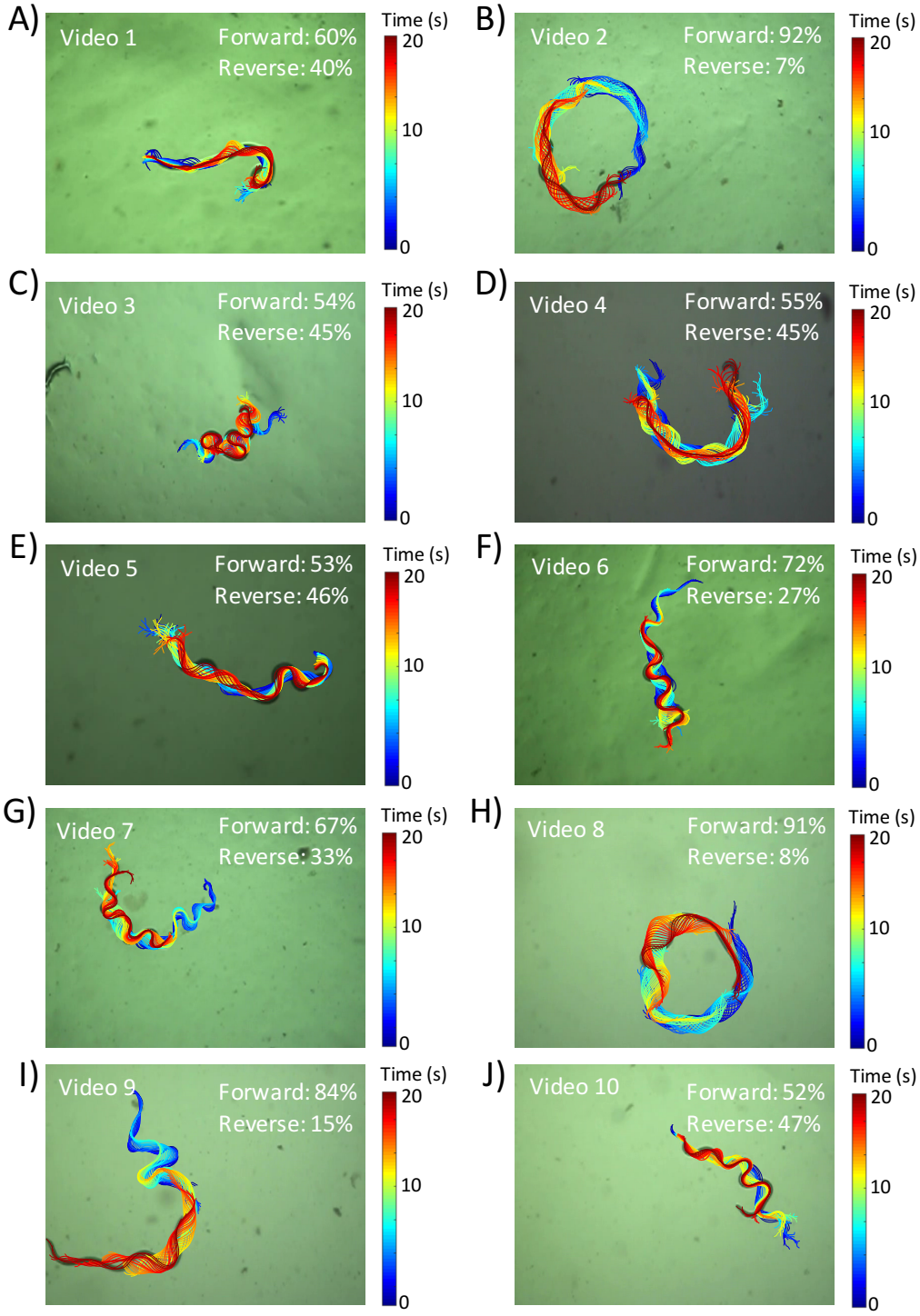

Fig. 5.7. Visual progression of the body position of a worm throughout a 20 second video. The percentage of time the head position of the worm was moving in the forward and reverse directions during the video is indicated as ”Forward” and “Reverse,” respectively.

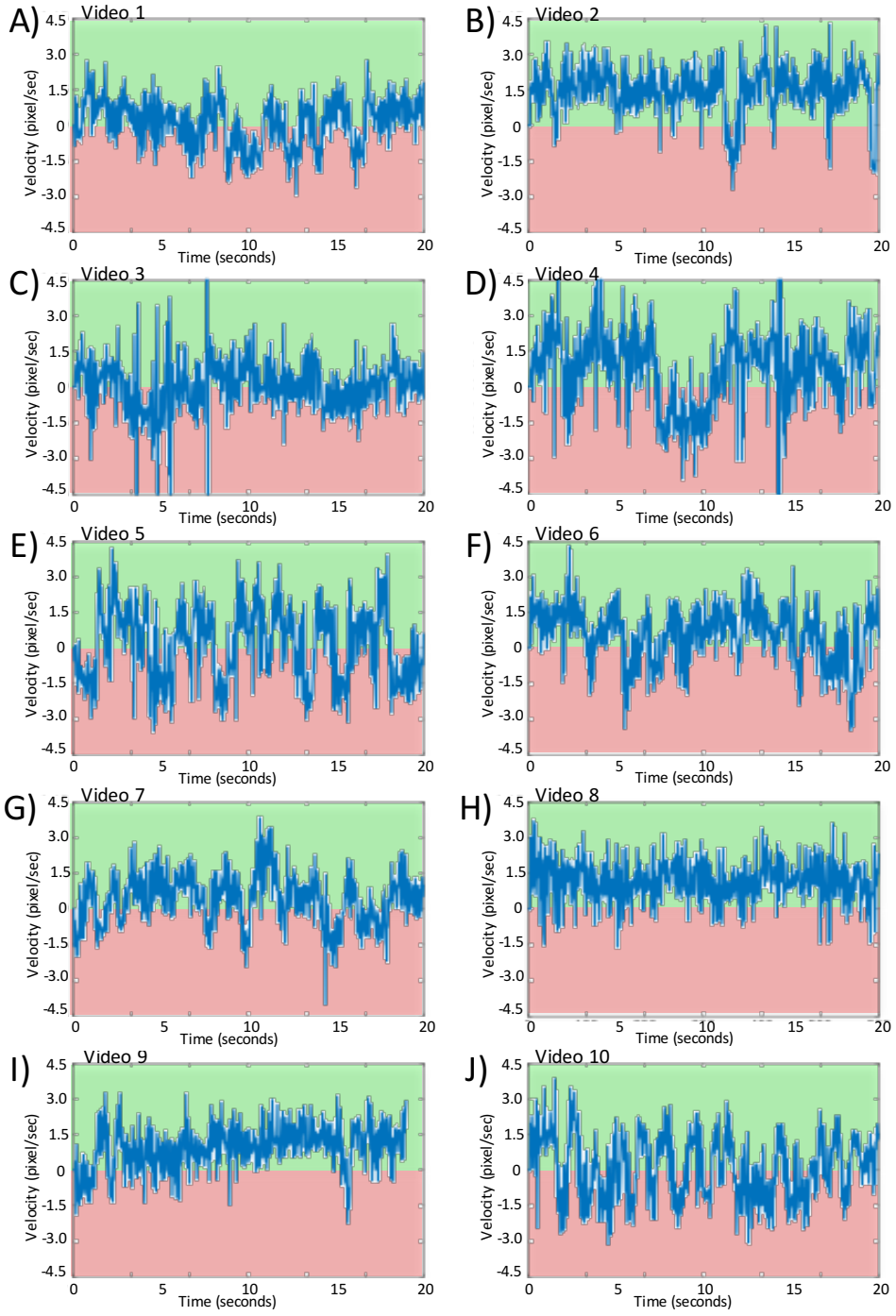

Fig. 5.8. Worm head velocity in the forward (green/ positive) and reverse (red/ negative) direction. Velocity is calculated as the change in position from frame to frame. The velocity direction is determined by measuring the distance from the current head location and the previous 3rd body location. If this distance has increased, then velocity is in the positive direction while if the distance has decrease it is in the negative direction.

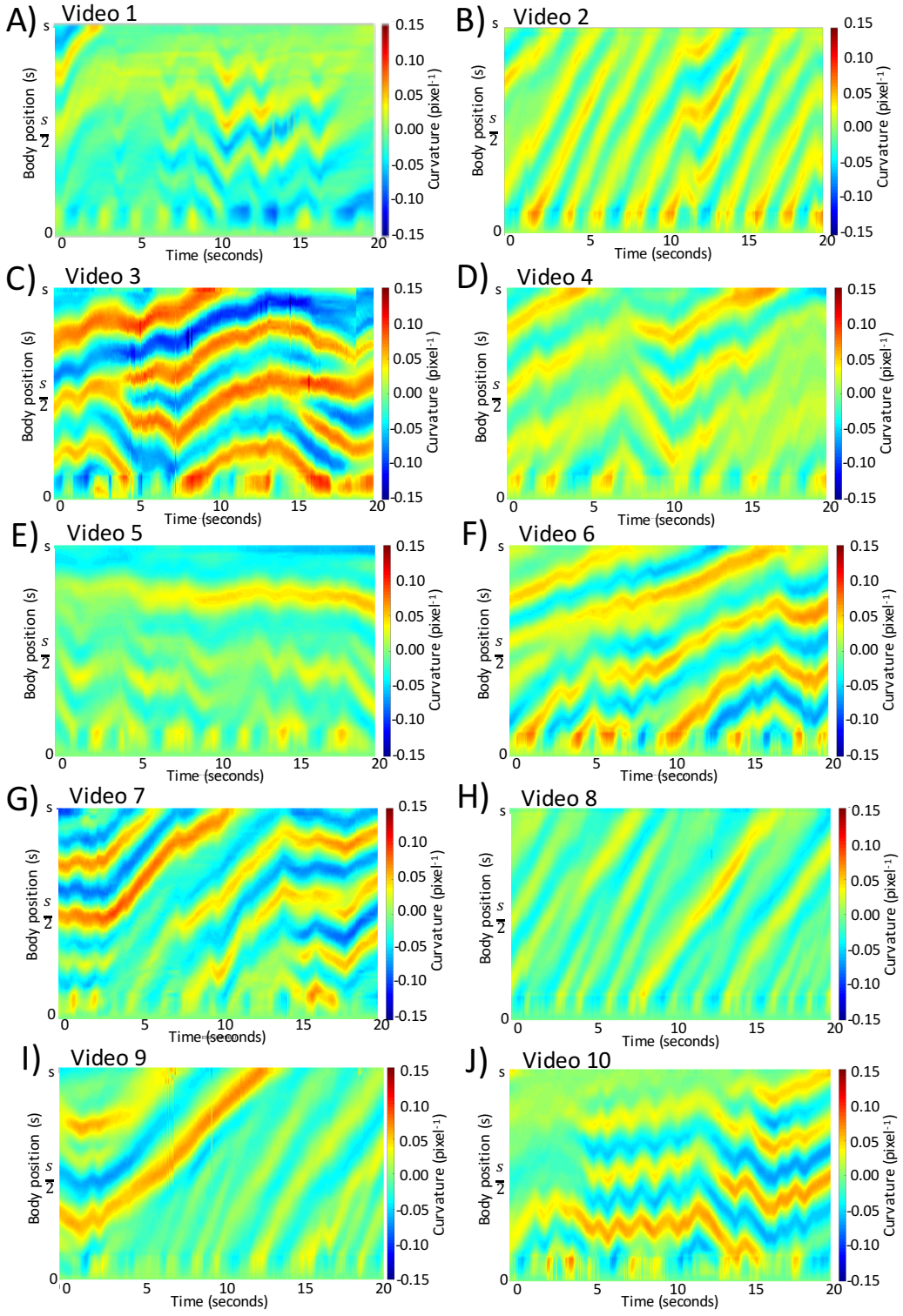

Fig. 5.9. Plot of the curvature at each midline point on the worm from the head s(0) to the tail s(1).

Number of Bends and Bending Severity

To accurately describe the shape of a nematode, the total curvature or total absolute bending along the midline of the worm should be monitored along with the number of bends present in the midline. The sum of the absolute value of the curvature provides information on how bent the worm is; however, this alone is not sufficient. Shapes such as omega (Ω) bends and coils can have very similar total curvature but visually appear different. By monitoring the number of bends in the body, it is possible to distinguish not only between omega and coiled postures but to also compare how similar the postures are. In Figure 7 the number of bends and sum of curvature are shown for multiple videos. From this data we can see that an increase in the number of bends in a body does not necessarily mean the total amount of curvature is going to increase (Fig. 5.10D). It can also be noted that the sum of curvature cannot be indicated by the number of bends, such as with Fig. 5.10B and C. Fig. 5.10B has a similar number of bends in the body as Fig. 5.10C; however, the sum of curvature of Fig. 5.10B is lower than Fig. 50.10C, indicating that the number of bend was similar but the severity of bends in Video 3 were much greater than the bends in Video 2.

Conclusion

In conclusion, we have developed a robust, user-friendly nematode tracking program that can detect and track the complex postures of *brugia malayi*. One of the challenges for nematode tracking programs is the ability to detect the worm's posture through occluding events, whether they are from self-occlusions or occlusions from other objects. As the focus of our program was *brugia malayi*, we desired that the program is able to track during occluding events of this filarial parasite without crashing or running out of memory. As shown in the Chapter, our program is successively able to track the worm movement through all occlusions

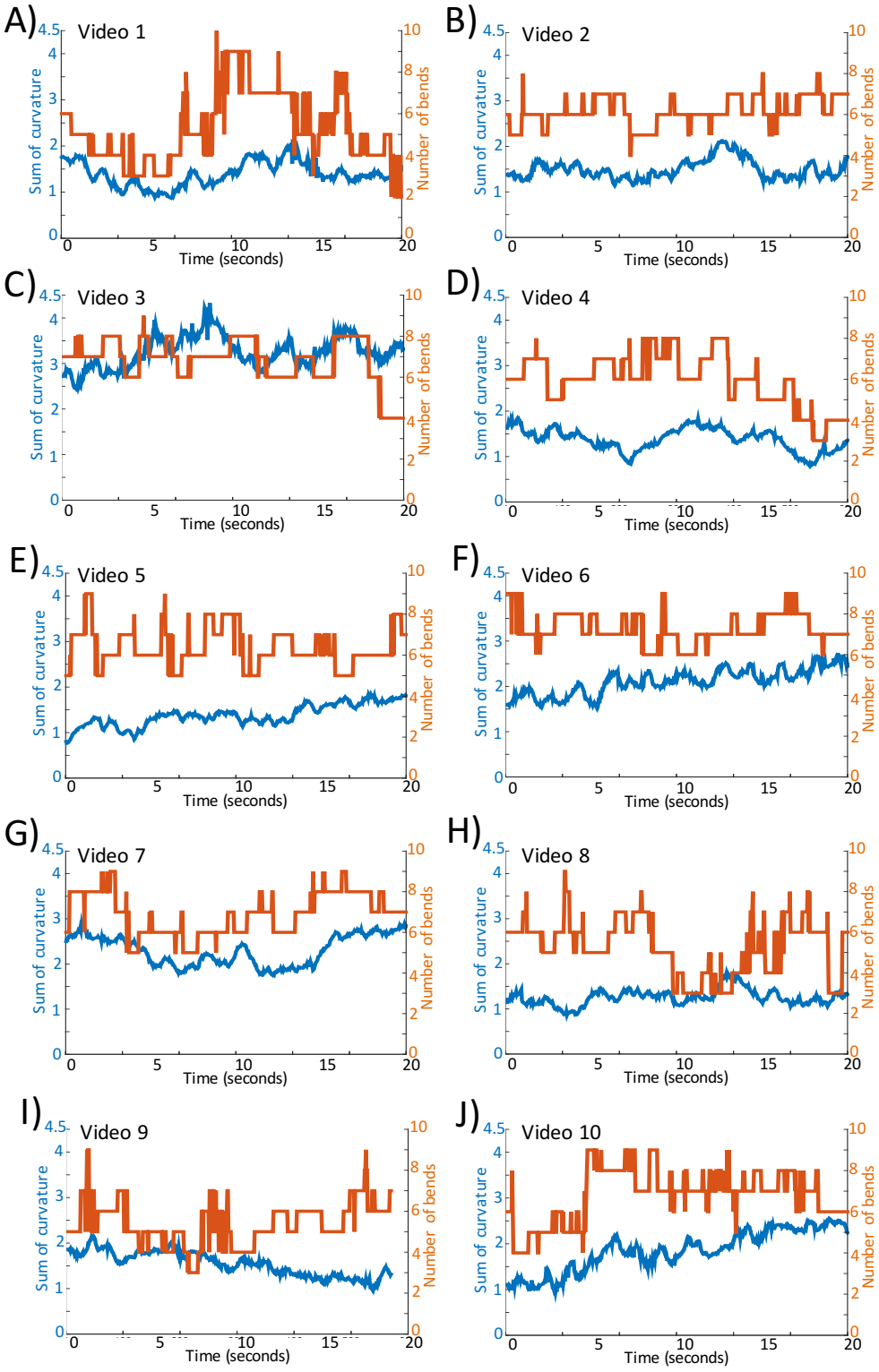

Fig. 5.10. Plot of the number of bends present in the body of the worm (orange) and the sum of the curvature along the midline of the worm (blue) at each instance of time.

and report values of user-defined parameters that are used in characterizing the movement behavior of *brugia malayi*. The parameters were chosen based on their apparent applicability to generalized nematode movement with some minor modifications to deal with *brugia malayi*.

Our program delivers a visual representation of every movement parameter to the user as well as a video sequence illustrating the worm's posture over time. With this information, a tracking error is easily detectable and can be rectified with minimal user intervention. In our view, this tracking program addresses the two key issues while detecting the posture of the nematode through a video: varying lighting conditions and even in the presence of occlusions. Since this work is one of few programs currently designed to track the *brugia malayi,* it would be possible to define new parameters that better describe the movement characteristics of the nematode. With the basic framework presented here to identify positions of the midline, it is possible to add new features and expand the functionality of the program.

Acknowledgements

We would like to thank Dr. Michael Kimber and Hirinu Harischandra for culturing the *brugia malayi* and recording the videos used in this publication.

References

[1] World Health Organization. (1987) WHO Expert Committee on Onchocerciasis. World Health Organization Technical Report Series. 752, 1-167.

[2] World Health Organization. (1995) Onchocerciasis and its control. World Health Organization Technical Report Series. 852, 1-103.

[3] World Health Organization. (2016) Lymphatic filariasis (Fact sheet 102). Retrieved from http://www.who.int/mediacentre/factsheets/fs102/en/

[4] Knopp S., Steinmann P., Hatz C., Keiser J., Utzinger J. (2012) Nematode infections: filariases. Infectious Disease Clinics of North America. 26(2), 359-81.

[5] Addiss D.G., Louis-Charles J., Roberts J., Leconte F., Wendt J.M., Milord M.D., (2010) Feasibility and effectiveness of basic lymphedema management in Leogane, Haiti, an area endemic for bancroftian filariasis. PLoS Neglected Tropical Diseases. 4(4), e668.

[6] Ottesen E., Duke B., Karam M., Behbehani K. (1997) Strategies and tools for the control/elimination of lymphatic filariasis. Bulletin of the World Health Organization, 75(6), 491–503.

[7] Ramaiah K.D., Das P.K., Michael E., Guyatt H. (2000) The economic burden of lymphatic filariasis in India. Parasitology Today. 16(6), 251-3.

[8] Cantey P.T., Rout J., Rao G., Williamson J., Fox L.M. (2010) Increasing Compliance with Mass Drug Administration Programs for Lymphatic Filariasis in India through Education and Lymphedema Management Programs. PLoS Neglected Tropical Diseases 4(6), e728.

[9] Moreno Y., Nabhan J., Solomon J., Mackenzie, C., Geary, T. (2010) Ivermectin disrupts the function of the excretory-secretory apparatus in microfilariae of Brugia malayi. Proceedings of the National Academy of Sciences of the United States of America, 107(46), 20120–20125.

[10] Rao R., Weil G., (2002) In Vitro Effects of Antibiotics on Brugia Malayi Worm Survival and Reproduction. Journal of Parasitology, 88(3):605-611.

[11] Storeya B., Marcellinoc C., Millera M., Macleana M., Mostafaa E., Howella S., Sakanaric J., Wolstenholmea A., Kaplana R. (2014) Utilization of computer processed high definition video imaging for measuring motility of microscopic nematode stages on a quantitative scale: "The Worminator." International Journal for Parasitology: Drugs and Drug Resistance, 4(3), 233–243.

[12] Huang K.M., Cosman P., Schafer W. (2007) Automated tracking of multiple c. elegans with articulated models. IEEE ISBI.

[13] Huang K., Cosman P., Schaferb W. (2008) Automated detection and analysis of foraging behavior in Caenorhabditis elegans. Journal of Neuroscience Methods, 171(1), 153–164.

[14] Geng W., (2004) Automatic tracking, feature extraction and classification of C elegans phenotypes. IEEE Transactions on Biomedical Engineering, 51(10), 1811–1820.

[15] Fontaine E., Burdick J., Barr A. (2006) Automated tracking of multiple C. Elegans. Conference Proceedings Engineering in Medicine and Biology Society.1:3716-9.

[16] Wang S.J., Wang Z.W. (2013) Track-A-Worm, An Open-Source System for Quantitative Assessment of C. elegans Locomotory and Bending Behavior. PLoS ONE 8(7), e69653.

[17] Nagy S, Goessling M, Amit Y, Biron D (2015) A Generative Statistical Algorithm for Automatic Detection of Complex Postures. PLoS Computational Biology 11(10), e1004517.

[18] Albrecht, D. Bargmann, C. (2011) High-content behavioral analysis of Caenorhabditis elegans in precise spatiotemporal chemical environments. Nature Methods 8(7), 599-605

[19] Palmer C., Barnett M., Copado S., Gardezy F., Kristan W. (2014) Multiplexed modulation of behavioral choice. Journal of Experimental Biology 217, 2963-2973

[20] Moore B., Jordan J., Baugh L. (2013) WormSizer: High-throughput Analysis of Nematode Size and Shape. PLoS ONE 8(2), e57142.

CHAPTER 6

SUMMARY AND CONCLUSIONS

In this thesis, I have presented microscale assays for testing the behavior of nematodes or worms, along with different versions of software solutions to ease the tasks of data collection, storage, analyses, and plotting.

Chapter 2 discussed whether *C. elegans* had the ability to sense static magnetic fields in the range of 5 milli Tesla to 120 milli Tesla. For this work, we designed and fabricated a microfluidic chip that constrained the movement of the *C. elegan* subjects in only one dimension. A permanent magnet was then placed at pre-specified distances from the microfluidic chip so the magnetic field lines ran parallel to the nematode's body. To automate the process of data collection and minimize and user bias, we designed a software program to quantify the worm's movement behavior when exposed to magnetic fields. We found that on the abovementioned range of magnetic field, the worms showed no significant change in movement behavior.

In Chapter 3, we studied two nematodes of agricultural importance: plant parasites soybean cyst nematode (SCN) and root knot nematode (RKN). It is thought that plant parasitic nematodes locate host plants in farmlands by detecting chemical gradients within the soil formed by exudates given off by the plant's root system. To test the attractive/repulsive nature of several ionic solutions as well as live root tissue, we designed two microfluidic devices. The first device contained four testing lanes arranged in a parallel configuration. Microscale filters allowed a chemical gradient to be formed over a period of 24 hours while simultaneously preventing the nematodes from exiting the testing chamber. The second device was designed to accommodate a 3-day-old soybean seedling along one side of the device which chemically connected all of the lanes together, while providing a physical barrier via the microscale filters. Because of large

scanning distances within the chip (~2cm) and long experimental time periods (18 to 24 hours), standard microscopy techniques could not be used. Using a high-resolution scanner and a custom control program, we were able to automate the process of imaging the experiment and aid the user in the process of data collection. Using these devices and the software program, we tested the response of SCN and RKN to various ionic solutions. We were also able to test the chemotaxis of SCN and RKN to four different locations along the root of a soybean seedling. We showed that the microfluidic chip technology, in combination with our nematode tracking program, can enable information-rich experiments on the chemotaxis of nematodes to live plant roots and serve as a useful platform to test the efficacy of crop resistance strategies in convenient laboratory settings.

While the applications of polymeric microfluidics are numerous and varied, their fabrication processes are often time-consuming, laborious, and expensive. This is precisely one of the fundamental reasons limiting the mass commercialization of microfluidic technology. In Chapter 4, we explore a new type of microfluidic device called *open air microfluidics* for the study of nematode behavior. We fabricated the two separate devices on two different substrates: paper and plastic. In both substrates, there is a supporting structure (i.e. base) with an area excised (i.e. hole). The excised area is filled with a liquid gel (i.e. agar or Pluronic gel) that eventually forms a suspended membrane. The materials and equipment involved in making these devices are low-cost and do not require any special training in photolithography or microscopy. The time for fabrication is within a few minutes compared to a few hours for polymeric microfluidic devices. We were able to successfully test the application of the paper- and plastic-based devices for drug screening and characterize the dose response curve of *C. elegans* to levamisole.

Chapter 5 presents my work to track and quantify the movement of a human filarial parasite, *Brugia Malayi*. Motion tracking software could lead to faster screening of new drugs and accelerate the process of finding a viable, safe vaccine. However, our previous nematode tracking and analysis algorithms do not adapt to this filarial parasite. The high length to width ratio of *brugia malayi* enables the nematode to form much more complex postures; often resulting in occlusions and peculiar movement behaviors. Our program is able to scan through a video, locate a frame to create an initial model of the nematode, and then track various positions along the nematode's midline. Based on our analysis of sample videos, minor assumptions were incorporated in the program regarding the shape, visual appearance and movement behavior. We were able to quantify various body and movement parameters of *brugia malayi*, including curvature along midline, forward or backward motion, and cruising or probing behavior.

Because of the diversity in behavioral patterns observed in different nematode species (free-living, animal parasitic, plant parasitic), it is challenging to develop a unified testbed or imaging software platform to suit all nematodes. Thus we have demonstrated movement assays for some specific applications, along with tracking software programs tailored for the application under study. To improve microfluidic accessibility to nematode researchers, it is worthwhile to consider cheaper, flexible testing designs beyond conventional microfluidics and build data-intensive software platforms that can extract useful behavioral information.

LIST OF PUBLICATIONS

Journal Publications

[1] Beeman, A.*, Njus, Z.*, Pandey, S., Tylka, G. (2016) Chip Technologies for Screening Chemical and Biological Agents Against Plant-Parasitic Nematodes. Phytopathology. 106(12), 1563-1571 * Joint first authors

[2] Kong, T., Brien, R., Njus, Z., Kalwa, U., Pandey, S. (2016) Motorized actuation system to perform droplet operations on printed plastic sheets. Lab on a Chip, 16(10), 1861-1872

[3] Njus Z., Feldmann D., Brien R., Kong T., Kalwa U., Pandey S. (2015) Characterizing the Effect of Static Magnetic Fields on *C. elegans* using Microfluidics. Advances in Bioscience and Biotechnology, 6, 583-591

Conference Publications

[4] Jensen, J., Njus, Z., Pandey, S., Tylka, G. (2016) Video analysis software to measure nematode movement with applicatinos for accurate screening of nematode control compounds. Society of Nematologists

[5] Beeman, A., Njus, Z., Pandey, S., Tylka, G. (2016) A scanner assay developed to quantify nematode population movement and its applications for nematicide screening. Society of Nematologists

[6] Agbedanu, P.N., Zamanian, M., Chan, J.D., Njus, Z.L., Pandey, S., Acharya, S., Kimber, M.J., Marchant, J.S., Day, T.A. (2014) Anthelmintics – From Discovery to Resistance, Schistosome Therapeutics: Assays and Receptors for Discovering New Schistosome Chemotherapies

[7] Cruz, D.R., Mayfield, D.A., Njus, Z.L., Pandey, S., Beattie, M.S., Leandro, L.F., Munkvold, G.P. (2014) Sensitivity of Fusarium species from soybean roots to seed treatment fungicides. Phytopathology, 104(11), 29-29

[8] Beeman, A.Q., Njus, Z., Jensen, J.P., Pandey, S., Tylka, G.L. (2014-2015) Center for Arthropod Management Technologies, Toward increased efficacy of soybean cyst nematode management tools

[9] Beeman, A.Q., Njus, Z., Jensen, J.P., Pandey, S., Tylka, G.L. (2014) A microfluidic device to study chemotaxis of plant-parasitic nematodes of soybean. Soy 2014